In vitro Characterisation of Foetal Human Neural Progenitors, their Astroglial Derivates, and Effects of Released Factors and Extracellular Matrix on Axon Regeneration

Von der Medizinischen Fakultät

der Rheinisch-Westfälischen Technischen Hochschule Aachen

zur Erlangung des akademischen Grades

einer Doktorin der Medizin

genehmigte Dissertation

vorgelegt von

Lisa Maria Hillen

aus Aachen

Berichter: Herr Privatdozent
Ph.D.B.Sc. Gary Brook

Frau Universitätsprofessorin
Dr. med. Ruth Knüchel-Clarke

Tag der mündlichen Prüfung: 31. Mai 2011

Diese Dissertation ist auf den Internetseiten der Hochschulbibliothek online verfügbar.

Lisa Maria Hillen

In vitro Characterisation of Foetal Human Neural Progenitors, their Astroglial Derivates, and Effects of Released Factors and Extracellular Matrix on Axon Regeneration

In vitro Characterisation of Foetal Human Neural Progenitors, their Astroglial Derivates, and Effects of Released Factors and Extracellular Matrix on Axon Regeneration

Lisa Maria Hillen

Abstract

Human neural progenitor cells (hNPC) and human mesenchymal stromal cells (hMSC) have both been reported to be able to promote improved functional recovery after grafting into experimental spinal cord injuries. Transplantation of pre-differentiated neural progenitor cells has been shown to be an effective strategy to support repair of the spinal cord. In particular, the implantation of astrocyte restricted precursors may represent a means of promoting spinal cord recovery through the maintenance and support of axonal regeneration.

Although it has been demonstrated by our group that foetal hNPC, pre-differentiated to type I astrocyte restricted precursors (hNP-AC), promote more extensive axon regeneration by adult rat dorsal root ganglia (DRG) neurons *in vitro* than non-differentiated hNPC or hMSC, the mechanisms of action to support neuritic outgrowth remained unclear. Therefore, hNPC were characterised before and after *in vitro* differentiation to hNP-AC to provide a clearer definition of the changes that the cells had undergone. Furthermore, possible contributions of released trophic factors (i.e. present in conditioned culture medium) or substrate-mediated mechanisms via the extracellular matrix (ECM) of hMSC and hNP-AC to support neuritic outgrowth were investigated.

In the first part of this study, the *in vitro* immunocytochemical- and mRNA expression profile of selected marker gens in hNPC and in the differentiated hNP-AC was quantified. Furthermore, proliferative activity was estimated with a metabolic and a morphological assay, whereby the latter, by measuring the increase in volume over time, provided an indirect indicator of proliferation within intact neurospheres. The hNPC grew as neurospheres, which were immunoreactive for the stem/progenitor cell related markers nestin ($91.0 \pm 3.4\%$), SOX2 ($89.2 \pm 2.7\%$) as well as musashi ($91.8 \pm 2.0\%$) and expressed CD133- and nestin mRNA. They showed spontaneous differentiation capacity into MAP2ab+ and TuJ1+ neuronal phenotypes as well as S100β+ (17.6

± 2.1%), GFAP+ (23.7 ± 2.3%) and vimentin+ (96.8 ± 1.1%) astroglial precursors. Whereas the differentiated hNP-AC demonstrated a similar immunocytochemical expression profile for the stem/ progenitor cell related markers nestin (89.2 ± 3.8%), SOX2 (88.0 ± 3.6%), musashi (89.2 ± 3.8%) and expressed CD133- and nestin mRNA in similar proportions to the hNPC, the expression of astroglial markers increased. A significantly higher proportion of hNP-AC were immunoreactive for S100β (79.4 ± 1.7%), GFAP (92.5 ± 3.4%) and CD44. Likewise, hNP-AC demonstrated significantly increased CD44- and GFAP mRNA expression than the non-differentiated hNPC. Estimation of proliferative activity of hNPC and hNP-AC showed a reduced doubling time (*DT*) in hNP-AC with a value of 5.1 days (morphological assay) and 3.2 days (metabolic assay), contrasting to hNPC prior to *in vitro* differentiation with a *DT* of 3.46 days (morphological assay) and 1.68 days (metabolic assay).

In the second part of this study, the contributions of trophic factors present in cell-conditioned medium (produced by either hNP-AC or hMSC) and their ECM in supporting DRG axon regeneration were investigated *in vitro*. Conditioned media from both cell types strongly supported neurite outgrowth over a defined PLL/laminin substrate. The ECM produced by the two cell types, however, demonstrated contrasting effects: hNP-AC ECM promoted substantial axon regeneration, but hMSC ECM supported relatively little axon growth. The combined application of hNP-AC ECM and hMSC conditioned media induced the greatest degree of axon outgrowth. The combination of hMSC ECM and hNP-AC conditioned medium, however, did not result in any enhanced axon growth over the values determined using hMSC ECM and control growth medium. Thus, although hNP-AC conditioned medium demonstrated potent trophic support for DRG axon growth, its effect was not supported by signals derived from hMSC ECM. This raises interesting questions for future experiments regarding the cross-talk between the intracellular signalling cascades activated by diffusible trophic factors and those activated by ECM-related molecules.

In vitro Characterisation of Foetal Human Neural Progenitors, their Astroglial Derivates, and Effects of Released Factors and Extracellular Matrix on Axon Regeneration

Lisa Maria Hillen

Zusammenfassung

Humanen neuralen Vorläuferzellen (human neural progenitor cells, hNPC) und humanen mesenchymalen Stromazellen (human mesenchymal stromal cells, hMSC) wird die Fähigkeit zugeschrieben funktionelle Genesung nach Transplantation in experimentell herbeigeführte Querschnittslähmung im Tiermodell zu fördern. Die Transplantation von prä-differenzierten neuralen Vorläuferzellen hat sich als effektive Strategie zur Unterstützung der Wiederherstellung nach experimentell herbeigeführte Querschnittslähmung erwiesen. Insbesondere, die Implantation von astrozytären Vorläufern, könnte einen Weg zur Genesung von Querschnittslähmung mittels Aufrechterhaltung und Unterstützung der axonalen Regeneration darstellen.
Obwohl unsere Gruppe *in vitro* demonstrieren konnte, das fetale hNPC, die zu Typ I astrozytären Vorläufern (human neural progenitor restricted Typ I astrocytes, hNP-AC) differenziert wurden, größere axonale Regeneration in Nervenzellen aus adulten Ratten Dorsal-/Spinalganglien (dorsal root ganglia, DRG) begünstigten als undifferenzierte hNPC oder hMSC, blieben die dazu führenden Wirkmechanismen unklar. Daher wurden in der vorliegenden Arbeit die hNPC vor und nach *in vitro* Differenzierung zu hNP-AC charakterisiert, um den vollzogenen zellulären Wandel eindeutiger zu bestimmen. Weiterhin, wurden mögliche Beiträge durch freigesetzte trophische Faktoren (d.h. Faktoren, die in konditioniertem Kulturmedium anwesend sind) oder substrat-vermittelte Mechanismen, via Extrazellulär Matrix (ECM) von hMSC und hNP-AC untersucht.

Im ersten Teil dieser Untersuchung wurde das *in vitro* immunocytochemische- und das mRNA Expressionsprofil von ausgewählten Markergenen in hNPC und differenzierten hNP-AC quantifiziert. Weiterhin wurde die Proliferationsaktivität mit einer metabolischen und einer morphologischen Untersuchung beurteilt, die mittels Vermessung der Volumenzunahme pro Zeiteinheit einen indirekten Indikator der Proliferation in intakten Neurospheren darbot. Die hNPC ent-

wickelten sich als Neurospheren, welche immunoreaktiv für die Stamm/Vorläuferzell verwandten Marker Nestin (91,0 ± 3,4%), SOX2 (89,2 ± 2,7%) sowie Musashi (89,2 ± 3,8%) waren und CD133- und Nestin mRNA exprimierten. Dabei wiesen die Zellen ein spontanes Differenzierungsvermögen in MAP2ab+ und TuJ1+ neuronale Phänotypen sowie S100β+ (17,6 ± 2,1%), GFAP+ (23,7 ± 2,3%) und Vimentin+ (96,8 ± 1,1%) astrogliale Vorläuferzellen auf. Während die differenzierten hNP-AC ein ähnliches immunocytochemisches Expressionsprofil für die Stamm/Vorläuferzell verwandten Marker Nestin (89,2 ± 3,8%), SOX2 (88,0 ± 3,6%) sowie Musashi (89,2 ± 3,8%) wie die hNPC aufwiesen und CD133- und Nestin mRNA in ähnlichem Verhältnis exprimierten, konnte ein Anstieg der Expression von astroglialen Markern beobachtet werden. Dies zeigte sich durch einen signifikanten Anstieg der Immunoreaktivität für S100β (79,4 ± 1,7%), GFAP (92,5 ± 3,4%) und CD44 in hNP-AC. Ebenso wurde in den hNP-AC ein signifikanter Anstieg der CD44- und GFAP mRNA Expression gegenüber den nicht-differenzierten hNPC nachgewiesen. Eine Bestimmung der Proliferationsaktivität von hNPC und hNP-AC ergab eine reduzierte Verdopplungszeit (doubling time, *DT*) in hNP-AC mit einem Wert von 5,1 Tagen (morphologische Untersuchung) und 3,2 Tagen (metabolische Untersuchung), im Gegensatz zu den hNPC vor der *in vitro* Differenzierung mit einer Verdopplungszeit von 3,5 Tagen (morphologische Untersuchung) und 1,7 Tagen (metabolische Untersuchung).

Im zweiten Teil dieser Arbeit wurden *in vitro* die Beiträge von trophischen Faktoren der hNP-AC bzw. der hMSC, welche in das Zellkulturmedium abgegeben wurden, sowie deren ECM im Hinblick auf die Unterstützung der axonalen Regeneration von DRG untersucht. Das konditionierte Medium beider Zelltypen induzierte einen weitreichenden, komplexen Neuritenauswuchs der DRG, wenn diese auf ein definiertes PLL/laminin Kontrollsubstrat platziert wurden. Allerdings zeigte die ECM der beiden untersuchten Zelltypen einen entgegengesetzten Effekt: Die hNP-AC ECM begünstigte eine beträchtliche axonale Regeneration, wohingegen die hMSC ECM einen signifikant geringeren axonalen Auswuchs induzierte. Die kombinierte Anwendung von hNP-AC ECM und konditionierten hMSC Medium induzierte das größte beobachtete Neuritenwachstum. Die Kombination von hMSC ECM und konditionierten hNP-AC Medium zeigte jedoch kein vergrößertes axonales Wachstum im Vergleich zu den Werten, die mit hMSC ECM und Kontrollkulturmedium erzielt wurden. Obwohl das konditionierte hNP-AC Medium mit seinen potenten trophischen Faktoren das axonale Wachstum von DRG förderte, war dieser Effekt nicht durch hMSC ECM bedingte Signale unterstützt. Hieraus resultieren interessante Fragestellungen für zukünftige Experimente zur genaueren Erforschung der Interaktion zwischen intrazellulären Signalkaskaden entweder aktiviert durch diffusionsfähige trophische Faktoren oder durch Wechselwirkungen mit ECM Molekülen.

Abstract

Human neural progenitor cells (hNPC) and human mesenchymal stromal cells (hMSC) have both been reported to be able to promote improved functional recovery after grafting into experimental spinal cord injuries. Transplantation of pre-differentiated neural progenitor cells has been shown to be an effective strategy to support repair of the spinal cord. In particular, the implantation of astrocyte restricted precursors may represent a means of promoting spinal cord recovery through the maintenance and support of axonal regeneration.

Although it has been demonstrated by our group that foetal hNPC, pre-differentiated to type I astrocyte restricted precursors (hNP-AC), promote more extensive axon regeneration by adult rat dorsal root ganglia (DRG) neurons *in vitro* than non-differentiated hNPC or hMSC, the mechanisms of action to support neuritic outgrowth remained unclear. Therefore, hNPC were characterised before and after *in vitro* differentiation to hNP-AC to provide a clearer definition of the changes that the cells had undergone. Furthermore, possible contributions of released trophic factors (i.e. present in conditioned culture medium) or substrate-mediated mechanisms via the extracellular matrix (ECM) of hMSC and hNP-AC to support neuritic outgrowth were investigated.

In the first part of this study, the *in vitro* immunocytochemical- and mRNA expression profile of selected marker gens in hNPC and in the differentiated hNP-AC was quantified. Furthermore, proliferative activity was estimated with a metabolic and a morphological assay, whereby the latter, by measuring the increase in volume over time, provided an indirect indicator of proliferation within intact neurospheres. The hNPC grew as neurospheres, which were immunoreactive for the stem/progenitor cell related markers nestin ($91.0 \pm 3.4\%$), SOX2 ($89.2 \pm 2.7\%$) as well as musashi ($91.8 \pm 2.0\%$) and expressed CD133- and nestin mRNA. They showed spontaneous differentiation capacity into MAP2ab+ and TuJ1+ neuronal phenotypes as well as S100β+ ($17.6 \pm 2.1\%$), GFAP+ ($23.7 \pm 2.3\%$) and vimentin+ ($96.8 \pm 1.1\%$) astroglial precursors. Whereas the differentiated hNP-AC demonstrated a similar immunocytochemical expression profile for the stem/ progenitor cell related markers nestin ($89.2 \pm 3.8\%$), SOX2 ($88.0 \pm 3.6\%$), musashi ($89.2 \pm 3.8\%$) and expressed CD133- and nestin mRNA in similar proportions to the hNPC, the expression of astroglial markers increased. A significantly higher proportion of hNP-AC were immunoreactive for S100β ($79.4 \pm 1.7\%$), GFAP ($92.5 \pm 3.4\%$) and CD44. Likewise,

hNP-AC demonstrated significantly increased CD44- and GFAP mRNA expression than the non-differentiated hNPC. Estimation of proliferative activity of hNPC and hNP-AC showed a reduced doubling time (DT) in hNP-AC with a value of 5.1 days (morphological assay) and 3.2 days (metabolic assay), contrasting to hNPC prior to *in vitro* differentiation with a DT of 3.46 days (morphological assay) and 1.68 days (metabolic assay).

In the second part of this study, the contributions of trophic factors present in cell-conditioned medium (produced by either hNP-AC or hMSC) and their ECM in supporting DRG axon regeneration were investigated *in vitro*. Conditioned media from both cell types strongly supported neurite outgrowth over a defined PLL/laminin substrate. The ECM produced by the two cell types, however, demonstrated contrasting effects: hNP-AC ECM promoted substantial axon regeneration, but hMSC ECM supported relatively little axon growth. The combined application of hNP-AC ECM and hMSC conditioned media induced the greatest degree of axon outgrowth. The combination of hMSC ECM and hNP-AC conditioned medium, however, did not result in any enhanced axon growth over the values determined using hMSC ECM and control growth medium. Thus, although hNP-AC conditioned medium demonstrated potent trophic support for DRG axon growth, its effect was not supported by signals derived from hMSC ECM. This raises interesting questions for future experiments regarding the cross-talk between the intracellular signalling cascades activated by diffusible trophic factors and those activated by ECM-related molecules.

Zusammenfassung

Humanen neuralen Vorläuferzellen (human neural progenitor cells, hNPC) und humanen mesenchymalen Stromazellen (human mesenchymal stromal cells, hMSC) wird die Fähigkeit zugeschrieben funktionelle Genesung nach Transplantation in experimentell herbeigeführter Querschnittslähmung im Tiermodell zu fördern. Die Transplantation von prä-differenzierten neuralen Vorläuferzellen hat sich als effektive Strategie zur Unterstützung der Wiederherstellung nach experimentell herbeigeführte Querschnittslähmung erwiesen. Insbesondere, die Implantation von astrozytären Vorläufern, könnte einen Weg zur Genesung von Querschnittslähmung mittels Aufrechterhaltung und Unterstützung der axonalen Regeneration darstellen.

Obwohl unsere Gruppe *in vitro* demonstrieren konnte, das fetale hNPC, die zu Typ I astrozytären Vorläufern (human neural progenitor restricted Typ I astrocytes, hNP-AC) differenziert wurden, größere axonale Regeneration in Nervenzellen aus adulten Ratten Dorsal-/Spinalganglien (dorsal root ganglia, DRG) begünstigten als undifferenzierte hNPC oder hMSC, blieben die dazu führenden Wirkmechanismen unklar. Daher wurden in der vorliegenden Arbeit die hNPC vor und nach *in vitro* Differenzierung zu hNP-AC charakterisiert, um den vollzogenen zellulären Wandel eindeutiger zu bestimmen. Weiterhin, wurden mögliche Beiträge durch freigesetzte trophische Faktoren (d.h. Faktoren, die in konditioniertem Kulturmedium anwesend sind) oder substrat-vermittelte Mechanismen, via Extrazellulär Matrix (ECM) von hMSC und hNP-AC untersucht.

Im ersten Teil dieser Untersuchung wurde das *in vitro* immunocytochemische- und das mRNA Expressionsprofil von ausgewählten Markergenen in hNPC und differenzierten hNP-AC quantifiziert. Weiterhin wurde die Proliferationsaktivität mit einer metabolischen und einer morphologischen Untersuchung beurteilt, die mittels Vermessung der Volumenzunahme pro Zeiteinheit einen indirekten Indikator der Proliferation in intakten Neurospheren darbot. Die hNPC entwickelten sich als Neurospheren, welche immunoreaktiv für die Stamm/Vorläuferzell verwandten Marker Nestin (91,0 $\pm$ 3,4%), SOX2 (89,2 $\pm$ 2,7%) sowie Musashi (89,2 $\pm$ 3,8%) waren und CD133- und Nestin mRNA exprimierten. Dabei wiesen die Zellen ein spontanes Differenzierungsvermögen in MAP2ab+ und TuJ1+ neuronale Phänotypen sowie S100β+ (17,6 $\pm$ 2,1%), GFAP+ (23,7 $\pm$ 2,3%) und Vimentin+ (96,8 $\pm$ 1,1%) astrogliale Vorläuferzellen auf. Während die differenzierten hNP-AC ein ähnliches immunocytochemisches Expressionsprofil

für die Stamm/Vorläuferzell verwandten Marker Nestin (89,2 ± 3,8%), SOX2 (88,0 ± 3,6%) sowie Musashi (89,2 ± 3,8%) wie die hNPC aufwiesen und CD133- und Nestin mRNA in ähnlichem Verhältnis exprimierten, konnte ein Anstieg der Expression von astroglialen Markern beobachtet werden. Dies zeigte sich durch einen signifikanten Anstieg der Immunoreaktivität für S100β (79,4 ± 1,7%), GFAP (92,5 ± 3,4%) und CD44 in hNP-AC. Ebenso wurde in den hNP-AC ein signifikanter Anstieg der CD44- und GFAP mRNA Expression gegenüber den nicht-differenzierten hNPC nachgewiesen. Eine Bestimmung der Proliferationsaktivität von hNPC und hNP-AC ergab eine reduzierte Verdopplungszeit (doubling time, *DT*) in hNP-AC mit einem Wert von 5,1 Tagen (morphologische Untersuchung) und 3,2 Tagen (metabolische Untersuchung), im Gegensatz zu den hNPC vor der *in vitro* Differenzierung mit einer Verdopplungszeit von 3,5 Tagen (morphologische Untersuchung) und 1,7 Tagen (metabolische Untersuchung).

Im zweiten Teil dieser Arbeit wurden *in vitro* die Beiträge von trophischen Faktoren der hNP-AC bzw. der hMSC, welche in das Zellkulturmedium abgegeben wurden, sowie deren ECM im Hinblick auf die Unterstützung der axonalen Regeneration von DRG untersucht. Das konditionierte Medium beider Zelltypen induzierte einen weitreichenden, komplexen Neuritenauswuchs der DRG, wenn diese auf ein definiertes PLL/laminin Kontrollsubstrat platziert wurden. Allerdings zeigte die ECM der beiden untersuchten Zelltypen einen entgegengesetzten Effekt: Die hNP-AC ECM begünstigte eine beträchtliche axonale Regeneration, wohingegen die hMSC ECM einen signifikant geringeren axonalen Auswuchs induzierte. Die kombinierte Anwendung von hNP-AC ECM und konditionierten hMSC Medium induzierte das größte beobachtete Neuritenwachstum. Die Kombination von hMSC ECM und konditionierten hNP-AC Medium zeigte jedoch kein vergrößertes axonales Wachstum im Vergleich zu den Werten, die mit hMSC ECM und Kontrollkulturmedium erzielt wurden. Obwohl das konditionierte hNP-AC Medium mit seinen potenten trophischen Faktoren das axonale Wachstum von DRG förderte, war dieser Effekt nicht durch hMSC ECM bedingte Signale unterstützt. Hieraus resultieren interessante Fragestellungen für zukünftige Experimente zur genaueren Erforschung der Interaktion zwischen intrazellulären Signalkaskaden entweder aktiviert durch diffusionsfähige trophische Faktoren oder durch Wechselwirkungen mit ECM Molekülen.

Contents

II Effects of Released Factors and ECM on Neurite Regeneration *in Vitro* 77

III Final Remarks 107

IV Appendix

111

Nomenclature

ΔV . . . . Difference in Volume V_1 and V_2

$\overline{V}$ . . . . Mean value of volume

D . . . . Diameter

DT . . . . Doubling time

N . . . . Number

N_H . . . . Number at t_{end}

N_I . . . . Number at t_0

r . . . . Multiplication rate

V . . . . Volume

a.d. . . . . aqua distilled

a.p. . . . . anterior-posterior

ABD . . . . Antibody dilution

ANOVA . . . . multifactorial analysis of variance

BBB . . . . Blood-brain barrier

BDNF . . . . Brain-derived neurotrophic factor

bFGF, FGF2 . . . . . basic Fibroblast growth factor 2

BMP-4 . . . . Bone morphogenetic protein 4

bp . . . . Base pair

BSA . . . . Bovine Serum Albumine

CD133 . . . . Prominin-1

CD44 . . . . Hermes antigen, H-CAM

cDNA . . . . Complementary desoxyribonucleic acid

CGRP . . . . Calcitonin gene related peptide

CNS . . . . Central nervous system

CSPG . . . . Chondroitin sulphate proteoglycans

d . . . . day

DAPI Diamidino-2-phenylindol

DMEM . . . . Dulbecco's Modified Eagle's Medium

DMSO . . . . Dimethyl sulfoxide

dNTP . . . . Deoxyribonucleotide triphosphate

NG2 . . . . Neuron-glial antigen 2

NGF . . . . Nerve growth factor

NPDM . . . . Neural progenitor differentiation media

NPPM . . . . Neural progenitor proliferation media

NT-3 . . . . Neurotrophin-3

OEC . . . . olfactory ensheathing cells

OMgp . . . . Oligodendrocyte myelin glykoprotein

PBS . . . . Phosphate Buffered Saline

PCR . . . . Polymerase chain reaction

PDGF . . . . Plateled derived growth factor

PDGF-BB . . . . Plateled derived growth factor BB

PFA . . . . Paraformaldehyde

PLL . . . . Poly-L-lysine

PNS . . . . Peripheral nervous system

PSA-NCAM . . . . Poly-sialated neural nell adhesion molecule

Px . . . . Culture passage number x

PxPy . . . . Culture Passage numbers with Px in NPPM, Py in NPDM

r . . . . number of PCR cycles

rpm . . . . Revolution per minute

RT-PCR . . . . Reverse transcriptase polymerase chain reaction

RV . . . . Reverse

SCF . . . . Stem cell factor

SDF-1 . . . . Stromal cell-derived factor 1

sec . . . . Seconds

SEM . . . . Standard error of the mean

SOX2 . . . . Sox2

SRY . . . . Sex-determining region Y

t . . . . time

T^A . . . . Annealing temperature

T3 . . . . Tri-iodothyronine hormone

TAE . . . . Tris-acetate-EDTA

TGFβ . . . . Transforming growth factor β

TuJ1 . . . . Tubulinβ, isotype III

VEGF . . . . Vascular endothelial growth factor

List of Figures

List of Tables

1 Introduction

1.1 Central Nervous System Injury

The inability of the central nervous system (CNS) to regenerate after injury has been one of the most challenging neuroscientific themes for decades. While lesioned axons in the peripheral nervous system (PNS) may undergo successful regeneration leading to the reinnervation of their targets (Guth, 1956; Hall, 1989; Stoll et al., 2002), damaged axons in the CNS regenerate less well, if at all (Cajal, 1928; Clemente, 1964; Franklin and Blakemore, 1990).

The earliest documentation of many of the key symptoms of individuals suffering paralysis due to spinal cord injury (SCI) is provided in the ancient Egyptian Edwin Smith papyrus from 1650-1550 B.C. (Breasted, 1930; Hughes, 1988). It has been suggested that the author was Imhotep (Anderberg et al., 2007; Donovan, 2007), whose advice that the condition was untreatable was followed down through the ensuing millennia. The lack of axonal regeneration in the adult mammalian CNS was accepted as "law of nature". Thus, brain and spinal cord lesions were considered irreversible.

In the early 20th century, Santiago Ramon y Cajal was the first to describe that damaged CNS axons are able to form sprouts, but that they did not extend for more than 1-2mm (Cajal, 1928). Since then, numerous scientific and medical studies have challenged the previous dogma of the irreversibility of CNS injury and dedicated their interest to better understand the cellular and molecular basis for abortive sprouting in the damaged CNS, the ultimate goal being the manipulation of these mechanisms to allow functional tissue repair following injury or disease.

The most important contributions have been published over the last 20-30 years. It has become evident that the CNS does, indeed, have the capacity to regenerate. However, this capacity is only transient and fails within a few days due to the development of a reactive growth inhibitory microenvironment around the axonal sprouts (Schwab and Bartholdi, 1996; Dumont et al., 2002). The discovery of many pathophysiological events that take place after SCI has resulted in the development of numerous highly innovative intervention strategies that were intended to enhance functional recovery after CNS injury. Nevertheless, there is still a paucity of clinically effective strategies for the treatment of severe CNS trauma such as SCI. Some of the major pathophysiological events following SCI and a number of corresponding treatment strategies will be highlighted in the following section.

1.2 Mechanisms Influencing Axon Regeneration in the CNS

Whereas the developing mammalian nervous system is endowed with a large capacity of plasticity, including the ability to regenerate, the potential for such adaptive behaviour decreases with increasing age, particularly in the adult CNS (Singer et al., 1979; Shewan et al., 1995; Bandtlow and Löschinger, 1997; Martin et al., 2000).

There are three main impediments to axon regeneration and functional recovery following CNS injury: namely the expression of potent axon growth inhibitory myelin associated proteins, the formation of a glial scar by reactive astrocytes and cell death (Beattie et al., 2000; Jones et al., 2001; Liu et al., 2006). The detrimental effects of these three processes are compounded by the formation of fluid filled cysts or cavities at the lesion epicentre.

1.2.1 Inhibition of Axonal Regeneration by Myelin Associated Proteins

Oligodendrocytes and degenerating myelin were discovered to be potent inhibitors of axon regeneration in the late 1980's (Schwab and Thoenen, 1985; Savio and Schwab, 1990). Much of the inhibitory effect of CNS myelin could be found in a protein fraction termed NI-220/250. The development and application of the antibody, IN-1, which blocked the activity of NI-220/250, resulted in a boosting of the extent of axonal growth over oligodendrocytes or CNS myelin *in vitro* (Caroni and Schwab, 1988; Caroni et al., 1988) and *in vivo* (Schnell and Schwab, 1990; Schwab, 2002). A decade later, the NI-220/250 antigen (named Nogo) was cloned independently by three groups (Chen et al., 2000b; GrandPré et al., 2000; Prinjha et al., 2000), with the isoform Nogo-A being identified as a major inhibitor to CNS regeneration (Pot et al., 2002).

Furthermore, other myelin associated proteins have been demonstrated to have potent axon growth inhibitory effects, i.e. myelin-associated glycoprotein (MAG) and oligodendrocyte myelin glycoprotein (OMgp; McKerracher et al., 1994; Mukhopadhyay et al., 1994; Wang et al., 2002). However, it seems that MAG plays no significant role in the inhibition of CNS axons *in vivo* (Bartsch et al., 1995; Li et al., 1996) and is lost or degraded very early after SCI (Buss and Schwab, 2003).

These discoveries and the identification of the receptors responsible for mediating the inhibitory effects of the myelin associated molecules have been the subject of numerous *in vitro* and *in vivo* studies (McGee and Strittmatter, 2003; Xie and Zheng, 2008).

1.2.2 The Astroglial Scar

Astrocytes are the key component of reactive gliosis (Eng et al., 1987) leading to the development of a scar tissue, similar to the process observed in other organs following injury as a protective and thereby beneficial reaction of the organism. However, the formation of an astroglial scar represents a major mechanical and molecular barrier to axonal regeneration (Hatten et al., 1991; Freire et al., 2004; Yiu and He, 2006). In lesions that spare the dura mater, the scar is composed primarily of astrocytes, but in more severe lesions, which open or rupture the meninges, invading connective tissue elements and Schwann cells mix with the reactive astrocytes (Shuman et al., 1997; Pérez-Bouza et al., 1998; Brook et al., 2000; Silver and Miller, 2004).

A prominent hallmark of reactive gliosis is hypertrophy of the astrocytic cell body and processes with increased production of intermediate filaments, such as glial fibrillary acidic protein (GFAP; Barrett et al., 1981; Eng, 1985), renewed expression of vimentin (Dahl et al., 1981a,b; Lin and Cai, 2004; Wilhelmsson et al., 2004) and nestin (Clarke et al., 1994; Frisén et al., 1995; Brook et al., 1999).

In the early 1990s, reactive astrocytosis was shown to be associated with the expression of axon-repulsive extracellular matrix (ECM) molecules such as tenascin and four classes of proteoglycans (Snow et al., 1990; Katoh-Semba et al., 1995; McKeon et al., 1999; Jones et al., 2003a; Tang et al., 2003) including the large family of chondroitin sulphate proteoglycans (CSPG) with aggrecan, brevican, neurocan, neuronglial antigen 2 (NG2), phosphocan and versican (Grimpe and Silver, 2002; Morgenstern et al., 2002). This led to the suggestion that certain ECM molecules in the area of the lesion site played a major role in the failure of CNS axon regeneration.

Nevertheless, axon growth-supportive molecules are also expressed by reactive astrocytes, for example the ECM molecules laminin and fibronectin as well as poly-sialated neural cell adhesion molecule (PSA-NCAM; Snow et al., 1996; Ridet et al., 1997; Silver and Miller, 2004; Gris et al., 2007; Tate et al., 2007). The interactions of these and other axon growth repulsive and growth promoting molecules results in an environment which provides either an overall support or inhibition of axon growth (Dou and Levine, 1995; Snow et al., 1996; Hynds and Snow, 2001).

Inflammatory cytokines such as interferon γ (IFNγ) and basic fibroblast growth factor (FGF-2, bFGF) seem to contribute to the development of the glial scar (Yong et al., 1991; Mocchetti et al., 1996). Furthermore, trophic factors such as the transforming growth factor β (TGFβ) have been reported to be potential trigger molecules for inhibitory gliosis inducing an up-regulation of the proteoglycan expression in astrocytes (Asher et al., 2000; Moon and Fawcett,

2001). The elevated levels of TGFβ-1 expression immediately after injury suggest a role in the acute inflammatory response and initiation of glial scar formation, whereas the later peak of TGFβ-2 expression may be associated with subsequent tissue repair processes (Lagord et al., 2002; Buss et al., 2008).

1.3 Cell-Transplantation Strategies to Enhance CNS Repair

The generation of an axon-growth promoting environment that is capable of bridging the cystic cavities and the developing scar tissue of the lesioned CNS has been extensively studied during the last three decades. Numerous strategies have been developed to promote CNS repair following SCI, which particularly focus on the transplantation of a variety of cell types, often in combination with other strategies: Cell-based repair strategies for promoting axon regeneration across spinal cord lesions have included grafting of CNS- or PNS glia into the lesion site. Transplantation of Schwann cells and/or olfactory ensheathing cells (OEC) provided promising results (Ramón-Cueto and Nieto-Sampedro, 1994; Ramón-Cueto et al., 1998, 2000; Sasaki et al., 2007; Oudega, 2007; Bunge, 2008).

Furthermore the combination of cell transplantation strategies with the delivery of neurotrophic factors (Jones et al., 2001; Bregman et al., 2002; Bunge, 2008) as treatment to override or degrade the glial scar, as well as the combination with structurally engineered biomaterials bridging the lesion for regenerating axons (Willerth and Sakiyama-Elbert, 2007) has promoted functional improvement in experimental CNS injury models.

More recently, the potential of stem/progenitor cell based strategies has become apparent. Numerous groups describe the benefits of stem/progenitor-cell based intervention strategies in promoting functional tissue repair following either CNS- or PNS injury (Enzmann et al., 2005; Someya et al., 2008; Eftekharpour et al., 2008; Bareyre, 2008; Willerth and Sakiyama-Elbert, 2008).

In this study main emphasis was laid on investigating the potential benefits of employing non-neural human mesenchymal stromal cells as well as astrocytic precursors derived from human foetal neural progenitor cells.

1.3.1 Human Mesenchymal Stromal Cells

Human mesenchymal stromal cells (hMSC) are non-neural cells isolated from bone marrow, adipose or other tissues. These cells are able to adhere to plastic culture plates and display a multi-potent differentiation capacity to osteoblasts, chondroblasts, adipocytes and myoblasts *in*

vitro (Prockop, 1997).

Ten years ago, Azizi and colleagues reported the survival and migration of hMSC that had been implanted in rat brains (Azizi et al., 1998). Since then, several groups have reported significant functional improvement after grafting these cells into animal models of SCI (Wu et al., 2003; Ohta et al., 2004; Li et al., 2005; Neuhuber et al., 2005; Himes et al., 2006).

However, the mechanism(s) of action by which grafted hMSC promote their beneficial effects in experimental SCI is still poorly understood and remains controversial. There is no consensus of opinion as to whether the reported transdifferentiation hMSC to neural cells contributes to recovery (Chen et al., 2000a; Hofstetter et al., 2002; Li et al., 2005; Montzka et al., 2009; Vaquero and Zurita, 2009).

Instead of serving as a cell replacement therapy, it is more likely that transplanted MSC affect SCI repair by the following mechanisms: hMSC can act as "feeder cells" supporting adjacent neurons and glia by the production of cytokines, growth- and neurotrophic factors including brain-derived neurotrophic factor (BDNF), vascular endothelial growth factor (VEGF), nerve growth factor (NGF), neurotrophin-3 (NT-3), interleukin 6 (IL-6), monocyte chemoattractant protein (MCP), stem cell factor (SCF) and stromal cell-derived factor 1 (SDF-1) (Cheng et al., 2003; Wu et al., 2003; Neuhuber et al., 2005; Shimode et al., 2007; Wagner et al., 2008).

Furthermore, it has been shown that MSC can provide an extensive ECM *in vitro*, consisting of collagen I, collagen IV, fibronectin and laminin (Grayson et al., 2004), that might represent a favourable substrate for axonal growth and contribute to the proliferation of endogenous CNS progenitor cells (Deans and Moseley, 2000; Neuhuber et al., 2005; Parr et al., 2007).

For a better understanding of the potential beneficial effects of hMSC in repair strategies for SCI, we have studied their direct effects on axon regeneration *in vitro* (Führmann et al., 2010b). Dissociated adult rat dorsal root ganglia (DRG) were plated onto semi-confluent hMSC monolayers and the extent of axon growth over a period of 24h was investigated. The study revealed substantial cell-substrate interactions between the regenerating DRG axons and the underlying hMSC monolayer. Viable hMSC were responsible for imparting a significant degree of directionality of axonal regrowth. Although the investigation confirmed the beneficial effect of hMSC on neurite regeneration, the mechanism of this effect still remained unclear.

1.3.2 Human Neural Progenitor Cells

Human neural progenitor cells (hNPC), are proliferative cells from CNS tissue with restricted self-renewal. Unlike stem cells, their ability to asymmetrically divide and to produce progeny indistinguishable from themselves is limited (Svendsen et al., 1999; Seaberg and van der Kooy, 2003; Sohur et al., 2006). A cardinal feature of hNPC is their multi-potency, being able to

differentiate into the three lineages of the CNS (i.e. oligodendroglial, astroglial and neuronal; McKay, 1997; Gage, 2000; Sohur et al., 2006).

Because of the current lack of markers to clearly distinguish CNS stem cells from progenitor cells (Uchida et al., 2000; Steindler and Laywell, 2003) the cells are usually characterised retrospectively on the basis of their behaviour after isolation *in vitro* (Carpenter et al., 1999; Weible and Chan-Ling, 2007). However, prospective attempts to characterise neural stem- and progenitor cells have been attempted (Maric and Barker, 2004).

The hNPC may be obtained from embryonic (Thomson et al., 1998; Klimanskaya et al., 2006) and foetal tissues (Svendsen et al., 1999; Uchida et al., 2000), as well as neurogenic regions in the adult CNS where hNPC continue to reside (Goldman, 2005; Sohur et al., 2006). Even *post mortem* CNS tissue has been suggested to be a source for hNPC (Schwartz et al., 2003).

Since the developing brain exhibits a high degree of plasticity, and can undergo regenerative axonal regrowth (Nicholls and Saunders, 1996; Kalia, 2008) special attention has been laid on the reparative potential effectiveness of neural stem/progenitor cells from embryonic (Wictorin and Björklund, 1992; McDonald et al., 1999; Davies et al., 2006) and foetal sources (Ogawa et al., 2002; Tarasenko et al., 2007; Ogawa et al., 2009) for therapeutical approaches in SCI.

For effective transplantation studies, large volumes of cells are essential (Björklund, 1993; Svendsen et al., 1999; Kanemura et al., 2002). However, ethical concerns surrounding the use of embryo- or foetus-derived cells, as well as the limited supply of donor tissues have strengthened the need and search for alternative sources of large numbers of donor cells.

Another important consideration in the use of hNPC for future clinical purposes is the clear establishment of the parameters for culturing the cells, for example how long or for how many passages can such cells be maintained in culture without loosing proliferative and differentiation characteristics (Kanemura et al., 2002; Wachs et al., 2003; Herszfeld et al., 2006; Zeng, 2007). Stem/progenitor cells isolated from embryonic tissues have been reported to possess properties that are similar to those of cancer cells, such as genetic instability (Ignatova et al., 2002; Herszfeld et al., 2006) and lack of senescence (Tsai and McKay, 2002; Zeng, 2007), leading to the transformation and tumorigenesis of the donor cells following grafting into the host Zheng et al. (2002). The use of hNPC isolated from foetal tissues attenuates the risk of oncogenic transformation, especially when they have undergone differentiation prior to transplantation (Keirstead et al., 2005).

Foetal hNPC have been transplanted into mice (Cummings et al., 2005; Ogawa et al., 2009), rat (Wu et al., 2002; Watanabe et al., 2004; Liang et al., 2006; Tarasenko et al., 2007) and monkey (Iwanami et al., 2005) SCI models. Spontaneous differentiation of donor foetal hNPC to glial and neuronal phenotypes after transplantation has been reported (Snyder et al., 1997; Watanabe et al., 2004; Liang et al., 2006; Tarasenko et al., 2007; Ogawa et al., 2009) and these have been

described to contribute to tissue repair at the lesion site. However, the majority of donor hNPC often fail to spontaneously differentiate into the desired cell types or differentiate at all, when grafted into non-neurogenic areas of the adult CNS (Nicholls and Saunders, 1996; Schultz, 2005; Davies et al., 2006). To overcome this impediment, epigenetic modulation of hNPC prior to transplantation has become popular. The transplantation of oligodendroglia, derived from differentiated hNPC has been shown to promote remyelination and improvement in locomotor function after SCI (Keirstead et al., 2005; Nistor et al., 2005; Faulkner and Keirstead, 2005). Following a similiar logic, the transplantation of astrocytes derived from foetal hNPC might represent an attractive cell type to support SCI repair.

1.3.3 Differentiation of Foetal hNPC to Astrocyte Restricted Precursors

At first glance, the beneficial effects of implanting astrocytes into the lesioned CNS might seem counter-intuitive, since reactive astrocytes represent the major component of the axon growth inhibitory glial scar (see section 1.2.2). However, the developmental stage of astroglia influences their ability to form scar tissue and the balance of their axon growth-inhibiting versus growth-promoting properties (Barrett et al., 1984; Silver and Miller, 2004). Their re-expression of developmental markers is suggestive of a phenotypic shift to a morphology that is supportive to regeneration. Indeed, cocultures of neurons and vimentin+/nestin+/GFAP+-astrocytes exhibit increased axonal growth, suggesting that this phenotype is one that encourages regeneration (Menet et al., 2000).

The first indications of the beneficial effects of immature astroglia in CNS injury were reported in the 1980s; astrocytes from the developing brain were suggested to be an ideal substrate for neuron regeneration *in vitro* (Noble et al., 1984; Fallon, 1985a,b; Tomaselli et al., 1986, 1988; Fawcett et al., 1989) and *in vivo* (Silver and Ogawa, 1983; Smith et al., 1986, 1990; Silver, 1988). Since then, numerous studies have suggested that young or immature astrocytes may provide a favourable substrate for axon regeneration following SCI (Fawcett et al., 1992; Biran et al., 2003; Tom et al., 2004; Davies et al., 2006).

In order to generate immature astrocytes for the repair of experimental CNS injuries, a technique for the rapid generation of a large, homogenous population of astrocytic cells has been developed: *in vitro* epigenetical differentiation of hNPC to human neural progenitor derived type I astrocyte restricted precursors (hNP-AC) by supplementing tissue culture medium with bone morphogenetic protein 4 (BMP4; Gross et al., 1996; Mehler et al., 1997, 2000; Zhang and Li, 2005) and leukemia inhibitory factor (LIF; Bonaguidi et al., 2005; Nakashima et al., 1999) encourages the generation of astrocyte restricted progenitors (Weible and Chan-Ling, 2007). Rat embryonic neural precursors have been used to generate astrocyte restricted precursors for

transplantation into experimental SCI and have promoted locomotor recovery, axon regrowth and the suppression of scar formation, in contrast to transplanted undifferentiated precursors (Davies et al., 2006). However, differentiation and grafting of type II astrocytes was reported to induce allodynia (Hofstetter et al., 2005). This observation was supported by Davies and colleagues who compared the effects of implanting type I and type II astrocytes into experimental SCI; type I astrocytes encouraged robust axon regeneration whereas type II astrocytes increased allodynia-like symptoms (Davies et al., 2008).

Recent studies performed in our research group have demonstrated that monolayers of foetal hNP-AC support significantly stronger DRG neurite outgrowth than non-differentiated hNPC or hMSC *in vitro* (Führmann et al., 2010a,b). It might be possible that the neural progenitor cell derived type I astrocytes secreted benefical substances into the culture media thereby supporting outgrowth of regenerating DRG neurites: it has been reported that astrocytes produce neurotrophic factors, such as BDNF (Ikeda et al., 2001), ciliary neurotrophic factor (CNTF; Lee et al., 1998), NGF (Krenz and Weaver, 2000), FGF-2 (do Carmo Cunha et al., 2007) and the neurogenic factors Neurogenesin-1 and Neuregulin 1 (Liberto et al., 2004; Ueki et al., 2003; Barkho et al., 2006).

In addition to diffusible factors, ECM-associated mechanisms contribute importantly to control axon growth in CNS development and after injury (Zhou and Snider, 2006). Although reactive astrocytes produce CSPGs, molecules that are inhibitory to neurite growth (see section 1.2.2), they also produce ECM molecules that are supportive to axon growth: especially, the ECM substrate generated by immature astrocytes has been reported to regulate cell adhesion, migration, morphogenesis as well as supporting neurite outgrowth (Powell et al., 1997; Pindzola et al., 1993; Kiryushko et al., 2004; Freire et al., 2004) via the presence of neural cell adhesion molecules (NCAM; Noble et al., 1985; Smith et al., 1993) with N-Cadherin (Tomaselli et al., 1988), laminin (Liesi et al., 1984; Liesi and Silver, 1988; Smith et al., 1993; Freire et al., 2004) and fibronectin (Tom et al., 2004). Several studies clearly demonstrated that *in vitro* derived astrocytes presented associated laminin matrices enabling neurite regeneration (Garcia-Abreu et al., 1995; Martinez and Gomes, 2002).

Finally, increasing evidence is emerging that theses influences contribute to enhance neurite regeneration and outgrowth via an intra- and intercellular cross-talk, that is coordinated by interactions of diffusible secreted factors and ECM-mediated mechanisms (Zhou and Snider, 2006).

1.4 Objectives of the Study

Although neural and non-neural stem/progenitor cell transplantation strategies have shown promising results as a therapeutical approach for SCI, the mechanisms of action remain poorly defined (Okano et al., 2003; Iwanami et al., 2005; Enzmann et al., 2005; Garbuzova-Davis et al., 2006; Oudega, 2007; Eftekharpour et al., 2008; Kitada and Dezawa, 2008).

In an attempt to better understand the beneficial interactions of stem/progenitor cells with regenerating neurites our group has studied the axon growth promoting effects of hMSC-, hNPC and hNP-AC monolayers *in vitro* with dissociated DRG neurons as model of repair after CNS injury (Führmann et al., 2010a,b). We could show that hNP-AC promoted stronger outgrowth than either non-differentiated hNPC or hMSC. Furthermore, hMSC were able to direct neurite regeneration.

1.4.1 Part I

Characterisation and Proliferative Activity of hNPC and hNP-AC

The following questions were addressed:

> I) To what extent has the *in vitro* differentiation process of hNPC altered the cellular characteristics in hNP-AC?

> II) Does the differentiation of hNPC to hNP-AC alter their proliferative activity?

Cell therapy strategies with hNP-AC in SCI would require substantial numbers of homogeneous, well defined populations of cells. Therefore, it was of interest to characterise the cell population of hNPC before and after differentiation *in vitro* and to investigate their proliferative activity.

For this purpose, immunocytochemistry and reverse transcription polymerase chain reaction (RT-PCR) were used to identify changes in the expression of stem/progenitor- and astrocyte-related markers. A metabolic and a morphological assay were used to assess proliferation.

1.4.2 Part II

Effects of Released Factors and ECM on Neurite Regeneration *in Vitro*

The mechanisms by which hMSC and hNP-AC supported neurite regeneration remained unclear. Therefore, the possible contributions of released trophic factors (i.e. present in conditioned medium) or substrate-mediated mechanisms (via the ECM) were investigated. The following hypotheses were tested and will be addressed in Part II of this thesis:

> I) Both, diffusible trophic factors (i.e. present in conditioned medium) and ECM-related mechanisms contribute to hNP-AC- and hMSC-mediated support of axonal regeneration.

> II) To what extent can the neuronal responses to diffusible trophic factors (i.e. present in conditioned medium) be modified by interactions with its environment (i.e. the ECM)? Similarly, to what extent are the responses of the cell to its ECM environment modified by the presence of diffusible trophic factors?

Morphological studies were used to determine to what extent cellular components (i.e conditioned medium and ECM) of hMSC or hNP-AC might influence neurite regeneration. A combinatory application of cellular components of hMSC and hNP-AC was used to investigate their interactions and possible effects on regenerating neurites.

It is anticipated that such information may contribute to the optimisation of future *in vivo* intervention strategies intended to promote functional repair following traumatic injury to the CNS. The study was performed with adult rat DRG neurons as an *in vitro* model for axon regeneration. Varying parameters were the ECM substrate deposited by either hMSC or hNP-AC and their trophic factors, which had been released into the applied culture media before.

1.4.3 Main Findings

In Part I of this thesis it will be shown that the hNPC represent a multipotent and heterogenous population of neural progenitor cells possessing the capacity to spontaneously differentiate into neuronal or astroglial phenotypes. Differentiated hNP-AC demonstrated a significant up-regulation of typical astroglial markers, whereas the expression of stem/progenitor-related markers remained constant. However, the rate of proliferation of hNP-AC was reduced when compared to that of non-differentiated hNPC.

12

In Part II of this thesis it will be shown that the ECM of hNP-AC strongly promoted neurite out-growth *in vitro*, whereas the ECM of hMSC promoted less robust outgrowth. Produced trophic factors released into the culture media from both stem/progenitor cell types strongly supported the outgrowth in regenerating neurites. The combination of hNP-AC derived ECM with hMSC derived trophic factors interacted in a benefical manner, thereby potentiating neurite outgrowth promotion in regenerating DRG.

Part I

In Vitro Characterisation and Proliferative Activity of hNPC and hNP-AC

2 Material and Methods

2.1 Cell Culture

2.1.1 Cultivation of hNPC Neurospheres

The hNPC used in this study were derived from 16-week human foetal forebrain and propagated by using the neurosphere technique. Neurospheres of human neural stem/progenitor cells are aggregates of more than a thousand individual cells and contain heterogeneous populations of neuronal, astroglial and oligodendroglial precursor cells (Reynolds and Weiss, 1996; Svendsen et al., 1999). The hNPC were purchased from Lonza (formerly Cambrex Bioscience, Belgium) and used according to all state and federal guidelines.

The neurospheres were cultivated in a humidified chamber at 37°C with 5% CO_2. To grow hNPC as monolayers or as adherent neurospheres, tissue culture plastic was treated with sterile poly-L-lysine (PLL, 0.01%, Sigma) for one hour, followed by two washing steps with 0.1M phosphate buffered saline (PBS) and the addition of the purified ECM molecule laminin (5μg/ml, Roche) in 0.1M PBS overnight. The next day the PLL/laminin surface was rinsed with medium (see below) and seeded with dissociated hNPC to form monolayers or with neurospheres.

Neurospheres were grown in suspension culture for up to 6-8 months using serum-free neural progenitor proliferation media (NPPM; Reynolds and Weiss, 1992, 1996; Svendsen et al., 1998, 1999). The medium contained:

Ham's F-12 nutrient mixture + GlutaMAX^{TM} (HAM F12, Invitrogen)
Dulbecco's Modified Eagle's Medium + GlutaMAX^{TM} + 4.5g/liter D-Glucose and Pyruvate (DMEM, Invitrogen)

with a concentration of HAM F12/DMEM (1:1 vol/vol)

Human recombinant epidermal growth factor (EGF, 20ng/ml, Cell Concepts)
Human recombinant basic fibroblast growth factor (bFGF/ FGF-2, 20ng/ml, Invitrogen)
B27 supplement (1:50 vol/vol, Invitrogen) without retinoid acid
Penicillin/streptomycin (1:100 vol/vol, PAA)

All components were sterile filtered (Millipore Stericap Plus, 0.22μm) and media was stored at 2-8°C. Before application to spheres, media was warmed to room temperature. Neurospheres were kept in T75 flasks (Greiner, Cellstar) and half of the medium was changed every other day.

2.1.2 Passaging of Neurospheres

Neurospheres were passaged every 7-10 days by incubation with Accutase (PAA, Innovative Cell Technologies Inc.) as described earlier (Wachs et al., 2003). Briefly, culture medium containing floating neurospheres was collected in a 15ml Falcon tube and centrifuged at 800 revolutions per minute (rpm) for 5 minutes. The cell pellet was resuspended in 200μl Accutase (ready to use solution), triturated with a 200μl pipette 10-15 times and incubated for 10 minutes at 37°C. Dissociated spheres were again triturated with a 200μl pipette 20-30 times to remove persisting cell bridges. Single cells were resuspended in NPPM and plated in T75 cell culture flasks with 10ml of fresh culture medium. The resultant single cell suspension formed new spheres within 1-3 days and were named passage 1 (P1), passage 2 (P2),... with increasing passage number after each Accutase treatment. Cells, that did not form new spheres after dissociation or became adherent in higher passages, were removed from culture.

2.1.3 hNP-AC Differentiation

At P4-P8 NPPM was changed to neural progenitor differentiation media (NPDM) to generate hNP-AC as described earlier (Weible and Chan-Ling, 2007). NPDM consisted of:

Neural basal media 1x (Invitrogen) mixed with

GlutaMAX^{TM} 0.5mM (1:100 vol:vol, Invitrogen)
B27 Supplement (1:50 vol:vol, Invitrogen) without retinoid acid
Human recombinant EGF (20ng/ml, Invitrogen)
Human recombinant bFGF (20ng/ml, Invitrogen)
Leukemia inhibitory factor (LIF, 10ng/ml, Chemicon)
Bone morphogenetic protein 4 (BMP4, 20ng/ml, R&D Systems)
Penicillin/streptomycin (1:100 vol/vol, PAA)

Cells were seeded at a densitiy of $2.5 \cdot 10^4$cells/ml in T75 flasks and initially half of the media was changed. The following day, media was changed completely to NPDM.

Half of the medium was replenished every other day. After 1-2 weeks neurospheres were passaged with Accutase and named PxP1, ..., PxP14 with increasing passage number after each Accutase treatment. The first passage number (x) shows for how long the cells were kept in an undifferentiated state with NPPM treatment before the differentiation treatment was started. The second passage number represents the differentiation phase with NPDM treatment to generate hNP-AC.

2.1.4 Cryopreservation and Retrieval from Frozen Storage

For cryopreservation, neurospheres or single cell suspensions of hNPC or hNP-AC were treated with the cryoprotective agent dimethyl sulfoxide (DMSO). Cryomedium consisting of 80% medium, 10% foetal calf serum (FCS; PAA) and 10% DMSO (Sigma Aldrich) was sterile filtered. Cryotubes (Nunc, Apogent) were loaded with 1.5ml cryomedium containing single cell suspensions of approximately $4 \cdot 10^6$ cells and cooled down slowly at 1°C/min to -80°C being placed in a freezing box (Roth) containing isopropyl alcohol. After 4-5 hours, the cryotubes were transferred to liquid nitrogen for long term storage.

To retrieve cells from frozen storage, cryotubes were immersed in a warm water bath (37-40°C) for 3 minutes to transfer cells in a semi-thawed state. After centrifugation to remove DMSO, cells were transferred rapidly to fresh culture medium and grown in PLL/laminin coated cell culture flasks as monolayers. When grown to confluence after 1-2 weeks, cells were dissociated using 2-3ml of Accutase (see section 2.1.2), transferred to non-coated cell culture flasks and cultured as floating neurospheres by spontaneous aggregation. Cells that returned to the substrate and grew as adherent cultures were excluded from the investigation.

2.2 Immunocytochemistry

2.2.1 Slide Preparation

Immunocytochemistry was performed on:

I) cryosections of intact neurospheres,

II) intact neurospheres adherent on PLL/laminin coated coverslips and

III) single cells from dissociated neurospheres adherent on PLL/laminin coated coverslips.

Free floating neurospheres as well as coverslips with adherent neurospheres or single cells were fixed for 1 hour in 4% paraformaldehyde (PFA) and washed three times in 0.1M PBS. To reduce cryoartefacts, non-adherent intact neurospheres were transferred to a 30% sucrose solution in 0.1M PBS for 72 hours at 4°C. Spheres were embedded in Tissue-Tec, frozen, cryosectioned (with 8μm thickness of slices) at -22°C and collected on objective slides (Superfrost Plus Gold, Menzel). Sections were either immediately processed for immunocytochemistry or were stored at -80°C for later use.

2.2.2 Double Immunofluorescence

All antibodies were diluted in antibody diluent consisting of 0.1M PBS containing 1% bovine serum albumin V (BSA, Serva). Sections were treated with antibody dilution (ABD) containing 1% Triton-X 100 and 3% normal goat serum followed by primary antibodies (see Table 2.1) overnight at room temperature in a humid atmosphere. The next day, sections were washed 3 times in 0.1M PBS followed by incubation in secondary antibodies (dilution 1:500; see Table 2.1) conjugated to either Alexa 594 (Molecular Probes) or Alexa 488 (Molecular Probes) for 2.5 hours in the dark. A nuclear counterstain with diamidino-2-phenylindol (DAPI, 1μg/ml stock solution, Molecular Probes) was added to the secondary antibody solution (dilution 1:1000). Primary antibodies were omitted for the negative control slides. After 3 washing steps in PBS the samples were coverslipped using Fluoroprep® (BioMerieux, Nurtingen, Germany). Probes were stored in the dark at 4°C before viewing with an inverted epi-fluorescence microscope (Leica, DMI 4000B).

2.2.3 Image Analysis of Immunofluorescence

Immunocytochemical analysis of hNPC was assessed on different passage numbers in culture (P2, P3, P6, P7, P11). Immunocytochemical analysis of hNP-AC was performed, after differentiation for at least 8 passages in NPDM according to Weible and colleagues (Weible and

Chan-Ling, 2007). Immunofluorescence was used to quantify the phenotype of cells migrating from neurospheres that had been seeded on to PLL/laminin coated surfaces over a period of 24 hours. This experimental approach allowed rapid adhesion of neurospheres and subsequent cell migration, resulting in the formation of cellular monolayers.

Quantification of the different phenotypes was accomplished by counting at least five non-overlapping, randomly chosen, microscopic fields (280μm x 212μm, magnification of 200x) from three independent experiments. Each field contained between 50-200 cells. The total number of cells within the fields were evaluated by counting the DAPI-positive nuclei. Then, the ratio (%) of monoclonal- and polyclonal antibody immunoreactive cells to total number of cells was calculated.

Neurosphere cryosections were used to investigate the spatial distribution of particular immunostained cells throughout the hNPC-spheres. In 8μm sections, the false indications of double immunoreactivity were minimal since cells diameters ranged from 7-13μm.

Table 2.1: **Summary of antibodies used in this study**

Antibody	Source	Dilution
Monoclonal Antibody		
Anti-CD44 (Hermes antigen, HCAM)	Sigma	1:200
Anti-vimentin	Sigma	1:10000
Anti-nestin	Chemicon	1:200
Anti-neurofilament, 200kD (NF200)	Sigma	1:2000
Anti-microtubule-associated protein 2a+b (MAP2a+b)	Sigma	1:500
Anti-tubulin β, isotype III (TuJ1)	Sigma	1:400
Anti-O1	Chemicon	1:200
Anti-O4	Chemicon	1:200
Anti Galactocerebrosidase C (GalC)	Chemicon	1:200
Polyclonal Antibody		
Anti-GFAP	Dako	1:2000
Anti-S100 beta (S100β)	Dako	1:2000
Anti-nestin	Chemicon	1:500
Anti-Sox 2 (SOX2)	Chemicon	1:2000
Anti-Musashi-1	Chemicon	1:400
Anti-Ki67	Chemicon	1:100
Secondary Antibody		
Alexa fluor 488 goat anti-rabbit	Molecular Probes	1:500
Alexa fluor 594 goat anti-mouse	Molecular Probes	1:500
Nuclear Staining		
Diamidino-2-phenylindol (DAPI)	Molecular Probes	1:1000

2.3 Reverse Transcription Polymerase Chain Reaction

2.3.1 Isolation of mRNA

A molecular biological approach was employed to obtain a semi-quantitative estimation of expression profiles of hNPC and their derivate hNP-AC. The expression level of a range of messenger ribonucleic acids (mRNA) was examined using reverse transcription PCR (RT-PCR) for hNPC (up to P7) and for hNP-AC (up to P12; Table 2.2).

The mRNA was isolated and enriched using the RNeasy-Mini-Kit (Qiagen) according to the manufacturers recommendations. To extract RNA from neurospheres of different passage numbers, $5 \cdot 10^6$ - $1 \cdot 10^7$ cells were harvested and centrifuged per sample. Cell pellets were stored at -20°C until isolation of RNA was performed.

Cell disruption and release of RNA was performed with the supplied lysis buffers (RLT®, 600μl). β-mercapthoethanol (6μl) was added as a stabilizing agent to each probe. Homogenisation of the lysed cells was carried out with a QIAshredder homogenizer to reduce viscosity of the cell lysates. All working steps were performed with RNase free reagents and instruments. The resulting lysate volume was then mixed with ethanol (70%, 600μl) and transferred to a RNeasy mini spin column. Centrifugation was carried out at 10,000rpm for 15 seconds (sec). The bound RNA in each column was washed with Buffer RW1® (700μl) and centrifuged at 10,000rpm for 15sec. Columns were washed twice with buffer RPE® (500μl), and finally centrifuged at 16,000rpm for 2 minutes to dry the columns. Then columns were transferred to new 1.5ml Eppendorf containers and RNA was eluted out of each column by addition of 30μl RNase free water and centrifugation at 10,000rpm for 15sec. Isolated RNA was stored at -20°C.

The concentration of RNA was measured using a thermo scientific spectrophotometer (Nano-Drop^{TM} 1000). Absorbance of each sample was measured within 10 seconds up to a concentration of 3700ng/μl.

To estimate quality and quantity of isolated RNA probes, the maximum of absorbance was used at a wavelength of $\lambda = 260$nm. To determine pureness of the RNA probes the amount of protein was also measured at a wavelength of $\lambda = 280$nm. Optical densiometry of RNase free water was used as blank value in the measurement. Since RNA samples were diluted in RNase free water a measurement in linear alignment could be assured. The ratio of absorbance at wavelength 260nm to wavelength 280nm (A260/A280) represents the degree of purity, which should be at least 1.7. The degree of purity of samples used in this study all had a value of at least 1.95 (see Table 2.2).

MCF-7 (a human mamma adenocarcinoma cell line), THP-1 (a human acute monocytic leukemia cell line) and U373 (a human glioblastoma cell line) were processed as described above and

used as positive controls for ongoing RT-PCR. H_20 served as negative control. The housekeeping gene glyceraldehyde-3-phosphate dehydrogenase (GAPDH) was used as internal control.

Table 2.2: **Summary of mRNA concentrations used in this study**

mRNA Sample	Ratio A260/A280	Concentration [ng/μl]
hNPC, culture passage (P)		
P2	2.01	285.69
P3	2.00	119.7
P7	2.11	348.45
P7	2.02	461.58
hNP-AC, culture passage (P)		
P4P5	2.03	224.81
P4P10	1.95	115.20
P8P4	2.01	215.94
P8P12	2.00	212.56
Positive Controls		
U373	2.05	166.5
MCF-7	2.03	597.8
THP-1	2.07	253.3
Negative Control		
mRNA free H_2O	-	-

2.3.2 Synthesis of Complementary DNA

For transcription of isolated RNA into complementary deoxyribonucleic acid (cDNA) the Omni-script^{TM} Reverse Transcriptase Kit (Qiagen) was used. To amplify the genes of interest, in a first step the mRNA was amplified by the reverse transcriptase enzyme. To accomplish reverse transcription, a specific oligo-(dT)-primer (Fermentas) was utilised. The primer hybridizes at the 3'-poly A-tale of the mRNA, allowing a complementary cDNA elongation of the mRNA single strand. Furthermore a random primer (Fermentas) was used to improve a continuous transcription. A mRNA-cDNA-hybrid was established, which was denatured with cDNA avail-

able for subsequent PCR as a single strand template.

According to the protocol, template RNA (xμg), RT-buffer, oligo-dT-primer, random primer, reverse transcriptase and RNase free water (11μl-x) were adjusted to an end volume of 20μl, while being stored on ice. Reaction batches were composed as follows:

10x RT-buffer	2μl
Deoxyribonucleotide triphosphate (dNTP) -mix (5mM)	2μl
oligo-(dT)-primer (10pM/μl)	2μl
random primer (10nM/μl)	2μl
omniscript reverese transcriptase (4U/μl)	1μl
RNase free water	11μl-x
template RNA (ng/μl)	xμg
total volume	**20μl**

Variable amounts of RNase free water were added, depending on the mRNA concentration (see Table 2.2). Reverse transcription proceeded for one hour at 37°C and was terminated by an enzyme inactivation step of 95°C for 5 minutes followed by a cooling step of 4°C. The cDNA products were either stored at -20°C or used immediately for RT-PCR.

2.3.3 Polymerase Chain Reaction

Polymerase chain reaction (PCR) serves as a method for *in vitro* amplification of cDNA fragments. Primer sequences for CD44 (Hermes antigen, HCAM) and CD133 (Prominin-1) were generated with genome information from Ensembl Data. The other primers used in this study relate to sequences described earlier (Montzka et al., 2009).

Table 2.3: **Reaction cycle of PCR**

reaction cycle	temperature	duration
denaturation	95°C	60sec
annealing	see T^A (see Table 2.4)	60sec
extension/ elongation	72°C	60sec
last elongation	72°C	10min
cool	4°C	∞

Each cycle was introduced by an initial denaturation step at 95°C for 60sec to achieve a complete separation of the double-stranded DNA. Primers annealed to the 5' and 3' end of the sought-after cDNA sequence.

Regulation of annealing temperature (T^A), design of primer pairs and the composition of reaction batch play an important role concerning sensitivity and specificity of the PCR and had to be optimised for each PCR (see Table 2.4). The specific T^A was adjusted to 60sec (see Table 2.3). A thermo stable DNA-dependant polymerase attached to the double stranded sequence consisting of primer and synthesised cDNA and started DNA-synthesis (72°C for 60sec). The final incubation at 72°C for 10min terminated the cycle (see Table 2.3). The specific DNA sequences of interest were exponentially amplified by repeating the cycles. The number of repetitions was optimised for each PCR as well.

Amplification was performed with the synthesised cDNA, Ready Mix REDTaq^{TM} PCR reaction mix (Sigma), as well as appropriate sense- and antisense oligunucleotide primers (MWG Biotech). Reaction batches were pipetted into a sterile RNase free PCR-tube (Biozym):

ready mix REDTaq^{TM}	12.5μl
distilled water	6.5μl
forward primer (10 pmol)	2μl
reverse primer (10 pmol)	2μl
cDNA (5ng/μl)	2μl
total volume	**25μl**

Denaturation, annealing and synthesis were performed in a Thermocycler (Biometra), whereas the temperature profiles of the PCR differed only in the specific annealing temperature of the particular primer (see T^A, Table 2.4). After termination of PCR, reaction products were either stored at 4°C or used directly for gel electrophoresis (agarose, 2%).

2.3.4 Agarose-Gel-Electrophoresis and Semi-Quantitative Analysis

Agarose (2%) was boiled in Tris-acetate-EDTA (TAE)-buffer (1x) and after cooling to 60°C, the suspension was poured into a gel-chamber. Ethidium-Bromide (EtBr; 0.05μg/ml, Roth) was added to visualise the DNA fragments in UV-light. The hardened gel was transferred into an electrophoresis apparatus (Subcell G, BioRad) and covered with TAE-buffer (1x). Samples of a complete reaction batch were pipetted in gel-bags on the side of the cathode and separated at 120 volt. A PCR-1kb-ladder (Gene-Ruler^{TM}, 0.5μg/μl, MBI Fermentas) was used to estimate the size of DNA fragments (see additional data, Fig. 9.1). Fluorescent DNA bands were visualised with a digital camera (Gel Doc 2000, BioRad) and processed with MultiAnalyst software 1.1. The number of pixels associated with the images of each DNA band was analysed semi-quantitatively with Image J 1.41o/Java 1.6.0-10 software and calculated as a ratio of the amount of pixels detected in the internal control, GAPDH band. Samples to be compared were adjusted

Table 2.4: **Forward (FW)- and reverse (RV) primers for reverse transcription PCR**

Gene	Primer Sequence 5'-3'	bp	T^A	r
GAPDH (FW) GAPDH (RV)	tga agg tcg gag tca acg gat ttg gt cat gtg ggc cat gag gtc cac cac	983	62°C	30
S100β (FW) S100β (RV)	gga gac aag cac aag ctg aag agc tac aac acg gct gga aag	322	63°C	30
GFAP (FW) GFAP (RV)	gtg gta ccg ctc caa gtt tgc ag aat ggt gat ccg gtt ctc ctc	373	59°C	40
Nestin (FW) Nestin (RV)	gcg ttg gaa cag agg ttg gag gca cag gtg tct caa ggg tag	385	65°C	30
Vimentin (FW) Vimentin (RV)	ccc tta aag gaa cca atg agt ccc tgg aac gag tga atc cag att agt ttc cct cag gtt c	301	64°C	30
CD44 (FW) CD44 (RV)	tgc ttc aat gct tca gct cc acct g tga ttc aga tcc atg agt ggt atg	375	64°C	33
CD133 (FW) CD133 (RV)	cca agt tct acc tca tgt ttg g cca aca ggg aga ttg caa agc	527	60°C	40

Human specific forward (FW)- and reverse (RV) primers for reverse transcription PCR with annealing temperature (T^A), number of PCR cycles (r) and base pair length (bp) of amplification products.

to an equal strength of GAPDH band strength (see additional data, Fig. 9.1).

For statistical evaluation, analysis of variance (ANOVA) with Bonferroni's post hoc Multiple Comparison Test were performed using Graph Pad Prism software. The results are presented as mean $\pm$ standard error of the mean (SEM) with $p < 0.05$ considered as significant.

2.4 Proliferation of hNPC and hNP-AC

Two different methods were used to estimate the proliferation rate:

I) a metabolic assay in which metabolic activity was determined by a fluorescent signal that was proportional to the number of viable cells in the sample;

II) a morphological assay, providing an indirect indicator of proliferation within intact neurospheres by measuring the increase in volume over time.

2.4.1 Cell Titer Blue Metabolic Assay

As metabolic assay the cell viability assay Cell Titer Blue® (Promega) was used. The Cell Titer Blue® reagent contains the indicator dye resazurin which, within the cytoplasm of viable cells, is converted to the highly fluorescent metabolite resorufin. The fluorescent signal correlates with the amount of resorufin produced and therefore represents the amount of living cells (Fig. 2.1A). Proliferation of hNPC and hNP-AC was measured in monolayer cell cultures adhering to a PLL/laminin substrate.

Cell Titer Blue® reagent was added to cell culture medium at a ratio of 1:5 incubated with the cells at 37°C for two hours. Fluorescent samples were transferred to an opaque 96-well plate for measurement. Fluorescence was measured with a fluoremeter (Fluostar Optima, BMG Laptech) at an extinction of 560nm and an emission of 590nm.

Empty wells without cells served as negative (no-cell) controls to determine the background fluorescence. Wells with untreated cells served as negative (vehicle) controls.

The average of fluorescence values of the culture medium controls (background) and the negative (no cell) controls were subtracted from all fluorescence values of experimental wells. Optima software 2.20 (BMG Laptech) was used for acquisition of data.

A standard curve for the metabolic assay was generated to examine, whether the indirect measurement of viable cells was accurate for both, hNPC and hNP-AC. For this purpose neurospheres were dissociated and the number of cells was counted in a Neubauer chamber. Cell suspension (1ml volume) was seeded on to PLL/laminin coated 12-well plates with an increasing concentrations of cells ($5 \cdot 10^4$ - $1.2 \cdot 10^6$ cells/ml) for calibration of fluorescence intensitiy. The calibration curve was determined on the basis of the mean values from 5 independent experiments. The standard curves revealed a significant linear relationship (r^2 = 0.93 for hNPC and r^2 = 0.97 for hNP-AC) between 590nm emission and the number of cells (Fig. 2.1B). The blank value with a fluorescence of 941 for hNPC and 875 for hNP-AC was substracted from all data, so that a best-fit line with linear approach resulted for ongoing calculations. The standard curves of hNPC and hNP-AC differed in their gradients with an overall higher fluores-

cence signal for hNP-AC compared to hNPC (Fig. 2.1B).

The hNPC and hNP-AC were prepared with a cell concentration of $1 \cdot 10^5$/ml (6 samples per cell line). Measurement was performed continuously every 3rd day (d) for a measure period of 22d.
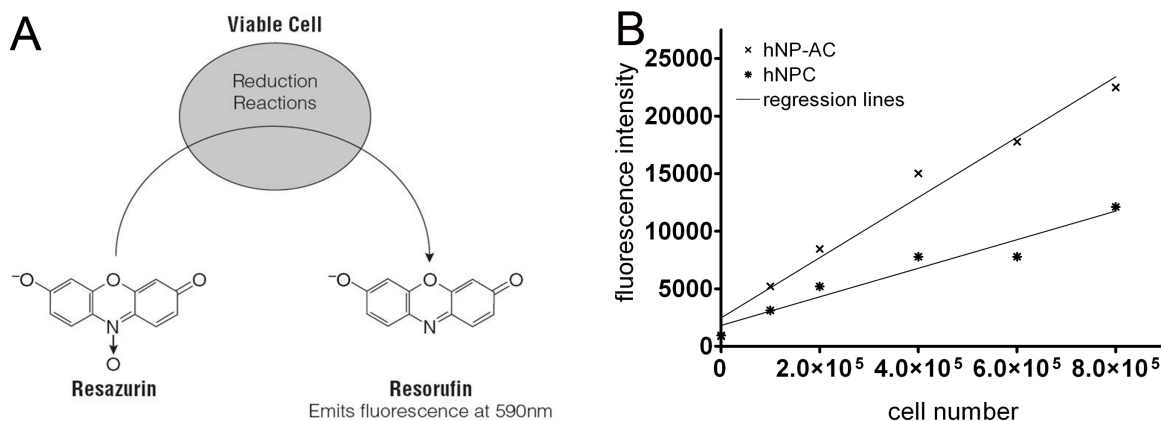
Figure 2.1: **Correlation between fluorescence and cell number for hNPC and hNP-AC.**
    A: Conversion of resazurin by metabolically active cells results in the generation of a fluorescent product proportional to the number of cells (Promega (2006), Technical bulletin).
    B: The standard curves for the metabolic assay of hNPC and hNP-AC show significant linear relationships between emission at 590nm and the number of serially diluted cells in the range from $1 \cdot 10^5$ - $8 \cdot 10^5$ cells/ml. Standard curves of hNPC and hNP-AC differed in their gradients. Fluorescence signal of hNP-AC was higher than the signal generated by hNPC. Regression lines show goodness of fit with $r^2 = 0.9374$ for hNPC, and $r^2 = 0.9748$ for hNP-AC. Data represent means $\pm$ SEM.

2.4.2 Morphological Assay

In vitro proliferation as self aggregating neurospheres is a characteristical feature of hNPC and offers excellent conditions for high expansion rates (Svendsen et al., 1997; Carpenter et al., 1999; Ostenfeld et al., 2002). Therefore, an examination under neurosphere culture conditions seemed reasonable. However, the metabolic assay was not appropriate for intact hNPC and hNP-AC spheres due to the lack of penetration of the kit components deep into the structures. Therefore, an alternative, morphological assay was established to estimate cell proliferation within intact spheres. The spherical nature of the neurospheres allowed the volume (*V*) to be determined from microscopical measurements of diameter (*D*, Fig. 2.2A) according to the following formula:

$$V = \frac{4}{3}\Pi\left(\frac{D}{2}\right)^3 \qquad (2.1)$$

To minimize systematic errors concerning the volume calculation of neurospheres, the following selection criteria were applied:

> I) Only ball-like spheres were assessed;
>
> II) As the shape of neurospheres changed during the experimental period, spheres were excluded from the experiment;
>
> III) Spheres located at the margin or adherent to the tissue culture plastic were excluded from the experiment.

The relationship between volume (V) of a sphere and cell number was investigated by the following method: neurospheres were carefully transferred with a pipette into 96 well plates (Microtest^{TM}) under microscopic control. After measurement of diameter, neurospheres were dissociated with Accutase (200μl, see chapter 2.1.2) to a single cell suspension. When cells had sedimented to the ground of the wells, five non-overlapping fields (0.242mm^2, magnification of 100x) were photographed and counted using ImageJ 1.41o software. To estimate the total number of cells of one neurosphere results were extrapolated to the complete well-surface (32mm^2). A significant linear correlation ($r^2 = 0.94$) between cell number (n) and diameter (D) of a sphere (Fig. 2.2B) was found, given by the following equation:

$$n(D) = 1.72 \cdot 10^5 \cdot D^3; \ [D \text{ in mm}] \tag{2.2}$$

Thus, it was possible to estimate the total cell number within hNPC neurospheres by measuring the sphere diameter, assuming that the linear correlation between the volume of the spheres and the number of cells within the spheres was maintained during cultivation. Proliferation was determined by measuring increasing neurosphere volume (ΔV) over time (t). Isolated neurospheres were cultured in 12-well culture plates (Greiner Bio-One) at 37°C in a 5% CO_2 atmosphere. The increase in size of neurospheres was monitored under the microscope (Leica, DMI 4000B), images captured using a digital camera (JVC, KY - F75U) and measured using the software Diskus 4.80. Two diameters in orthographic projection were recorded (Fig. 2.2A). The arrithmetic mean of the two diameters was used for further calculations, assuming a nearly round sphere. Media was changed every other day. Growth of approximately 80 individual neurospheres was documented every 24h for a time period of 14d.

Different sizes of neurospheres were monitored to investigate, whether proliferation of spheres depends on their size. Selected spheres showed diameters in between 70μm (smallest spheres) to 450μm (largest spheres) at the beginning of the experiment (day 1; d1). Measurement was terminated when spheres reached a diameter greater than 1000μm.
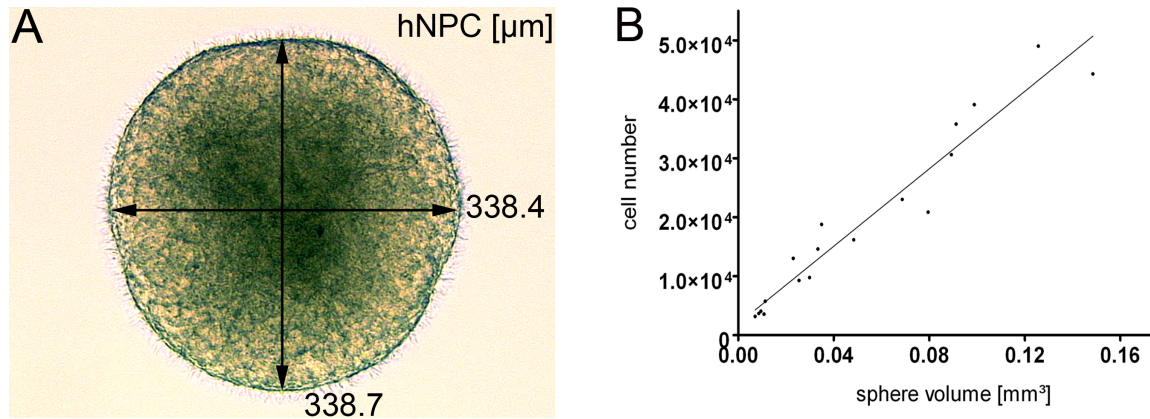
Figure 2.2: **Correlation between neurosphere volume and cell number.**
A: The lightmicroscopic image shows a hNPC-neurosphere that was cultured individually for the morpholocial assay. The diameters were registered in orthographic projection each 24 hours and used for ongoing calculations. **B:** The diagram shows the standard curve of the morphological assay with a positive linear correlation ($r^2 = 0.94$) between cell number and volume of a sphere (n = 18).

2.4.3 Calculations of Proliferation and Doubling Time

Proliferation activity of cells in culture is characterised by a sigmoidal pattern containing four different phases of growth (Fig. 2.3). Within the first phase, when cells adapt to culture, the number of cells is nearly constant. Thereafter, the culture proliferates exponentially, illustrated by a constant slope in the logarithmic scaled diagram (log phase), until saturation is achieved (plateau phase). Due to a faster cell death compared to cell division, the latest phase is characterised by a declining cell number.

Cell proliferation kinetics during log phase are characteristic for a particular cell line and it is during this phase when the multiplication rate or the Doubling Time is calculated (McAteer J.A, 2001). The multiplication rate (r) is the number of generations that occur per time unit and is expressed as population doublings per time. The doubling time (DT) is reciprocal to r and expresses the time in hours taken for cell number to double:

$$DT = \frac{1}{r}.$$

(2.3)

As the DT varies strongly in the different growth phases the cell line is currently in (Fig. 2.3), a time averaged value over all growth phases has no significance. Therefore the analysis was performed on the logarithmic growth phase. A time interval of $\delta t = 72$ for the metabolic assay and a time interval of $\delta t = 24$ for the morphological assay was chosen.
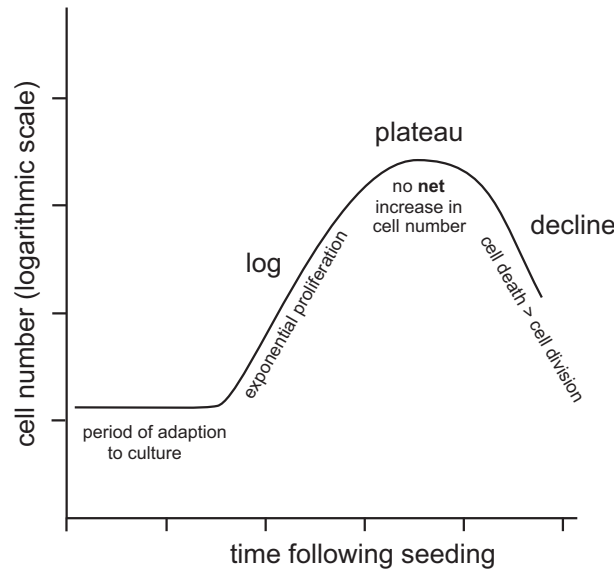
Figure 2.3: **Schematic drawing of growth phases for cells in culture.**
The graph outlines the classical phases of growth under cell culture conditions of non-transformed cell lines. Cell proliferation kinetics during the log phase are characteristic for a particular cell type under defined conditions.

In the metabolic assay *DT* could be calculated with a cell number over time function. Mean values of cell amount over the series of experiments could be easily generated. However, for the morphological assay a calculation of a mean value concerning cell amount would have been inaccurate, because differently sized spheres showed different cell numbers at the beginning and throughout the experiment. Thus, a calculation of *DT* using a cell number over time function would have only been possible for one single sphere. Since a result including data of only one series of sphere measurements, would have lacked general significance, a calculation of *DT* including data of more spheres was needed. Therefore, a correlation between the expansion of the cell volume expressed by the difference volume (ΔV) and the mean cell volume ($\overline{V}_{t1,t2}$) was used. The difference volume (increasement) per time ($\Delta V/\Delta t$) was calculated by

$$\frac{\Delta V}{\Delta t} = \frac{V_{t2} - V_{t1}}{t_2 - t_1},$$

(2.4)

where V_{t1} represents the volume of a sphere at the point in time t_1 and V_{t2} the volume of the same sphere at the point in time t_2. The mean volume ($\overline{V}_{t1,t2}$) was determined by

$$\overline{V}_{t1,t2} = \frac{V_{t2} + V_{t1}}{2}.$$

(2.5)

In case of an exponential growth, the increasement of the sphere correlates linear with the mean volume (see Fig. 2.4), whereby the constant correlation coefficient, the slope (α) of the plot, is reciprocal to the desired doubling time:

$$DT = \frac{ln2}{\alpha}.$$ (2.6)

The derivation of this correlation is given in the appendix (see additonal data, chapter 9.1). The averaged doubling time was calculated by the slope of the regression line, found by plotting the data of all neurospheres.

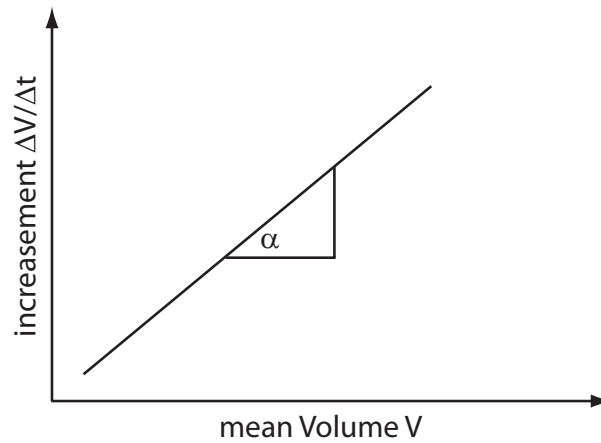Figure 2.4: **Correlation between the increasement of the neurospheres and their mean volume in case of logarithmic growth.**

3 Results

3.1 Characterisation of hNPC

One goal of this study was to define the cell population in the hNPC-neurospheres. Characterisation of the hNPC cells was necessary because it provides the baseline phenotype for the *in vitro* differentiation of hNP-AC, a prerequisite for later *in vivo* transplantation studies.

3.1.1 Progenitor/Stem Cell Related Markers in hNPC

In a first stage the expression profile of the stem cell related markers nestin, SOX2, musashi and CD133 (Prominin-1) was investigated. The hNPC grew as neurospheres which appeared as large, tightly bound clusters of cells. Plating of the neurospheres on to PLL/laminin coated dishes induced rapid adherence to the substrate with flattening of the sphere as cells migrated away in a radial pattern (Fig. 3.1B).

Quantitative immunocytochemistry of the monolayers around the spheres revealed that the majority of the hNPC were immunopositive (+) for nestin (Fig. 3.1B and C), an intermediate filament protein expressed in undifferentiated neuroepithelial stem and precursor cells derived from human first trimester forebrain- and spinal cord tissue (Carpenter et al., 1999; Wright et al., 2003). Quantification revealed that $91 \pm 3.4\%$ of hNPC were nestin-positive (Fig. 3.11). Cryosections of hNPC-neurospheres showed an even, ubiquitous distribution of nestin staining within the spheres (Fig. 3.1A).

The migrating, nestin-positive cells displayed heterogeneous morphologies including small round-, bipolar as well as large polymorphic appearances (Fig. 3.1C). Interestingly, some bipolar cells were able to grow on top of the polymorphic cells (Fig. 3.2D, white arrows).

The proportion of nestin immunoreactive cells was maintained during *in vitro* expansion (investigation was performed up to P11). Likewise, there was no significant alteration of nestin mRNA expression during *in vitro* expansion (Fig. 3.1D). Complete images of mRNA samples with kb-ladder, GAPDH internal controls as well as positive- and negative controls for each investigated marker are attached in the appendix (see additional data, Fig. 9.1).

Figure 3.1: **Expression of the stem cell marker nestin by hNPC.**
A: The cryosection of a hNPC-neurosphere (P6) showed an even and ubiquitous staining pattern for nestin immunoreactivity (red). **B**: A hNPC-neurosphere (P11) plated on to PLL/laminin for one day prior to fixation showed rapid attachment and a wave of radial cell migration. The boxed region exemplarily shows one out of four areas per neurosphere, which were counted for statistical evaluation of immunoreactivity. **C**: Nestin+ cells (red) with heterogeneous morphologies migrate out of the neurosphere; nuclei were counterstained with DAPI (blue). **D**: RT-PCR shows that nestin mRNA was continuously expressed in different hNPC passages over time in culture (P2, P3, P7).

The hNPC were immunoreactive for SOX2 (Fig. 3.2), a nuclear transcription factor of the sex-determining region Y (SRY)-related high mobility group (HMG) box family, which is most commonly associated with non-committed stem and precursor cells in the developing nervous system (Ellis et al., 2004; Fong et al., 2008). There was an even distribution of SOX2+ cells in hNPC-neurosphere cryosections (Fig. 3.2A), showing co-expression for nestin (Fig. 3.2C). Quantification demonstrated that $89.2 \pm 2.7\%$ of hNPC were SOX2+ within the wave of migration cells (Fig. 3.2B and Fig. 3.11). Immunoreactivity for SOX2 was mainly localized in the cell nuclei with a slight cytoplasmatic component. Co-expression of the two stem cell related markers (nestin and SOX2) was observed in $82.7 \pm 3.4\%$ of hNPC (Fig. 3.2C, D and E). Only $6.9 \pm 2.8\%$ of hNPC, whose nuclei were visible with DAPI staining, showed no immunoreactivity for SOX2 or nestin antibody.
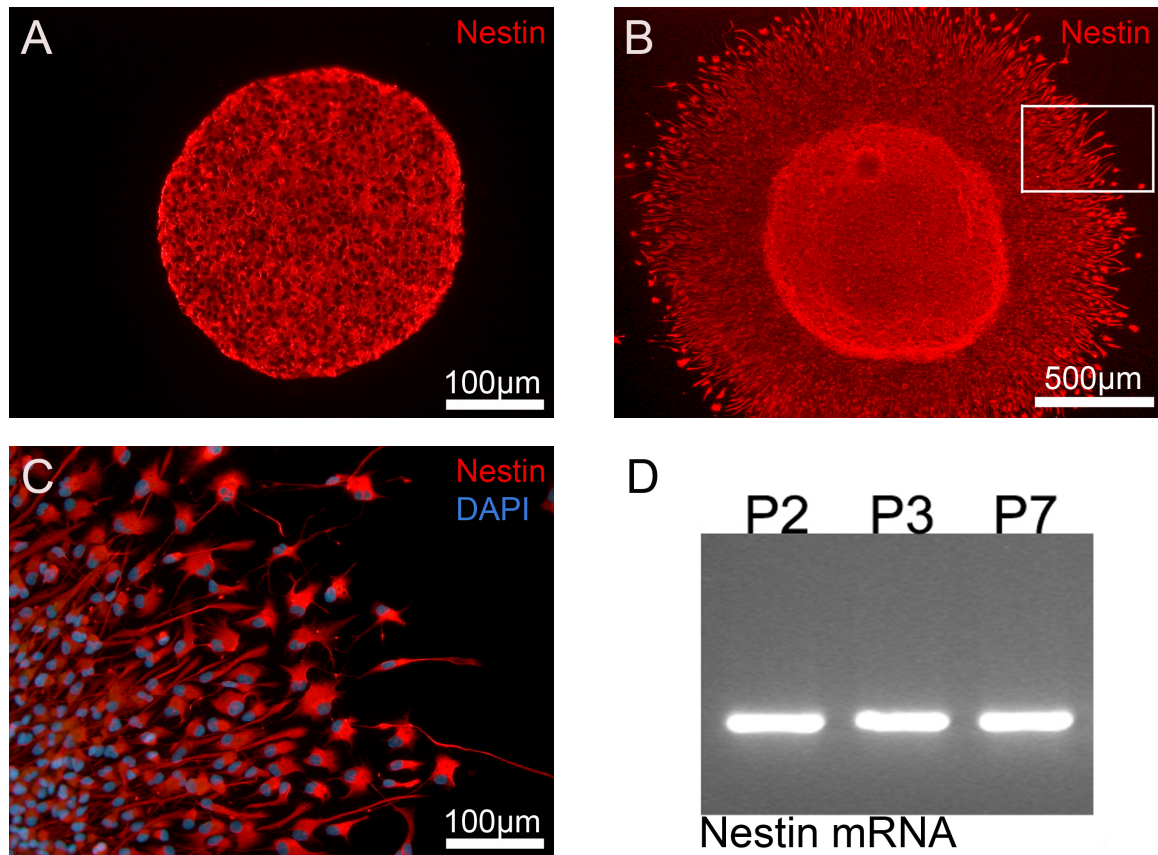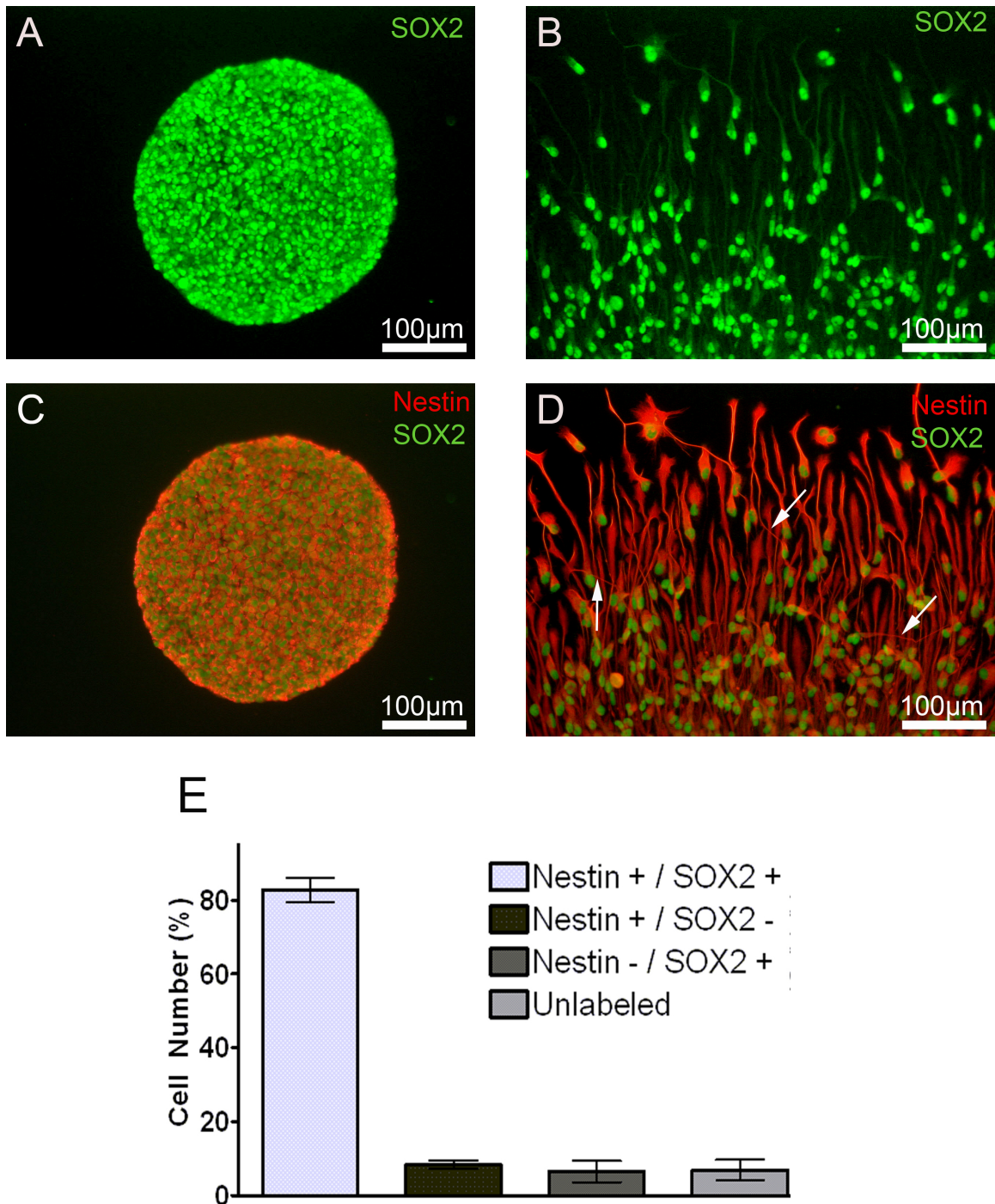
Figure 3.2: **Co-expression of the stem cell markers SOX2 and nestin by hNPC.**
     A, C: The cryosection of a hNPC-neurosphere (P6) shows an even and ubiquitous distribution of SOX2+ (green) cells with co-expression of nestin (red, **C**).
     B, D: SOX2+ (green) hNPC migrated out of a PLL/laminin plated neurospheres (located outside the image frame). SOX2 is co-expressed with nestin (red, **D**). The arrows indicate bipolar cells with long processes that grow on top of other hNPC.
     E: Quantification shows that the majority of cells co-expressed SOX2 and nestin (left column). A small percentage of hNPC expressed only one of the markers (centre columns) while some cells did not express either markers (right column). Data are means $\pm$ SEM of P3-P11 of hNPC.

37

The hNPC were immunoreactive for Musashi-1 (Fig. 3.3A and B), an evolutionary conserved stem-cell RNA-binding protein, that controls neural cell fate (Okano et al., 2002). There was an even staining pattern of Musashi-1 immunopositive cells in cryosections of hNPC-neurospheres (Fig. 3.3A). Musashi-1 immunopositive cells, which had established aggregates of cells at the limit of the migration wave showed heterogeneous morphologies with bipolar and polymorphic cells (Fig. 3.3B). About $91.8 \pm 2.0\%$ of hNPC were immunoreactive for Musashi-1 (Fig. 3.11). This proportion remained constant over time in culture.

The hNPC expressed mRNA of CD133 (Prominin-1, Fig. 3.3C), a surface marker endowing self-renewal and multi-lineage differentiation capacity in neurosphere-initiating cells (Uchida et al., 2000; Piao et al., 2006). The expression profile for CD133 mRNA was constant over time in culture.
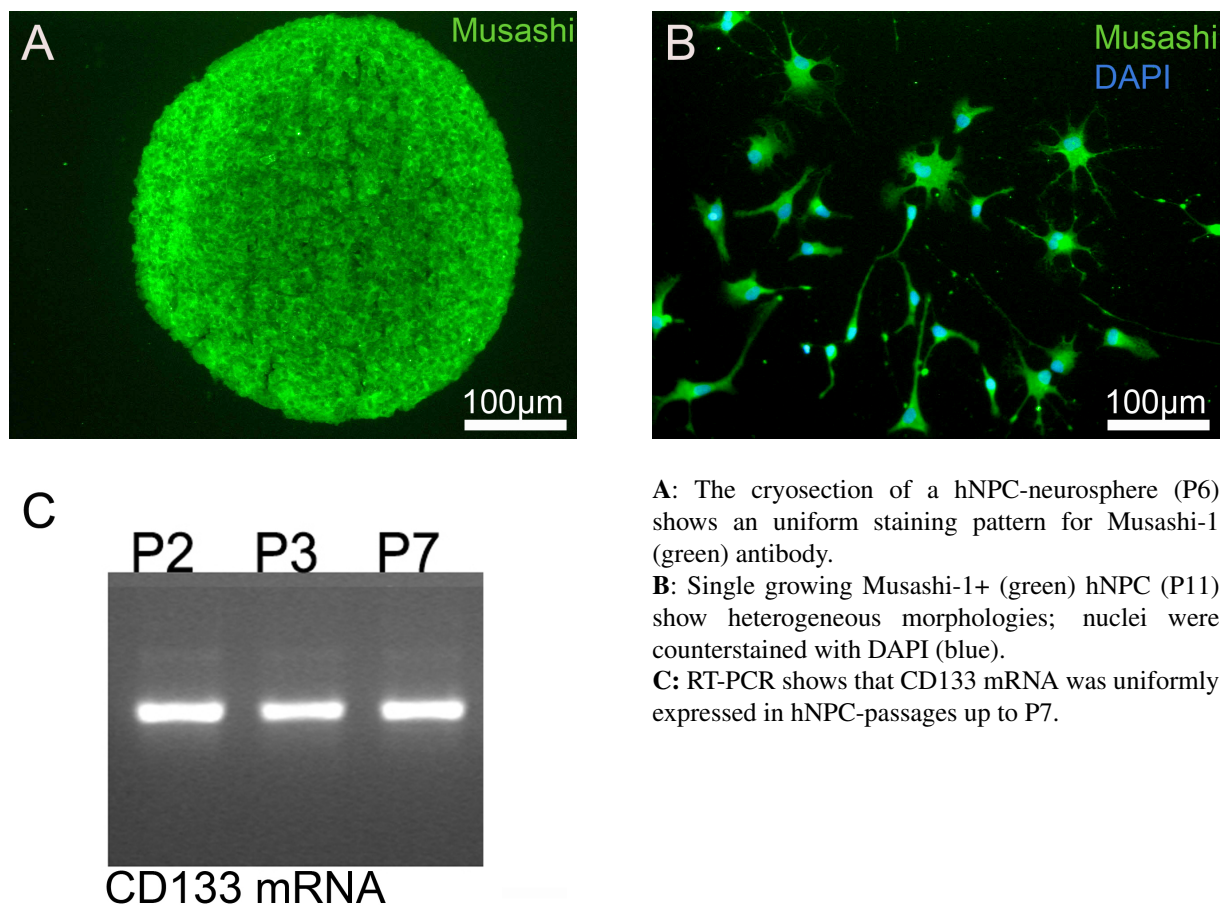
A: The cryosection of a hNPC-neurosphere (P6) shows an uniform staining pattern for Musashi-1 (green) antibody.

B: Single growing Musashi-1+ (green) hNPC (P11) show heterogeneous morphologies; nuclei were counterstained with DAPI (blue).

C: RT-PCR shows that CD133 mRNA was uniformly expressed in hNPC-passages up to P7.

Figure 3.3: **hNPC immunoreactivity for Musashi-1 and expression of CD133 mRNA.**

3.1.2 Multipotency of hNPC

Immunostaining for TuJ1 and MAP2ab was used to identify spontaneously differentiating neurons of variable maturity (Dehmelt and Halpain, 2005). Staining for TuJ1 identified individual cells scattered throughout the hNPC-neurospheres. These cells showed no distributional preference within the neurospheres, being located at the outermost margins as well as the center (Fig. 3.4A). Many cells showed a weak immunoreactivity for TuJ1. Only a few cells with an intensive staining migrated out of the hNPC-neurospheres (white arrow Fig. 3.4B).
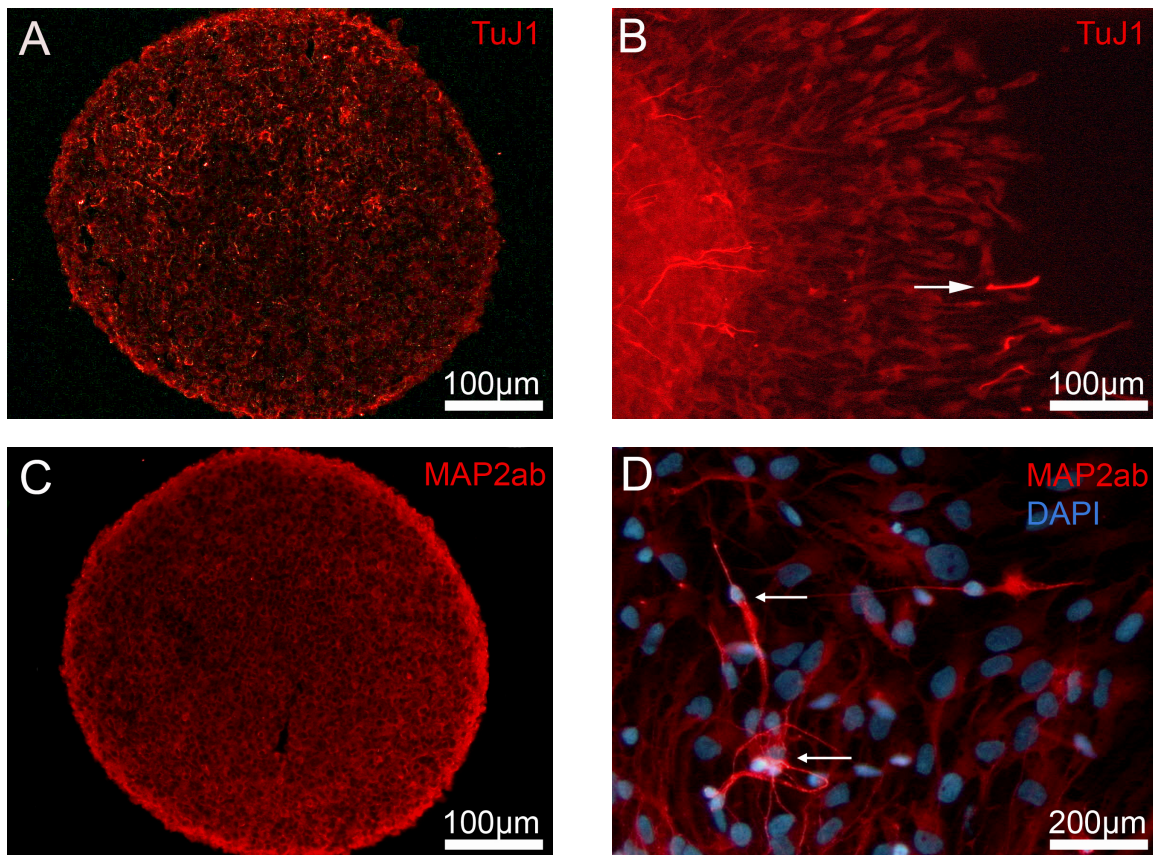
Figure 3.4: **Scattered expression of neuronal markers TuJ1 and MAP2ab by hNPC.**
A: Cryosection of a hNPC-neurosphere (P6) shows a few randomly localized TuJ1+ (red) cells. B: A wave of migrating cells forming around the plated sphere with many weakly stained, non-committed TuJ+ cells. The white arrow indicates an intensively stained migrating TuJ1+ (red) cell. C: Cryosection of a hNPC-neurosphere (P6) shows a thin band of strong MAP2ab immunoreactivity (red) around the neurosphere. D: Some MAP2ab+ (red) hNPC migrate out of a neurosphere (P3). Nuclei were counterstained with DAPI (blue). The white arrows mark two bipolar, intensely stained MAP2ab+ cells growing over more weakly stained- or unstained cells.

Staining of cryosections of hNPC-neurospheres with anti-MAP2ab showed weak immunore-
activity in the center of spheres (Fig. 3.4C). At the outer margin, there was a thin band of
relatively strong MAP2ab immunoreactivity (Fig. 3.4C), which extended annularly around the
neurosphere. Some migrating bipolar hNPC were intensely MAP2ab immunoreactive (white
arrows Fig. 3.4D and Fig. 3.6). MAP2ab+ cells had a bipolar morphology and adhered singu-
larly on PLL/laminin coated surface (Fig. 3.6) or on top of other cells (Fig. 3.4D, white arrows).
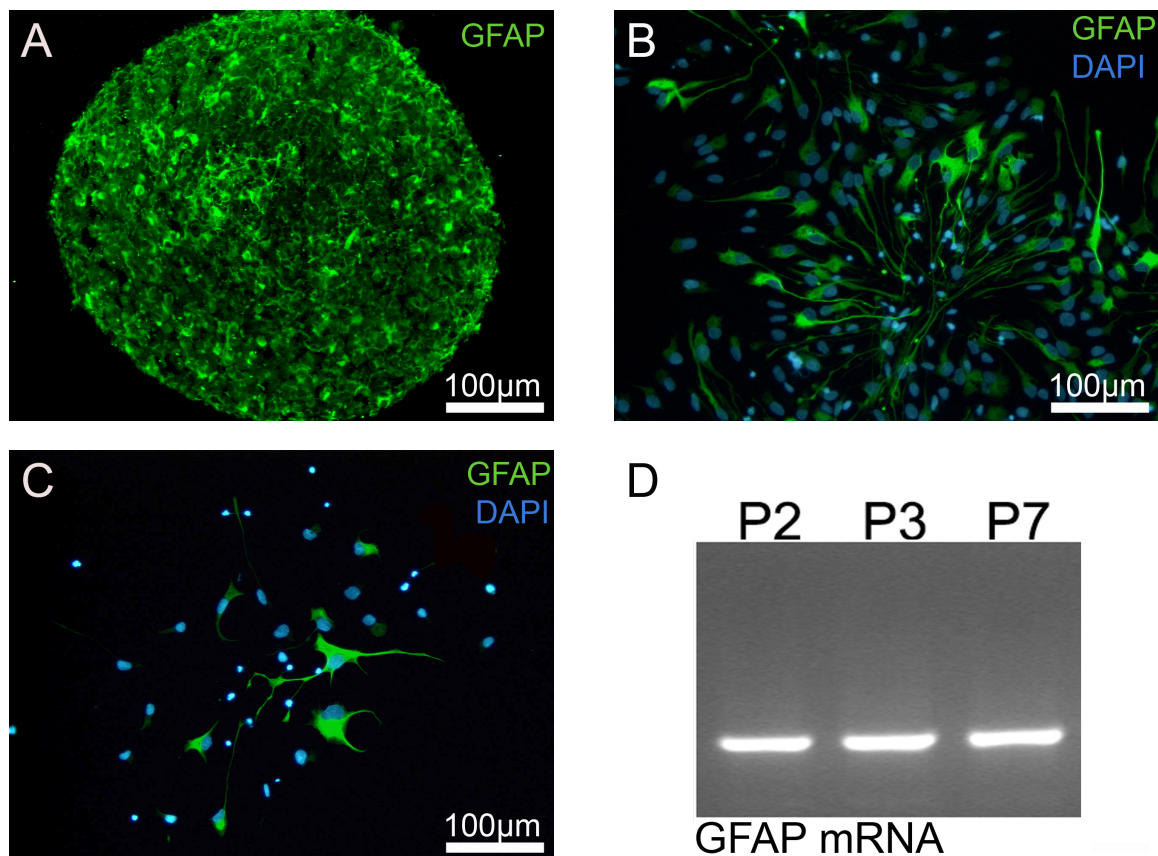
Figure 3.5: **Expression of the astrocytic marker GFAP by hNPC.**
A: A cryosectioned hNPC-neurosphere (P6) shows randomly distributed GFAP+ cells (green). **B,C**:
Clusters of individual GFAP+ cells (P6, green) migrating on PLL/laminin were big in size and adopted
polygonal morphologies. Many DAPI stained nuclei (blue) labelled cells, negative for GFAP staining.
D: A thin band of GFAP mRNA was expressed in hNPC.

To indicate presence of astrocytic precursor cells, immunofluorescence for GFAP, CD44 (HCAM/
Hermes antigen), vimentin and S100β was performed. Furthermore, the mRNA-expression
profile of these markers was also examined with RT-PCR.

Some hNPC were immunoreactive for GFAP (Fig. 3.5A, B and C), an astrocyte-specific type
III intermediate filament protein widely used in CNS cell characterisation (Eng, 1985). The
GFAP staining pattern in cryosectioned spheres was not ubiquitous; individual GFAP+ cells

were scattered throughout the sphere (Fig. 3.5A). GFAP+ cells, that had established aggregates at the limit of the migration wave, were large in size and had a polygonal, flat epithelial cell-like morphology (Fig. 3.5C). Quantification demonstrated the presence of $23.7 \pm 2.3\%$ of GFAP+ cells in younger (P3) and older (P11) culture passages of hNPC (Fig. 3.11). The apparently constant proportion of cells differentiating to an astrocytic phenotype was supported by RT-PCR, which demonstrated the presence of a similarly thin band of GFAP mRNA expression at different passages in hNPC (Fig. 3.5D).

Double immunofluorescence revealed many non-committed hNPC with only weak staining for GFAP and/or MAP2ab antibody. Occasional cells, which had migrated out from the sphere, sometimes intensely labelled for either MAP2ab or GFAP, but never for both antigens. These 2 populations of cells were morphologically and antigenically different: the large epitheloid GFAP+ cells were readily discernable from the smaller bipolar MAP2ab+ cells; other cells nearby the sphere were negative for both antigens (see arrows Fig. 3.6).
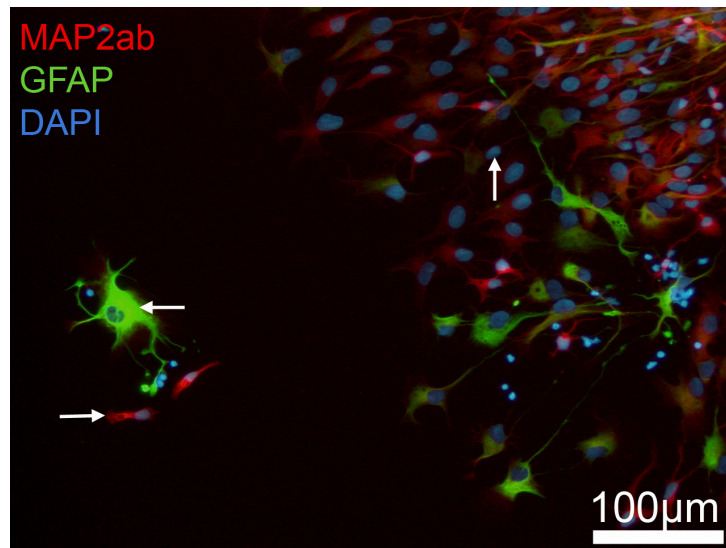
Figure 3.6: **MAP2ab+ hNPC and GFAP+ hNPC develop heterogeneous morphologies.**
GFAP+ (green) cells with a large, polygonaland morphology (arrow pointing to the left) contrasted to MAP2ab+ (red) cells, which were smaller and adopted a bipolar morphology (arrow pointing to the right). Some cells with small densely packed nuclei were negative for both antigens (arrow pointing upwards).

The majority of hNPC was immunoreactive for vimentin (Fig. 3.7A, B and C), another type III intermediate filament protein, expressed in astrocytic progenitor cells (Chu et al., 2001). Vimentin+ cells were ubiquitously distributed within cryosections of spheres with an even staining pattern (Fig. 3.7A). Quantitative analysis revealed a presence of $96.8 \pm 1.1\%$ vimentin+ cells (Fig. 3.11). Solitary localized vimentin+ cells were polymorphic with large cell bodies (Fig. 3.7C). The size of the mRNA vimentin band, generated by RT-PCR, was constant in different hNPC passages (Fig. 3.7D). Vimentin+ cells also co-expressed either Musashi-1, S100β or GFAP (Fig. 3.8). Figure 3.8 demonstrates the heterogeneous morphologies adopted by the hNPC population, when exposed to the PLL/laminin substrate.
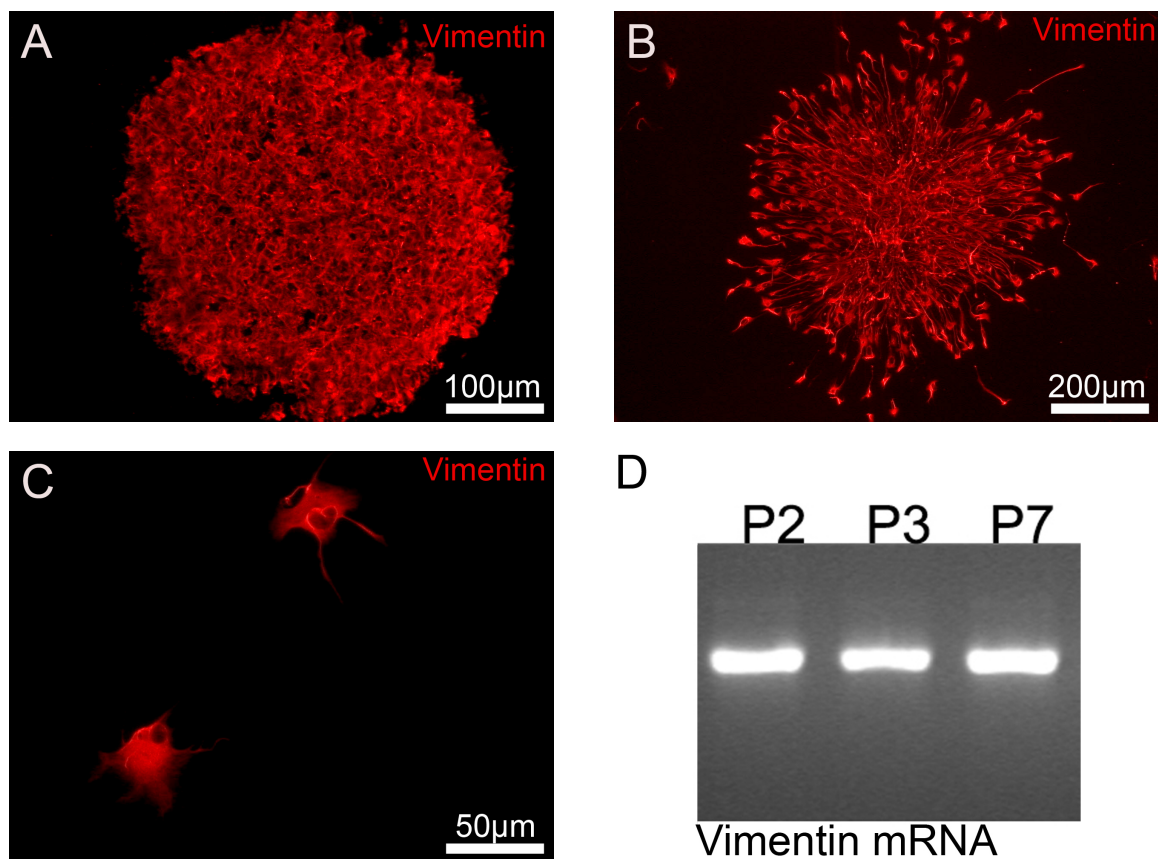
Figure 3.7: **Vimentin expression by hNPC.**
A: Vimentin+ (red) cells were evenly distributed within a cryosection of a hNPC-neurosphere (P3). B: Vimentin+ hNPC grew in a radial manner when plated on to PLL/laminin (P3). C: Individual vimentin+ hNPC (P11) were large and polymorphic in shape. D: RT-PCR revealed similarly sized bands of vimentin mRNA from hNPC at different passages in culture (P2, P3, P7).
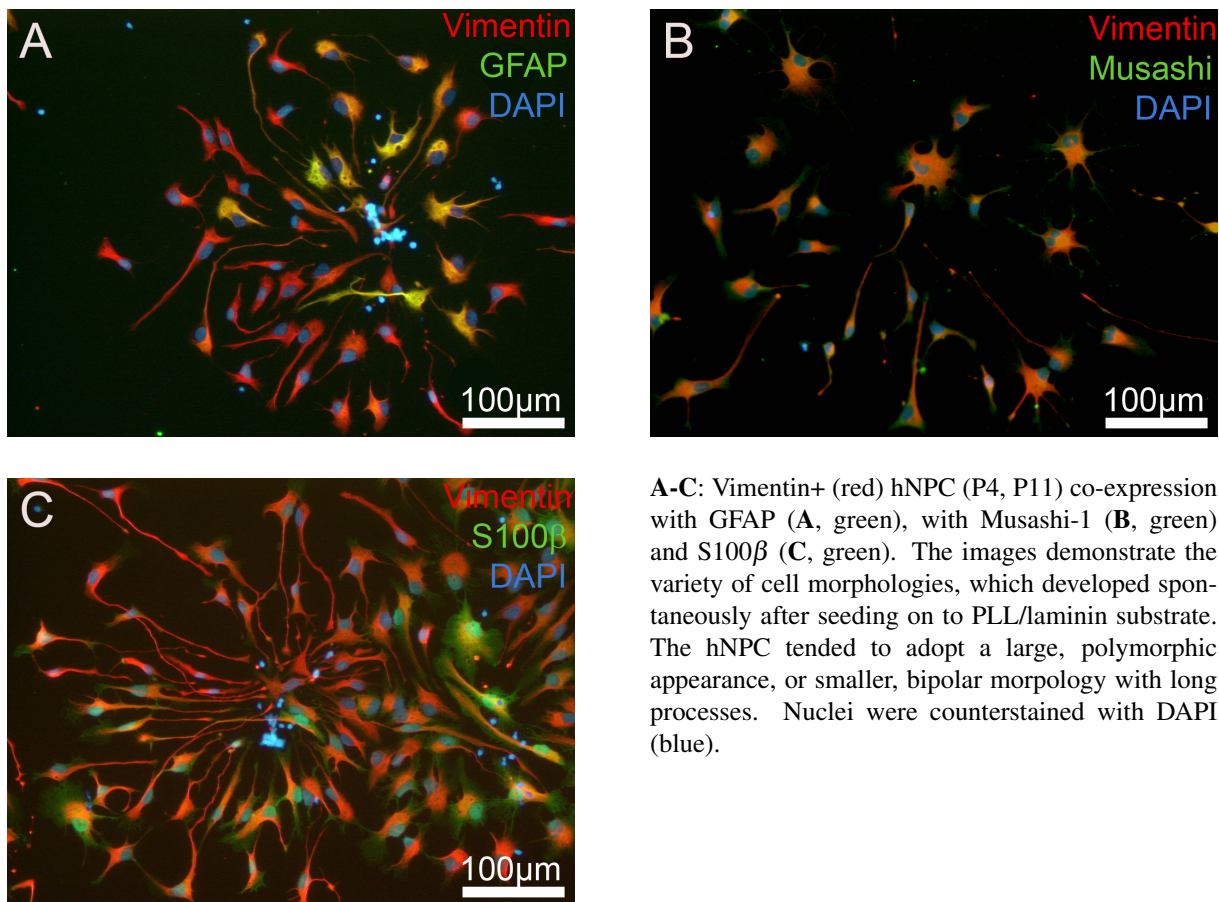
A-C: Vimentin+ (red) hNPC (P4, P11) co-expression with GFAP (**A**, green), with Musashi-1 (**B**, green) and S100β (**C**, green). The images demonstrate the variety of cell morphologies, which developed spontaneously after seeding on to PLL/laminin substrate. The hNPC tended to adopt a large, polymorphic appearance, or smaller, bipolar morpology with long processes. Nuclei were counterstained with DAPI (blue).

Figure 3.8: **hNPC co-express vimentin with GFAP, Musashi-1 or S100β.**

The hNPC were immunoreactive for S100β (Fig. 3.9A, B and D), a Ca^{2+}, Cu^{2+} and Zn^{2+} binding member of the S100-calmodulin-troponin superfamily that participates in remodelling components of the astrocytic cytoskeleton such as microtubules, GFAP or vimentin (Bianchi et al., 1993; Sorci et al., 1998). S100β+ cells were randomly, but not ubiquitously, localized within cryosections of hNPC-neurospheres (Fig. 3.9A). Quantification revealed that $17.6 \pm 2.1\%$ of hNPC were immunoreactive for S100β (Fig. 3.11). Preferentially the hNPC-population, which adopted a polymorphic appearance (Fig. 3.9B and D) demonstrated S100β immunoreactivity. The intensity of the staining within a cell was uneven: the nucleus with higher fluorescence intensity could be clearly discerned from the cytoplasm (Fig. 3.9B). S100β mRNA of hNPC was expressed at a constant level in the different passages (Fig. 3.9C).

In early hNPC passages (e.g. P3) of hNPC there were hardly any CD44 (Hermes antigen, HCAM) immunoreactive cells detectable. The CD44 transmembrane glycoprotein has been implicated in cell-matrix adhesion and matrix-mediated cell signaling (Naor et al., 1997) and is expressed by astrocyte-restricted progenitor cells (Liu et al., 2004). It has been identified as
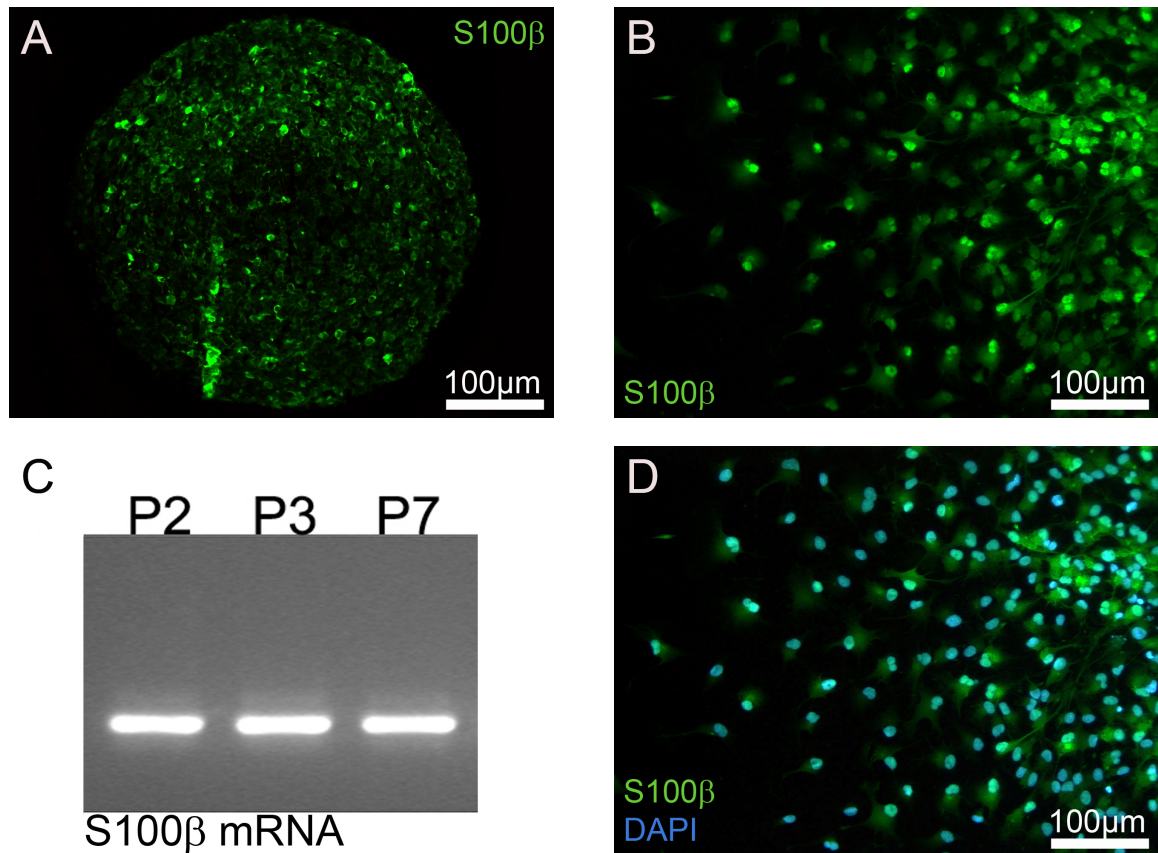
Figure 3.9: **S100β expression by hNPC.**
  A: Some S100β+ (green) cells were randomly localized within a cryosection of a hNPC-neurosphere (P6). **B, D**: S100β+ cells migrated out of a neurosphere (P11) with their nuclei showing higher fluoresence intensity compared to their cytoplasmn. Cell nuclei were counterstained with DAPI (blue, **D**). **C**: S100β mRNA was expressed constantly in different hNPC passages.

an early marker of astrocytic differentiation (Vogel et al., 1992; Moretto et al., 1993). In older hNPC culture passages (e.g. P11) CD44+ cells were rarely detectable (data not shown). A thin band of CD44 mRNA was expressed in hNPC, that remained constant in different hNPC passages (Fig. 3.10).

A spontaneous differentiation to cells of the oligodendroglial lineage was not observed. Staining with the oligodendroglial markers, for example anti-O1, anti-O4 and anti-GalC showed no immunoreactivity (data not shown).

In summary, the immunocytochemical characterisation and mRNA expression analyses confirmed that the purchased hNPC contained cells, which demonstrated typical neural progenitor characteristics. Approximately 90% of hNPC expressed the stem/progenitor cell markers nestin, SOX2 and Musashi-1 (Fig. 3.11).
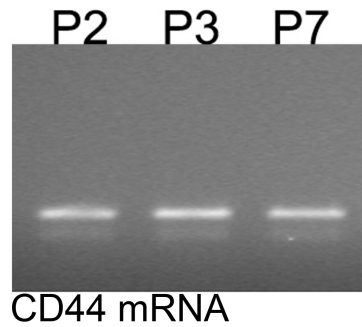
Figure 3.10: **CD44 mRNA expression by hNPC.**
RT-PCR shows a thin band of CD44 mRNA in different hNPC culture passages.

Furthermore, hNPC represented a heterogeneous population, varying in morphology and marker expression. The hNPC expression patterns could be attributed to undifferentiated-, astrocytic or neuronal progenitor cells, but not to an oligodendroglial cell lineage.

The amount of cells expressing characteristic astrocyte-related markers (i.e. S100β, GFAP) was less than 25% in hNPC (Fig. 3.11). A table summarizing percentage of phenotypes is attached in the appendix (see additional data, Table. 9.1).
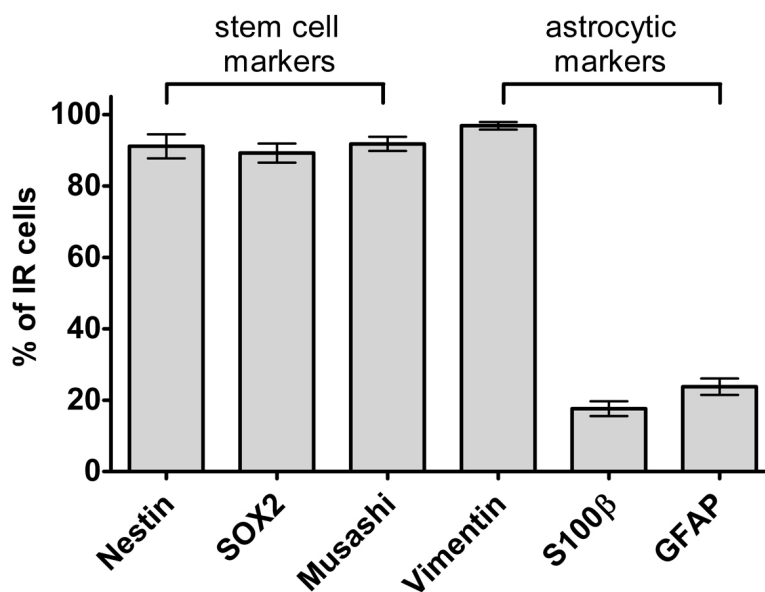
Figure 3.11: **Immunocytochemical expression profile of hNPC for stem/progenitor cell and astrocytic markers.**
The diagram shows the proportion of cells that were immunoreactive for stem/progenitor cell-related markers (nestin, SOX2, Musashi-1) and astrocyte-related markers (vimentin, S100β, GFAP). Provided data are means $\pm$ SEM of immunoreactivity profile for hNPC (P3-P11), migrating out of spheres, which had been plated on to PLL/laminin for one day.

3.2 Proliferative Activity of hNPC

In presence of growth factors EGF and bFGF, the hNPC were kept in a proliferative state and could be cultured over a period of 6-8 months. The hNPC showed immunoreactivity for the proliferation marker Ki67, which is expressed in late G1/S/G2/M phases of the cell cycle (Verheijen et al., 1989; Schlüter et al., 1993). Adherent cell monolayers as well as neurosphere-cryosections showed Ki67+ hNPC (Fig. 3.12B and C). The DAPI+ nuclei showed a normal appearance within the spheres (Fig. 3.12A) without indications of cell death, such as by the presence of nuclear fragmentation. Ki67+ hNPC nuclei were evenly distributed in the sphere without any preference for being located at the outermost margin or at the centre (Fig. 3.12B).
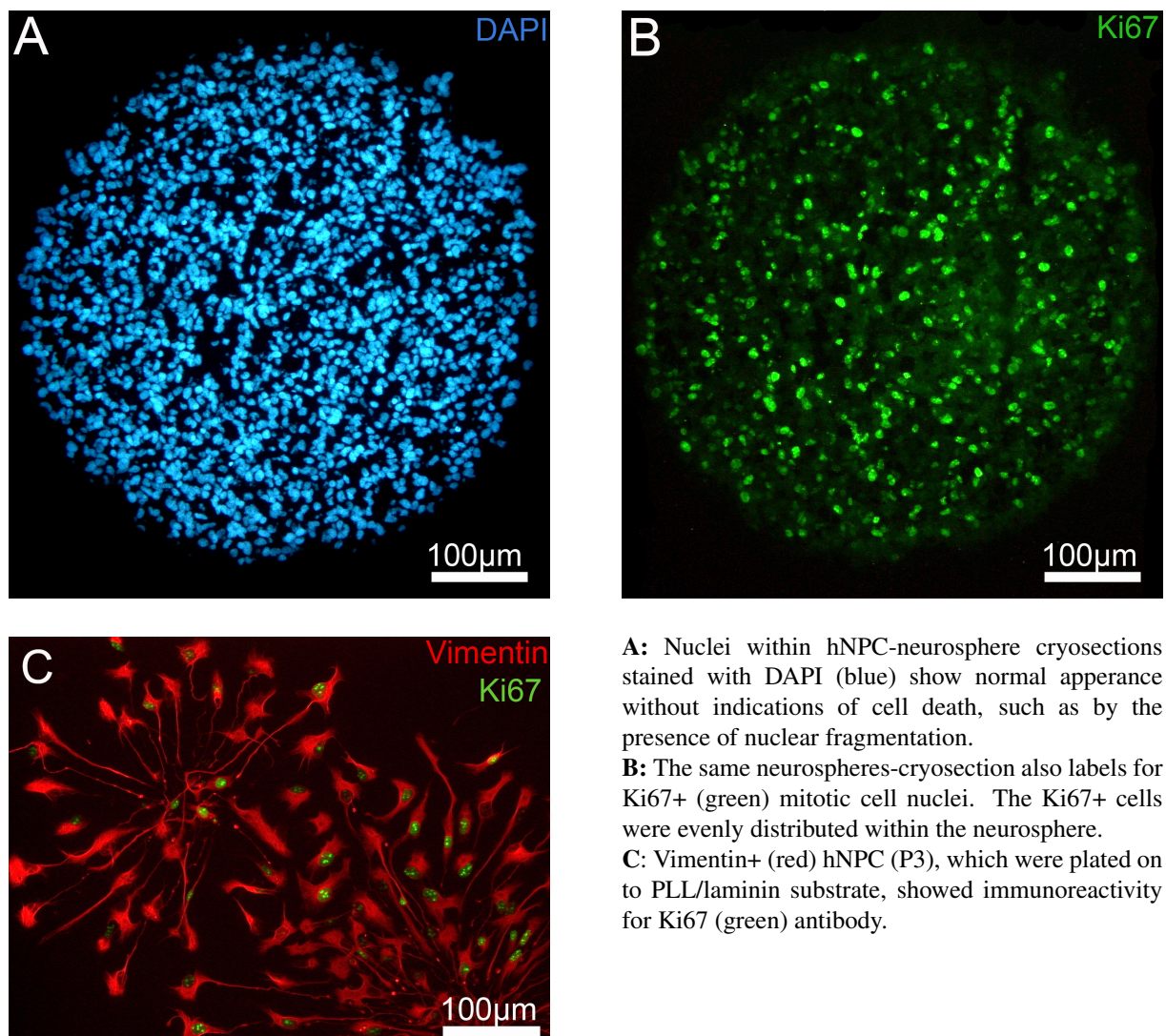
A: Nuclei within hNPC-neurosphere cryosections stained with DAPI (blue) show normal apperance without indications of cell death, such as by the presence of nuclear fragmentation.

B: The same neurospheres-cryosection also labels for Ki67+ (green) mitotic cell nuclei. The Ki67+ cells were evenly distributed within the neurosphere.

C: Vimentin+ (red) hNPC (P3), which were plated on to PLL/laminin substrate, showed immunoreactivity for Ki67 (green) antibody.

Figure 3.12: **Ki67 expression by hNPC.**

3.2.1 Metabolic Assay

To quantify the proliferative activity in hNPC a 2D metabolic assay and a 3D morphological analysis (see chapter 3.2.2) were performed. Thus, *DT* and *r* could be determined.

The metabolic assay measured proliferation of hNPC, which were grown as adherent cell cultures on PLL/laminin substrate. The hNPC (P3) showed a sigmoidal growth curve over the 22 days of measurement (Fig. 3.13A). From day 1-7, growth followed a logarithmic function. In this phase the characteristic *DT* of 1.68 $\pm$ SEM 0.1 days was determined. Between day 17-20 the cell number reached its maximum with $2.5 \cdot 10^6$ cells/ml (i.e. $6.5 \cdot 10^5/cm^2$). Subsequently, the number of cells decreased and measurement was stopped.

Values for *r*, which is reciprocal to *DT* (see chapter 2.4.3) changed over time (Fig. 3.13B). In the logarithmic growth phase, *r* was maximal with values of 0.6/24h (Fig. 3.13B, day 4 and 7). When monolayer cultures of hNPC reached confluency, *r* decreased. Negative values for *r* indicate cell loss (Fig. 3.13B, day 19 and 22).
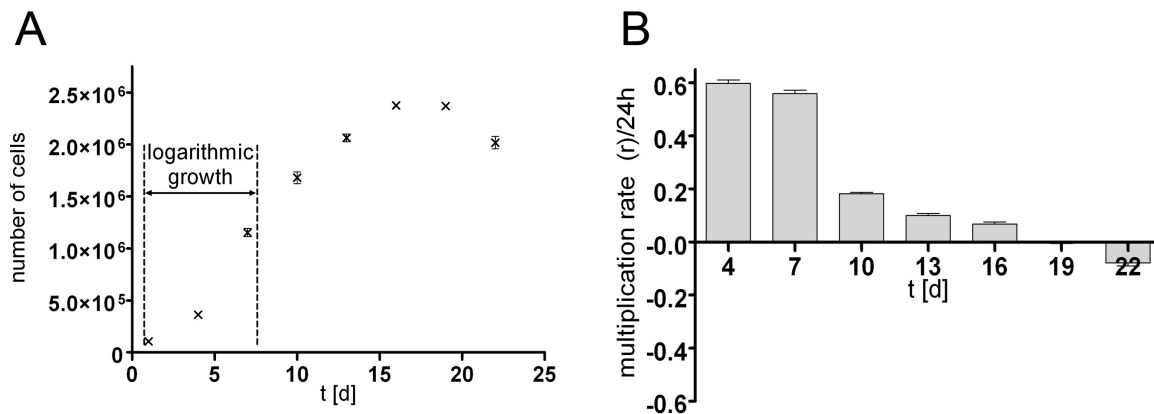
Figure 3.13: **Growth curve of hNPC and decline of multiplication rate in the metabolic assay.**
A: The hNPC (P3) showed a sigmoidal pattern of growth. In the beginning growth could be described by a logarithmic function (*DT* = 1.68 $\pm$ SEM 0.1 days). Between day 17 and 20 there was a maximum with $2.5 \cdot 10^6$ cells/ml. **B**: Multiplication rate (*r*) of hNPC (P3) decreased over time in the metabolic experiment. Values for *r* were highest in the logarithmic growth phase at day 1-7. At day 19 and 22 *r* was negative due to cell decline. Data are means $\pm$ SEM of six independent cultures.

3.2.2 Morphological Assay

The 3D morphological assay performed in this study allowed an estimation of cell proliferation in intact neurospheres. An example of the increase of neurosphere volume over time (as well as the estimated cell number) is demonstrated for one individual hNPC-neurosphere (P3) in Figure 3.14A. The growth curve describes an exponential function, with the neurosphere volume quadruplicating over the 14 day measuring period. All hNPC-neurospheres selected for this experiment followed an exponential function of growth. The hNPC-neurospheres observed in this experiment were selected from both, young (P3) and older (P11) passages.

The volume [mm^3] over time [d] diagram (Fig. 3.14A) did not allow a general conclusion and calculation of a mean DT, because the plotting of data from all hNPC-neurospheres was not possible with this function (see chapter 2.4.3). Therefore a data plot of the difference in volume (ΔV) as a function of mean sphere volume ($\overline{V}_{t1,t2}$) was selected (Fig. 3.14B). A pair of values represents the volume difference of a sphere (ΔV) over the period of time (t_2 - t_1; i.e. 24 hours) in relation to the mean volume of the sphere at time point t_1 and t_2.
Figure 3.14B reflects data from all hNP-neurospheres selected for this experiment. The scatterplot describes a linear function (r^2 = 0.84) with a constant logarithmic increase of sphere volume, i.e. increase in cell number of the spheres. As described earlier (see chapter 2.4.3, formula 9.1) the slope (α) of the regression line represents the exponent of growth with α = 0.1923 $\pm$ 0.007347. Thus, DT resulted from the given formula:

$$DT = \frac{ln2}{\alpha} = 3.46 \qquad\qquad (3.1)$$

The growth curve in the 3D morphological assay described constant logarithmic growth, so that the DT of 3.46 days (i.e. r of 0.28), did not decline over duration of the experiment, in contrast to the calculated DT and r in the 2D metabolic assay.
Distribution of values is not even in diagram 3.14B, because more values were available for small- and middle-sized spheres, varying from 0.03 to 0.13mm^3 in volume. Large spheres, achieving a volume greater than 0.2mm^3, often had to be excluded from the experiment due to their shape change from spherical to ovoid.
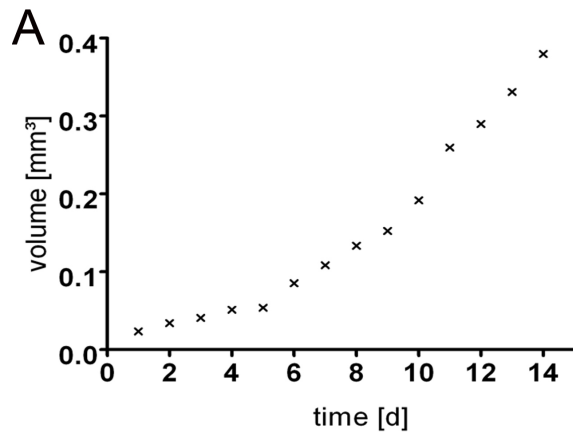
A: The graph shows one hNPC-neurosphere increasing in volume over a time period of 14 days. The function describes exponential growth. The increase of volume was monitored every 24 hours, serving as an indirect measure for the increase in cell number.

B: This dataplot depicts the correlation between the absolute change of the sphere volume and the mean sphere volume for all hNPC-neurospheres (n = 133). The regression line describes a constant logarithmic growth throughout the duration of the experiment (r^2 = 0.84), whereby the slope (α = 0.19) corresponds to a mean doubling time (DT) of 3.46 days.
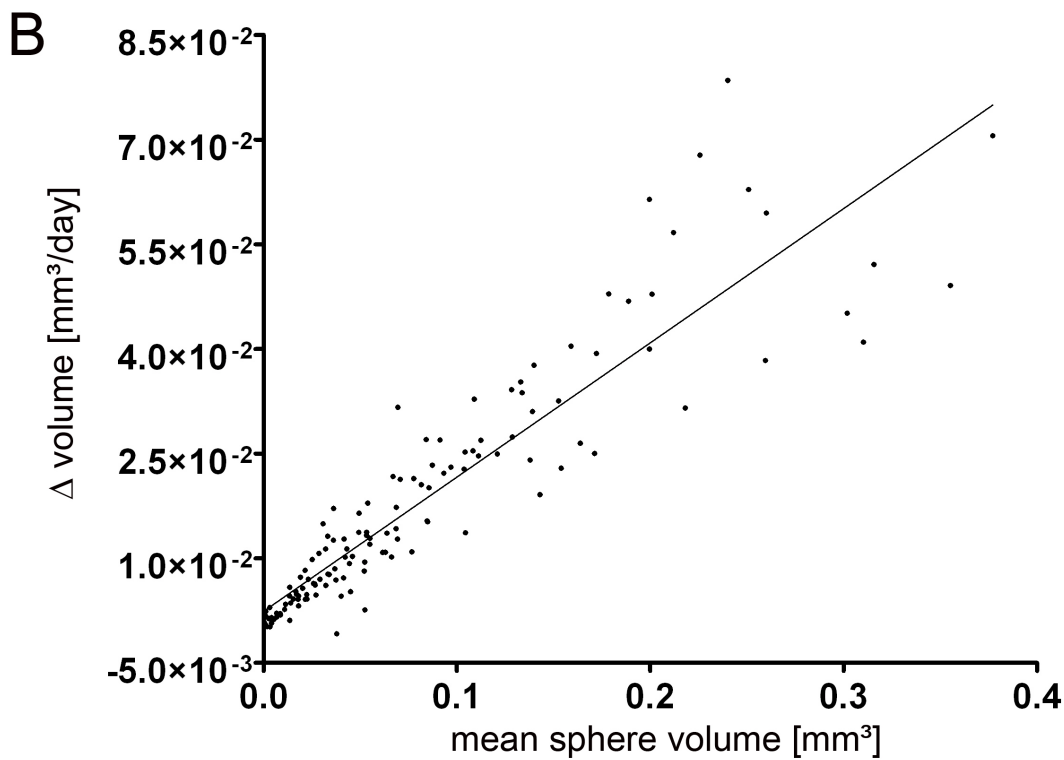
Figure 3.14: **Constant logarithmic growth of all hNPC-neurospheres.**

The volume of spheres and time point of measurement did not influence *DT* critically: the data of the hNPC-neurospheres examined for 14 days in this experiment did not provide a significant correlation for change of *DT* with increase of sphere volume (Fig. 3.15A). Smaller spheres showed no characteristic difference in *DT* compared to larger spheres. There was no significant correlation between *DT* and point in time during the measurement (Fig. 3.15B). Both graphs in Figure 3.15 show continuous variation of *DT*.

The *DT* did not decrease over time, in contrast to the calculated *DT* in the metabolic assay.
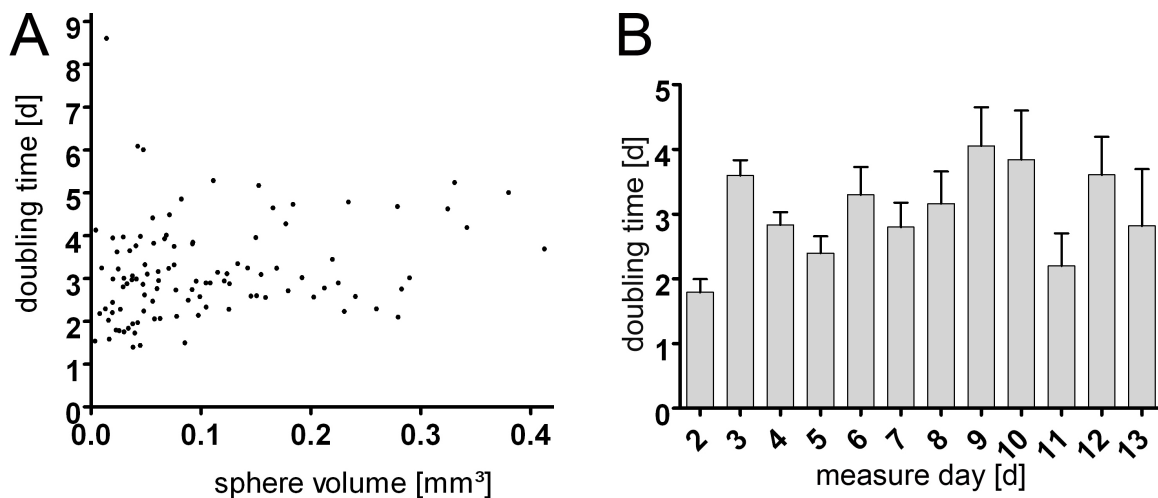
Figure 3.15: **Doubling Time (*DT*) does not correlate with sphere volume (A), or with point in time during the measure period (B)**.
A: Variation of *DT* for single spheres with different volumes.
B: Variation of *DT* for single spheres when measure time [d] proceeded.

3.3 Characterisation of hNP-AC

To generate unipotent aggregates from hNPC capable of giving rise to pure populations of hNPC-derived type I astrocytes (hNP-AC), that are subscribed to comprise CNS regenerative capacity, neurospheres were incubated with the media supplements LIF and BMP4 (Weible and Chan-Ling, 2007) for at least 8 passages.

The next section outlines the contrast in between the hNPC prior to- and after differentiation to hNP-AC. Characterisation of the differentiated cells was performed using the same immunocytochemical- and RT-PCR mRNA-expression analyses as were used for hNPC. The results for hNP-AC will be compared to those obtained for hNPC (see chapter 3.1).

It will be shown, that the expression of stem/progenitor cell-related markers did not significantly change following differentiation to hNP-AC, whereas the proportion of cells expressing astrocyte-related markers increased significantly.

3.3.1 Stem/Progenitor Cell Related Markers in hNP-AC

The hNP-AC were investigated for expression of the stem/progenitor cell-related markers nestin, SOX2, Musashi-1 and CD133, which had already shown to be expressed in a high number in hNPC prior to differentiation (see chapter 3.1.1).

Immunocytochemistry showed that the stem cell markers nestin, SOX2 and Musashi-1 were evenly and ubiquitously distributed within cryosections of the spheres without any preference to being located at the centre- or at the outermost margins of the spheres (Fig. 3.18A, C and Fig. 3.17A). The vast majority of cells migrating out of spheres that had been seeded on to PLL/laminin substrate showed immunoreactivity for nestin (Fig. 3.18B), SOX2 (Fig. 3.18D) and Musashi-1 (Fig. 3.17B). Quantification demonstrated that $89.2 \pm 3.8\%$ of hNP-AC were immunoreactive for nestin, not significantly differing from the percentage of nestin+ cells in hNPC. Similarly, the level of nestin mRNA (Fig. 3.16) was maintained during *in vitro* differentiation from hNPC to hNP-AC and remained unchanged at the different culture passages (Fig. 3.16). The CD133 mRNA expression also showed no change in hNP-AC when compared to hNPC (Fig. 3.16).

SOX2 expression was detected in $88.0 \pm 3.6\%$ of hNP-AC migrating on the PLL/laminin substrate; not significantly different from the proportion of SOX2 expressing cells in hNPC cultures (Fig. 3.25). Similiar to hNPC, the distribution of SOX2 immunoreactivity in hNP-AC was mainly localized to the nuclei (Fig. 3.18D and F). Cells in cryosections of spheres (Fig. 3.18E) as well as migrating cells (Fig. 3.18F) demonstrated co-localization for the stem/progenitor cell
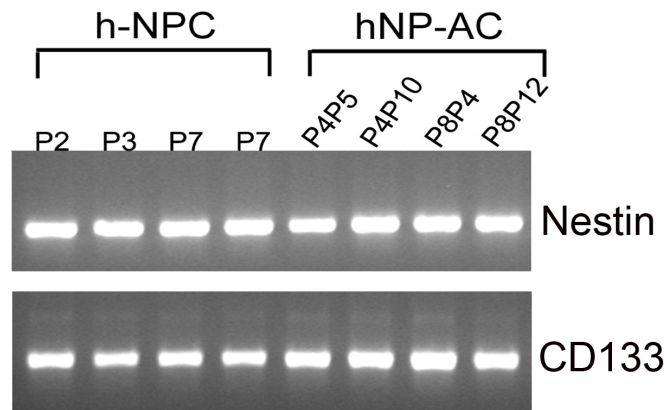
Figure 3.16: **Nestin and CD133 mRNA expression profiles during the BMP4/LIF-mediated differentiation of hNPC to hNP-AC.**
RT-PCR of the expression of nestin and CD133 mRNA for hNPC (four bands on the left) and the differentiated hNP-AC (four bands on the right). There was no significant change in mRNA expression of either mRNA following BMP4/LIF treatment. Samples were selected from different passages of hNPC (P2, P3, P7) and from different passages of hNP-AC (P4P5, P4P10, P8P4, P8P12).

markers nestin and SOX2 in hNP-AC.

Immunoreactivity for Musashi-1 was present in $89.2 \pm 3.8\%$ of hNP-AC migrating out of plated spheres (Fig. 3.17B and Fig. 3.25). Although the quantity of Musashi-1 immunoreactive cells did not significantly change, there was a qualitative change in the staining compared to Musashi-1 immunoreactive hNPC: in hNPC, staining with Musashi-1 antibody showed an even distribution, smoothly filling out the cell (see chapter 3.1.1, Fig. 3.3B), whereas the Musashi-1 staining in hNP-AC appeared more patchy (Fig. 3.17B).
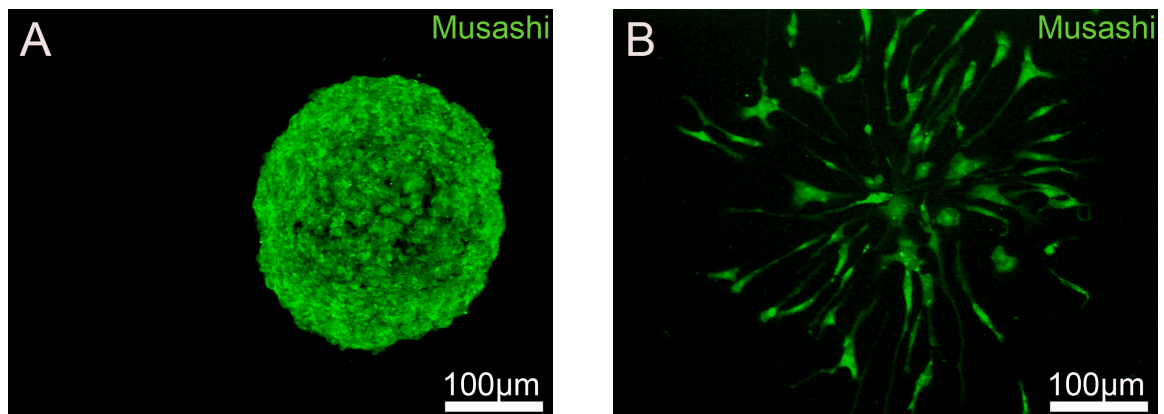
Figure 3.17: **Musashi-1 expression by hNP-AC.**
A cryosection of an hNP-AC sphere (**A**) and single cells migrating over PLL/laminin substrate (**B**) demonstrate immunoreactivity for Musashi-1 (green). Musashi-1+ hNP-AC display a patchy staining pattern (**B**) throughout the cell cytoplasm.
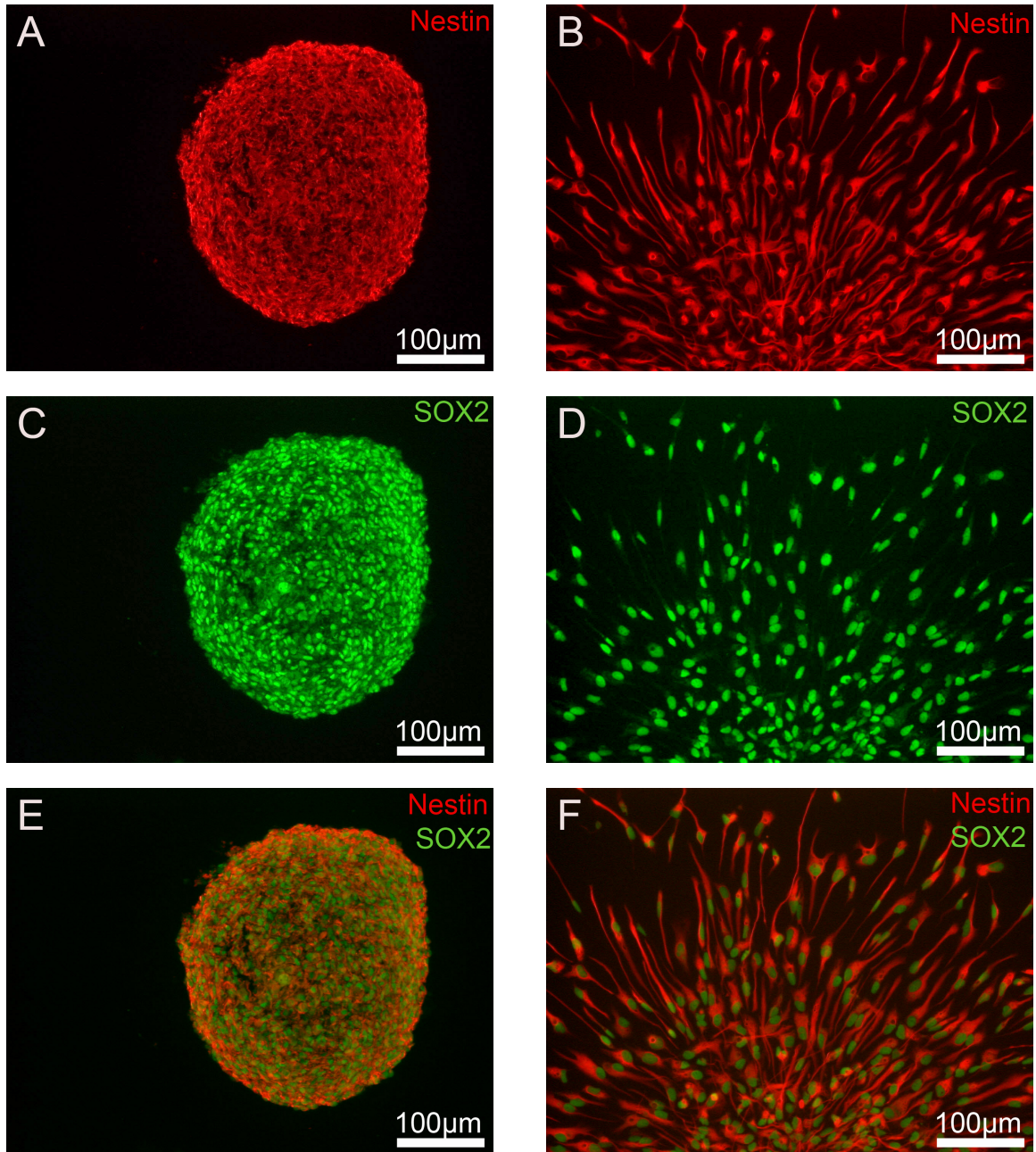
Figure 3.18: **Co-expression of the stem cell markers nestin and SOX2 by hNP-AC.**
A cryosection of a hNP-AC sphere (**A,C,E**) and cells migrating out of spheres plated on to PLL/laminin (**B,D,F**) show immunoreactivity for nestin (red) and SOX2 (green). Both stem cell markers colocalize in hNP-AC cryosections (**E**) and in migrating cells (**F**).

3.3.2 Differentiation Results in a Highly Enriched Population of hNP-AC

Most hNP-AC were immunoreactive for vimentin (92.9 $\pm$ 3.8%) and GFAP (92.5 $\pm$ 3.4%; Fig. 3.20A-F). The values for vimentin+ cells were similar between hNP-AC and hNPC, however the number of GFAP+ hNP-AC was significantly greater than that of hNPC (Fig. 3.25). These observations were supported by RT-PCR: whereas only a thin band of GFAP mRNA was detectable in the hNPC (Fig. 3.19A), a broad band of GFAP mRNA was observed in the hNP-AC. Semi quantitative analysis of GFAP mRNA expression in ratio to the expression of the house keeping gene GAPDH (Fig. 3.19B) resulted in a change, that was significant ($p < 0.05$).

The vimentin+/GFAP+ cells were ubiquitously distributed within cryosections of hNP-AC spheres and when plated on to PLL/laminin substrate adopted a large, polygonal, flattened morphology sometimes with process indicating their orientation of migration away from the position of the plated sphere. Vimentin and GFAP co-localized within the cytoplasm of these cells (Fig. 3.20E and F).
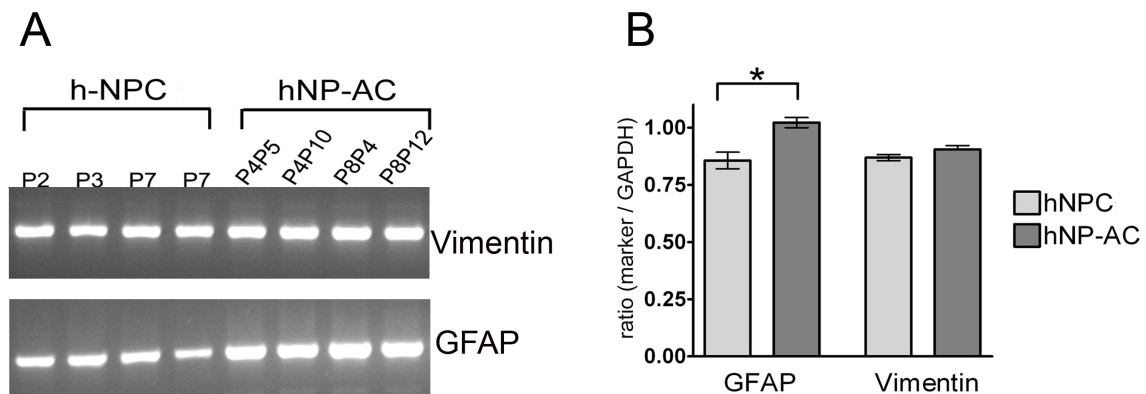
Figure 3.19: **Significant increase in GFAP-mRNA expression by hNP-AC.**
Expression of vimentin and GFAP mRNA is shown for hNPC (**A**, four bands on the left) and the differentiated hNP-AC (**A**, four bands on the right) in comparison. Samples were selected from different passages of hNPC and hNP-AC (as indicated). **A:** Differentiation to hNP-AC resulted in an increase of GFAP mRNA expression. Vimentin mRNA expression did not change after differentiation.
B: Statistical analysis of the marker genes showed a significant increase of GFAP mRNA expression in hNP-AC ($\ast$: $p < 0.05$).
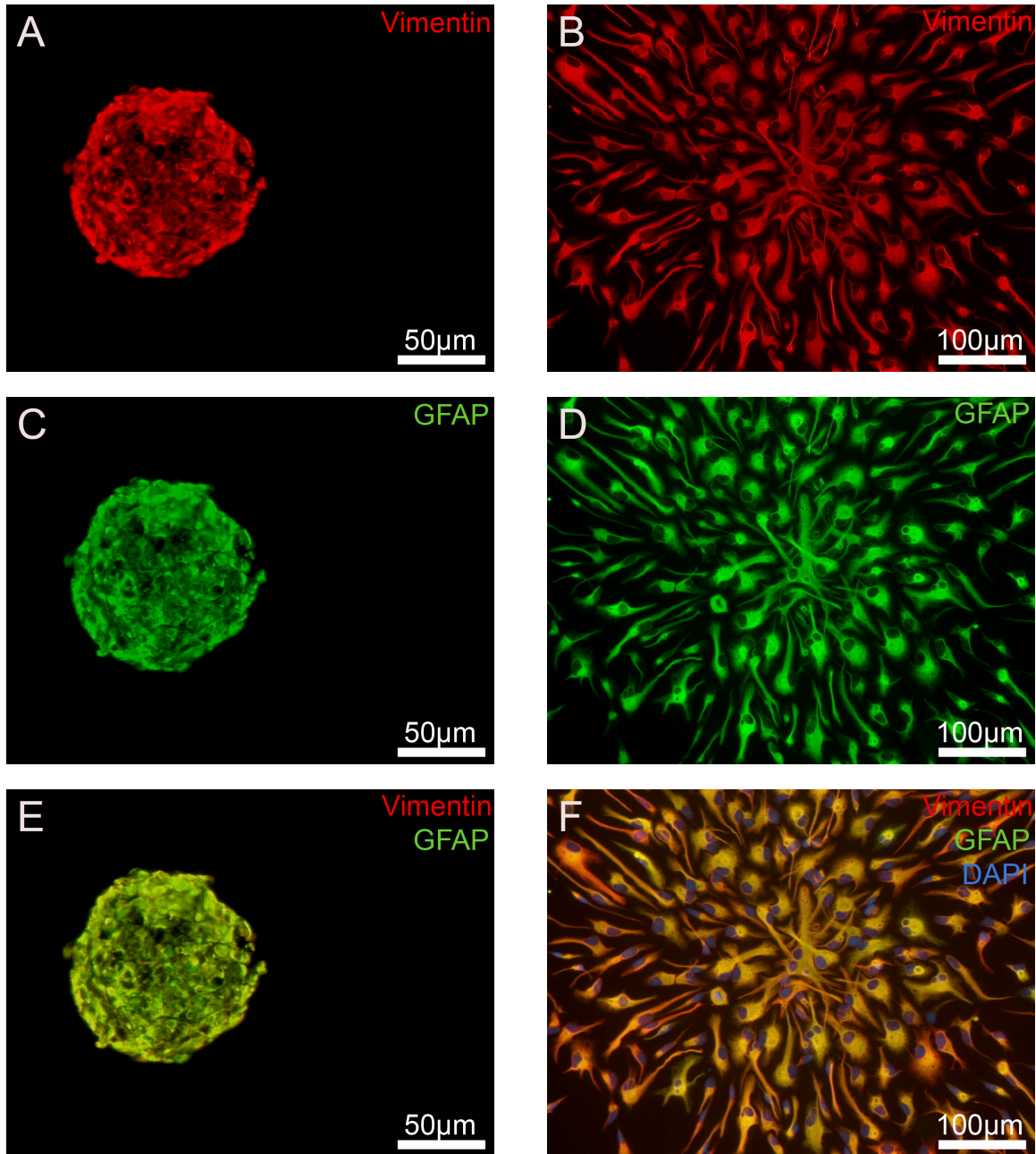
Figure 3.20: **Expression of the astrocyte-related markers vimentin and GFAP in hNP-AC.**
A-F: hNP-AC show immunoreactivity for vimentin (red) and GFAP (green). **A,C**: Vimentin+ (**A**) and GFAP+ (**C**) cells are ubiquitously distributed within a cryosection of a hNP-AC-sphere.
B,D: Vimentin+ (**B**) and GFAP+ (**D**) cells, migrating on PLL/laminin substrate. **E,F**: Colocalization of vimentin and GFAP within a cryosectioned sphere (**E**) and in individual cells migrating on the PLL/laminin substrate (**F**). Cell nuclei were counterstained with DAPI (blue, **F**).

The differentiated hNP-AC also showed immunoreactivity for S100β (Fig. 3.21) colocalizing with vimentin (Fig. 3.21D). The vimentin+/ S100β+ hNP-AC adopted, as described earlier, a polygonal morphology with processes indicating the route of migration away from the plated sphere. Quantification of RT-PCR indicated that S100β mRNA expression remained constant over time in culture, even after differentiation to hNP-AC (Fig. 3.23). However, the cellular distribution of S100ß protein, identified by immunocytochemistry, showed a significant increase from $17.6 \pm 2.1\%$ to $79.4 \pm 1.7\%$ (Fig. 3.25). In addition, cryosections of hNP-AC demonstrated a homogeneous distribution of S100β immunoreactivity (Fig. 3.21A) in contrast to the heterogeneous distribution in hNPC spheres (see chapter 3.1.2, Fig. 3.9A). Furthermore, staining of adherent S100β+ hNPC revealed that the nucleus had an intense fluorescence that allowed its clear visual discrimination from the lower immunoreactivity of the cytoplasm (see chapter 3.1.2, Fig. 3.9D). In contrast, the S100β+ hNP-AC appeared uniformly immunoreactive, with their nuclei hardly distinguishable from the cytoplasm (Fig. 3.21B and C).
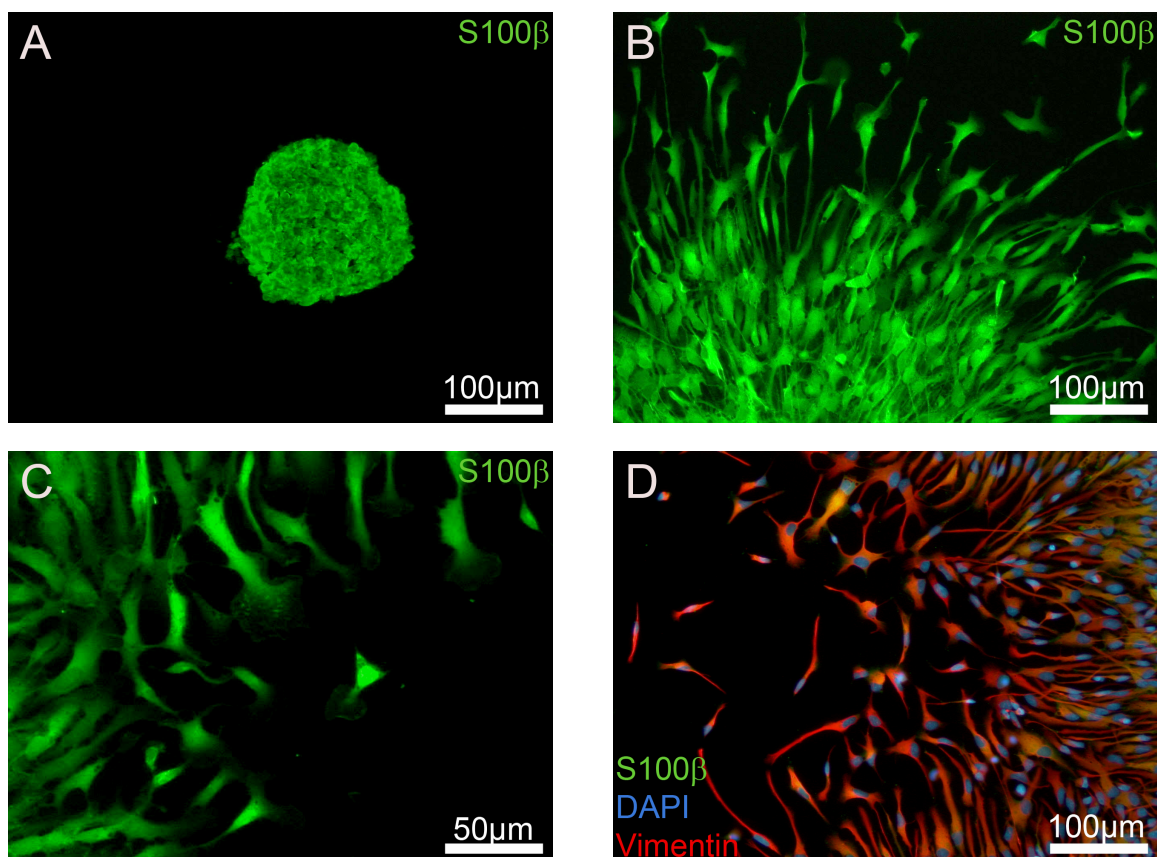
Figure 3.21: **Expression of the astrocyte related markers vimentin and S100β by hNP-AC.**
A: The cryosection of a S100β+ (green) hNP-AC-sphere shows an even and area wide staining pattern. **B, C**: S100β+ hNP-AC migrate out of PLL/laminin plated spheres. The hNP-AC show an uniform staining pattern, such that nuclei could hardly be distinguished from the cytoplasm. **D**: The S100β+ hNP-AC co-express vimentin (red). Nuclei were counterstained with DAPI (blue).

The hNP-AC expressed the CD44 surface antigen on the cell bodies and processes, that adhered to the PLL/laminin substrate showing a distribution consistent with the reported localisation within the plasma membrane (Fig. 3.22B and C; Naor et al., 1997). Almost all CD44+ cells co-expressed GFAP (Fig. 3.22D). The CD44+ cells were ubiquitously localized within cryosections of hNP-AC-spheres with an apparent increase of staining intensity towards the outer margins (Fig. 3.22A). This observation contrasted to immunocytochemical analysis of hNPC, where CD44+ cells were hardly detectable.

The increase of CD44 expression detected by immunocytochemistry Fig. 3.22), was supported by the semi-quantitative RT-PCR analysis that showed a statistically significant increase of CD44 mRNA ($p < 0.05$; Fig. 3.23).
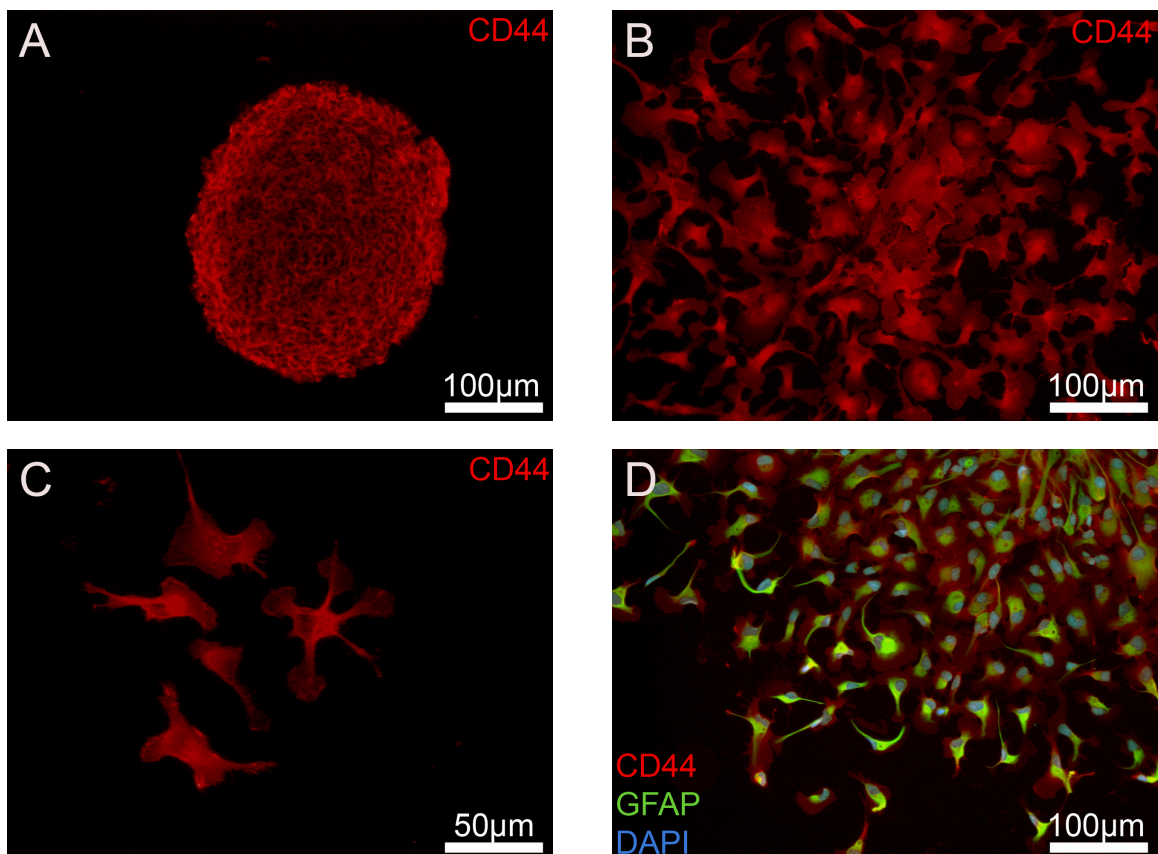
Figure 3.22: **Co-expression of GFAP and the surface marker CD44 by hNP-AC.**
A: CD44+ (red) cells are evenly distributed within a cryosection of a hNP-AC-sphere. **B**: CD44+ (red) cells migrate out of spheres, which had been plated on to PLL/laminin for one day. Cells show a distribution consistent with the reported localisation within the plasma membrane. **C**: Higher magnification of CD44+ (red) hNP-AC visualizes their stellate cell processes, which expanded at their tips as they spread over the laminin-coated substrate. **D**: All CD44+ (red) hNP-AC co-express GFAP (green). Nuclei were counterstained with DAPI (blue).
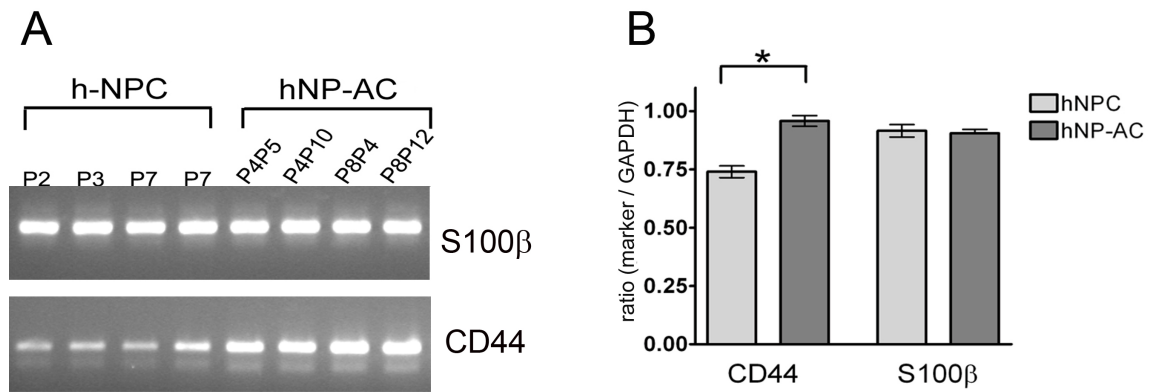
Figure 3.23: **Increase in CD44-mRNA expression following differentiation to hNP-AC.**
A: Expression of S100β- and CD44 mRNA is shown for hNPC (**A**, four bands on the left) and the differentiated hNP-AC (**A**, four bands on the right). Samples were selected from different hNPC and hNP-AC culture passages (as indicated). There was an increase of CD44 mRNA expression in hNP-AC compared to hNPC, whereas the S100β-mRNA expression profile did not change. **B**: Statistical analysis of marker genes shows a significant increase in CD44 mRNA expression in hNP-AC compared to hNPC ($p < 0.05$).

In order to characterise the small population of cells that were negative for markers of the astrocytic lineage, immunocytochemistry for oligodendroglial and neuronal cell lineage markers was performed.

No cells were immunoreactive for the oligodendroglial antigens O1, O4 or GalC. TuJ1 and MAP2ab immunocytochemistry was used to identify residual cells of the neuronal lineage. Immunocytochemistry of cryosections failed to demonstrate any TuJ1+ or MAP2ab+ neurons. However, occasional migrating TuJ1+ (Fig. 3.24A and B) and MAP2ab+ bipolar cells could be found amongst the differentiated hNP-AC.
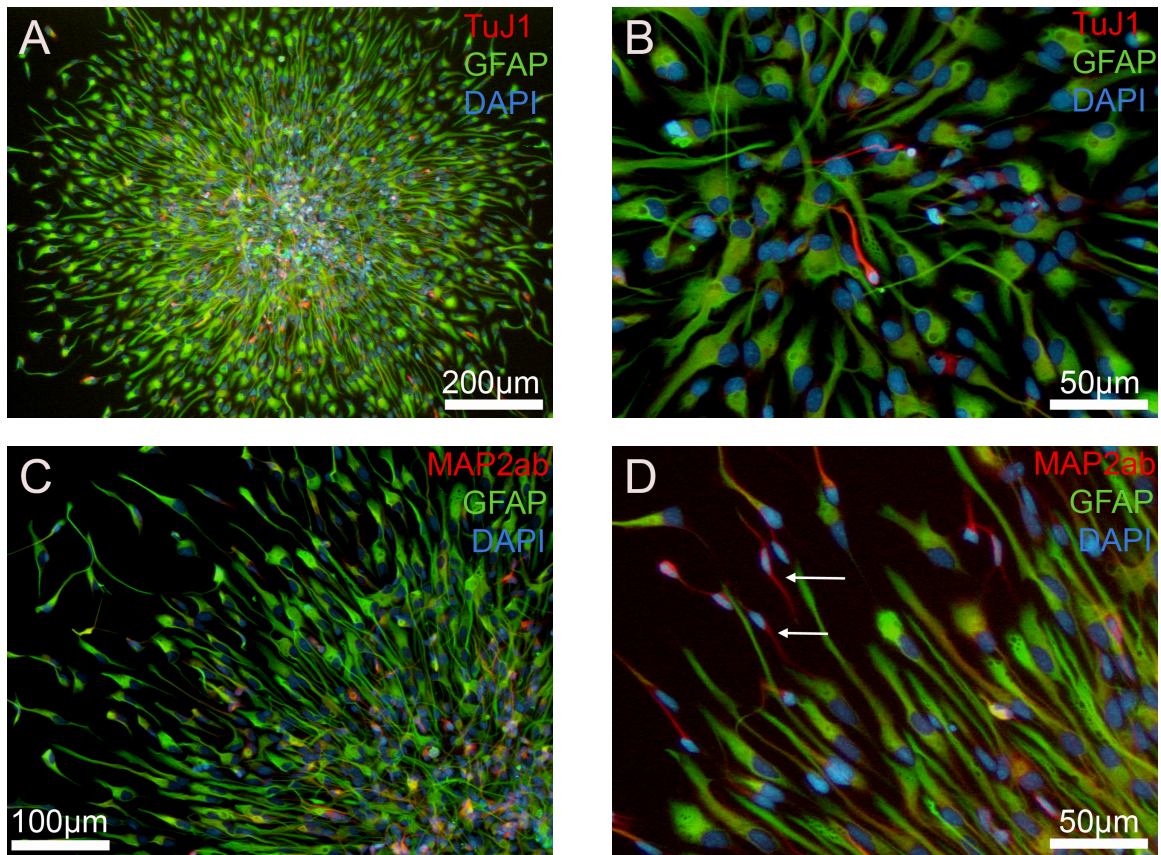
Figure 3.24: **Following differentiation to hNP-AC, only a few cells express markers for neuronal lineage.**
The majority of hNP-AC (P4P12), migrating out of PLL/laminin plated spheres, show immunoreactivity for GFAP antibody (green, **A-D**). Morphology of GFAP+ cells often resembles astrocytic cells. Only a few residual small sized, bipolar cells show immunoreactivity for TuJ1 (red, **A,B**) or MAP2ab (red **C,D**). Nuclei were counterstained with DAPI (blue).

In summary - following differentiation - hNP-AC continued to express stem/progenitor cell-related antigens such as nestin, SOX2 and Musashi-1 (Fig. 3.25, see columns on the left). Furthermore hNP-AC showed a clear and statistically significant increase of astrocyte-related antigens such as vimentin, GFAP, S100β (Fig. 3.25, columns on the right) and CD44 co-expression in all GFAP+ cells.

Only a few residual TuJ+ or MAP2ab+ neurons could be detected within the hNP-AC population. A table summarizing the immunohistochemical phenotypes is attached in the appendix (see additional data, Fig. 9.1).

Concluding, the investigation shows that the hNPC had successfully elaborated towards a highly enriched population of cells constituting astrocytic lineage characteristics, termed hNP-AC.
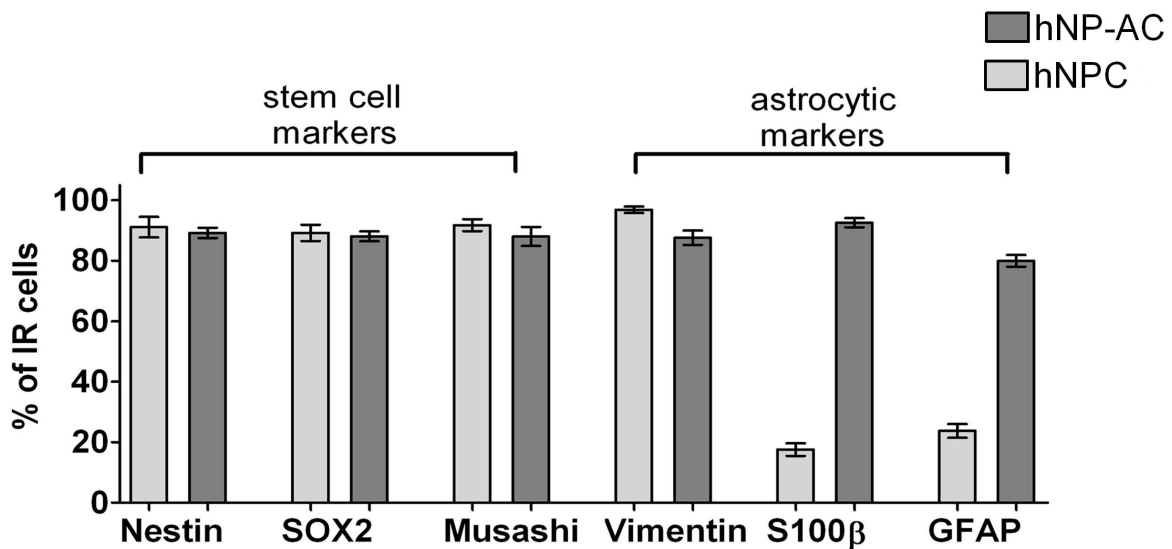
Figure 3.25: **Overview of immunoreactivity profile of hNP-AC compared to hNPC.**
The diagram compares percentages of hNPC (light grey) and hNP-AC (dark grey) plated on to PLL/laminin for one day that were immunoreactive for the stem/progenitor cell-related markers nestin, SOX2 and Musashi-1 as well as the astrocyte-related markers vimentin, S100β and GFAP. Data are means $\pm$ SEM. Expression profile data of hNPC are identical to those in Figure 3.11 in chapter 3.1.2.

3.4 Proliferative Activity of hNP-AC

Proliferation of hNP-AC was investigated to find out whether the expansion rate differed between hNPC and differentiated hNP-AC. To determine the *DT* of hNP-AC the 2D metabolic assay and 3D morphological analysis were performed as described above for hNPC (see chapter 3.2). In the following it will be shown that both assays resulted in a significantly decreased *DT* in hNP-AC, when compared to *DT* of hNPC.

There were Ki67+ cell nuclei present in long term cultures (P4P13) of hNP-AC (Fig. 3.26B and C). The Ki67+ nuclei could also be detected in cryosections of hNP-AC-spheres, where they were distributed evenly throughout the spheres. DAPI staining visualized normal shaped nuclei within the central part of the spheres without indications of cell death (i.e the presence of nuclear fragmentation). (Fig. 3.26A and B). The black holes in the sphere, where no DAPI+ nuclei can be detected (Fig. 3.26A), probably result from cryo-preservation artefacts.
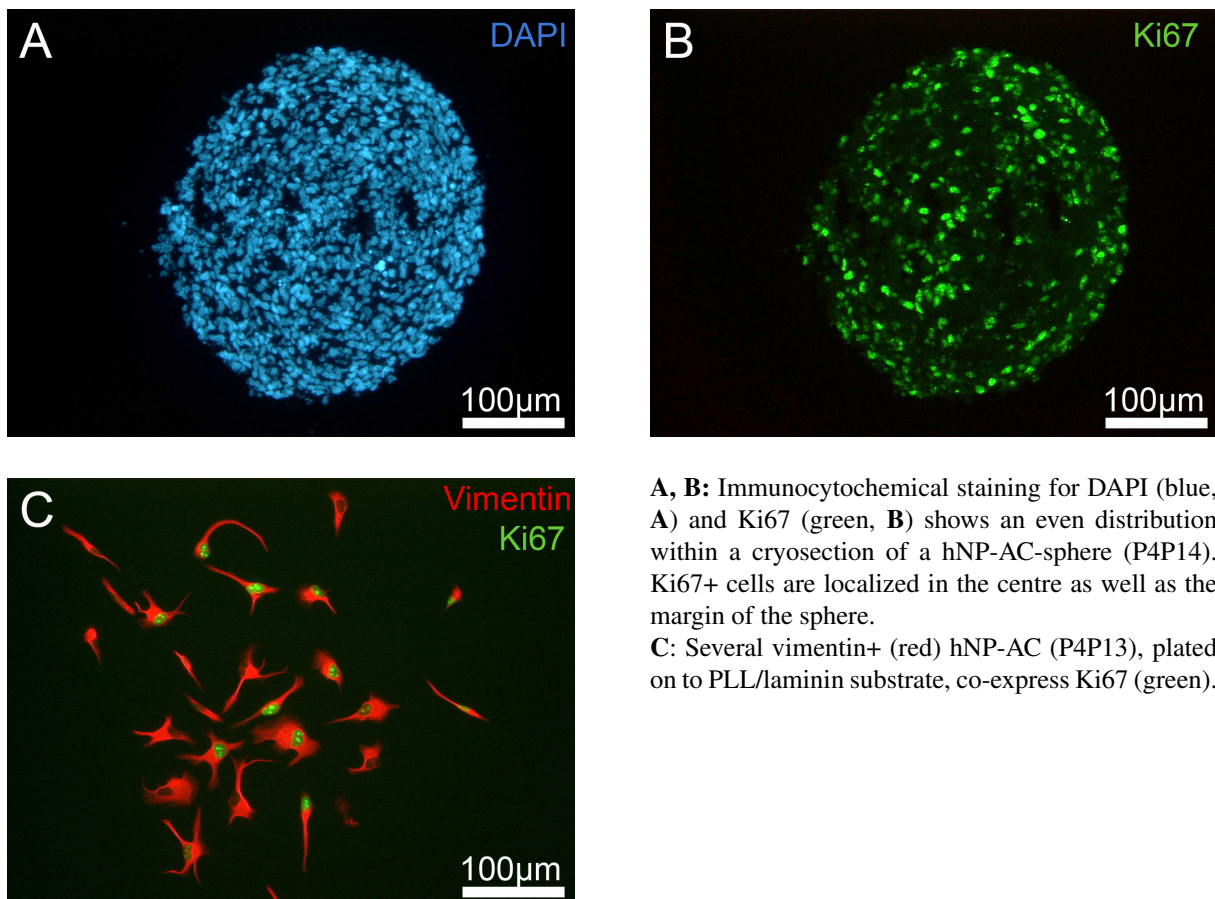
A, B: Immunocytochemical staining for DAPI (blue, **A**) and Ki67 (green, **B**) shows an even distribution within a cryosection of a hNP-AC-sphere (P4P14). Ki67+ cells are localized in the centre as well as the margin of the sphere.
C: Several vimentin+ (red) hNP-AC (P4P13), plated on to PLL/laminin substrate, co-express Ki67 (green).

Figure 3.26: **Ki-67 expression by hNP-AC.**

3.4.1 Metabolic Assay

The metabolic assay measured proliferation of hNP-AC, which were grown as adherent cell cultures for 22 days. The graph in Figure 3.27A includes mean values of 6 independent cultures. From day 1-4, growth of hNP-AC described a logarithmic function with its characteristic DT. From day 5-16 the increase of cell number was constant, reaching a maximum of $1 \cdot 10^6$ cells/ml (i.e. $2.6 \cdot 10^5$cells/cm^2). Later the amount of cells declined and measurement was determined. The diagram 3.27B shows 6 mean values for r of adherent hNP-AC (P4P8) with increasing time. Values for r decreased when hNP-AC-monolayers reached confluency. Negative values for r at day 19-22 describe reduction of cells. This growth pattern was similiar to that for hNPC (see chapter 3.2.1).

Statistical analysis with the Student's t-test showed a significant difference ($p < 0.001$) in mean DT of hNP-AC during the logarithmic growth phase ($3.2 \pm$ SEM 0.06d) in comparison to that for hNPC ($1.68 \pm$ SEM 0.03d).
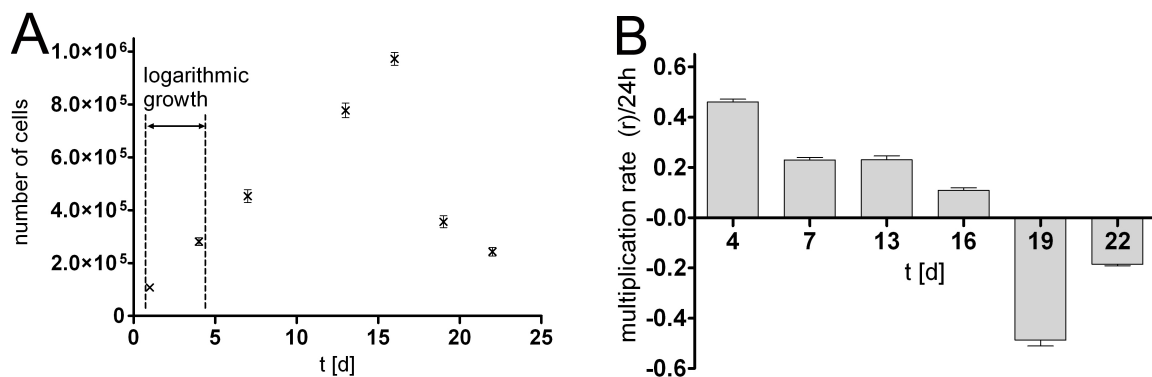
Figure 3.27: **Proliferation of hNP-AC in the metabolic assay.**
A: Proliferative activity of the hNP-AC (P4P8) was observed for 22 days using the metabolic assay. Day 1-4 describe a logarithmic growth ($DT = 3.2 \pm$ SEM 0.06d). When hNP-AC monolayers became confluent, proliferation slowed down and after some time, a reduction of cell number was detectable. **B:** The values for r of hNP-AC (P4P8) decrease over time in the metabolic experiment with maximum r in the logarithmic growth phase at day 1-4. At day 19-22 r is negative due to reduced cell numbers. Data represent means $\pm$ SEM of six independent cultures.

3.4.2 Morphological Assay

To determine proliferation of hNP-AC under sphere culture conditions, an additional estimation of the growth rate with the morphologic assay was performed. As described before the calculation of DT required a volume difference (ΔV) over mean cell volume ($\overline{V}_{t1,t2}$) data-plot (Fig. 3.28).
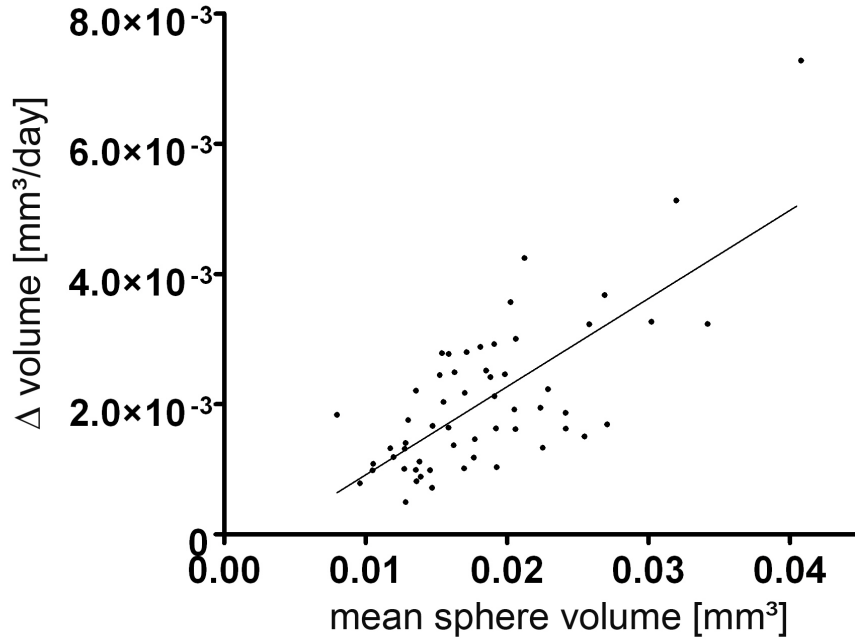
Figure 3.28: **Data-plot to calculate DT of all hNP-AC-spheres using the morphological assay**.
The graph shows data plotted from all hNP-AC-spheres (n = 57). The linear function describes constant logarithmic growth within the duration of the experiment (r^2= 0.52). The slope (α = 0.1355) of the regression line corresponds to a DT of 5,1d.

The investigated hNP-AC spheres showed a similar growth pattern. The scatter-plot describes a linear function ($r^2 = 0.52$) with constant logarithmic increase in volume of spheres, i.e. increase in cell number of spheres. As described earlier (see chapter 2.4.3, equation 9.1) the slope (α) of the regression line represents the exponent of growth with $\alpha = 0.1355 \pm 0.01750$.
A DT with

$$= \frac{ln2}{\alpha} = 5.1 \tag{3.2}$$

days resulted, i.e. r of 0.19 days. The growth curve in the morphological assay described a constant logarithmic growth, so that there was no change of DT (i.e. r) with increasing time in contrast to r in the metabolic assay.

In support of the metabolic assay, the morphological-based calculation of hNP-AC *DT* (5.1 ± 0.19d) was significantly slower than that of the hNPC (3.46 ± 0.28d; $p < 0.001$).

There was no apparent correlation between DT and the increase of sphere volume (Fig. 3.29A), nor with the advancement of time (Fig. 3.29B). A continuous variation of *DT* within the measuring period was observed, giving no indication of a linear correlation. Small spheres demonstrated similar *DT* to larger spheres.
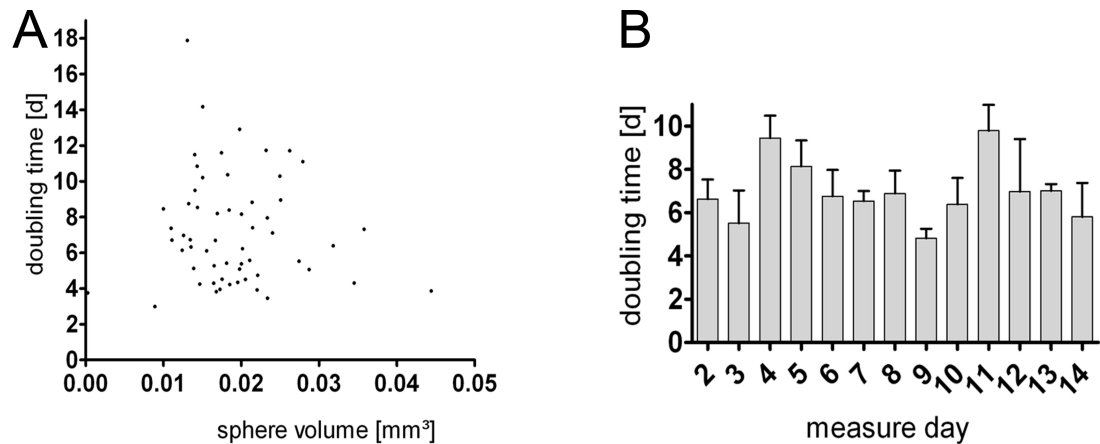
Figure 3.29: *DT* **does not correlate with sphere volume, or with point in time in the measuring period**.
The *DT* showed no significant correlation with volume of the spheres or with progress in time within the 14 day experiment. There was a continous variation in *DT*. **A**: Variation of *DT* for single spheres at different volumes, **B**: DT of single spheres at different measuring days within the experiment.

4 Discussion

In the present study the following questions were addressed:

I) To what extent has the *in vitro* differentiation process altered the cellular characteristic in hNP-AC?

II) Does the differentiation of hNPC to hNP-AC alter their proliferative activity?

First, the present results confirm that the hNPC demonstrate neural progenitor cell characteristics. Results were obtained using RT-PCR and double immunofluorescence for particular markers. The differentiation of hNPC to hNP-AC provoked a significant increase in the proportion of cells labelled with astroglial markers, indicating the generation of a highly enriched population of astrocytes.

Second, differentiation was also accompanied by a decrease in proliferative activity, as indicated by the 2D metabolic assay and the 3D morphological analysis.

4.1 Characterisation of hNPC and hNP-AC

Populations of hNPC were characterised prior to- and after *in vitro* differentiation to hNP-AC by investigating the proportion of cells expressing stem/progenitor cell-, astrocyte-, neuronal- and oligodendroglial lineage-related markers.

4.1.1 Methods for Identification of Cellular Content

Double immunofluorescence immunocytochemistry and RT-PCR were applied to observe protein- and mRNA-expression profiles in both hNPC and differentiated hNP-AC.

Immunocytochemistry is a well established method for cell characterisation. Especially the cell morphology and marker distribution can be easily observed with this method. Neurospheres were plated on to PLL/laminin-coated substrates and processed for double immunofluorescence. The range of cellular phenotypes were quantified in the migrating cell monolayers, which formed around the neurospheres, according to quantification methods described earlier (Svendsen et al., 1998; Ostenfeld and Svendsen, 2004; Piao et al., 2006). In this study, a growth and spreading period of only 24 hours was selected, because the greater cell density resulting

from longer growth periods, generated difficulties for accurate cell counting (Carpenter et al., 1999).

It has been reported that neuronal markers are down-regulated following trituration to a single cell suspension before seeding, in contrast to seeding intact spheres (Svendsen et al., 1998). Therefore, the present analysis was performed by maintaining constant seeding conditions for intact spheres. Furthermore, the central parts of neurospheres were analysed using sphere cryosections similar to analyses described earlier (Svendsen et al., 1998; Kim et al., 2006; Piao et al., 2006; Weible and Chan-Ling, 2007).

Even though analysis with immunocytochemistry represents an ideal method to identify the cellular content, only the protein expression level can be determined. Therefore additional analyses for the stem/progenitor cell-related markers CD133 and nestin were performed using RT-PCR for mRNA expression profiles. In an attempt to better define the mechanism of differentiation from hNPC to hNP-AC, the investigation of the astrocytic markers GFAP, vimentin, CD44 and S100β was also extended to the mRNA level.

However, it should be considered that an interpretation problem remains concerning data from mRNA expression analysis in contrast to those from immunocytochemistry. It is not clear, whether a low mRNA expression level represents a general low expression of the investigated mRNA across the whole population, or whether a few cells expressing high levels of mRNA may be scattered throughout a generally non-expressing population. Thus, it remains essential to regard the results of each method in relation to each other.

4.1.2 Stem/Progenitor Cell-Related Markers in hNPC

The first important stage of this investigation was to confirm the neural progenitor cell characteristics of the hNPC. Markers previously reported to label neural stem/progenitor cells were used to show the presence of neural progenitors. Immunocytochemistry of the monolayers that had emerged from plated hNPC-spheres showed $91.0 \pm 3.4\%$ nestin-, $91.8 \pm 2.0\%$ Musashi-1- and $89.2 \pm 2.7\%$ SOX2- immunoreactive cells. These proportions indicate that the hNPC-spheres were largely composed of non-committed progenitor cells.

Nestin is expressed in the majority of human first trimester-derived forebrain- and spinal cord neurospheres (Carpenter et al., 1999; Wright et al., 2003; Piao et al., 2006). The high proportion of nestin protein expression relates to the strong bands of nestin mRNA observed in different hNPC passages. In addition, the cryosections of hNPC-spheres confirmed nestin expression throughout the spheres. This supports findings by others in which the majority ($> 95\%$) of human neural progenitors within neurospheres were reported to be positive for nestin (Svendsen

66

et al., 1998).

Co-expression of the markers nestin and SOX2 was present in 82.7 ± 3.4% of hNPC. SOX2 expression has been most commonly associated with non-committed stem and precursor cells in the developing nervous system (Fong et al., 2008). The 6.9 ± 2.8% of hNPC which were not immunoreactive for either nestin or SOX2 may include spontaneously differentiated- cells or apoptotic cells, whose nuclei were not yet degraded and may still be visible with DAPI staining.

The evolutionarily conserved, neural RNA-binding protein Musashi-1 functions in maintenance of stem cell fate and differentiation by repressing particular mRNA translation (Good et al., 1998; Okano et al., 2002). The hNPC in the present study showed 91.8 ± 2.0% immunoreactivity for Musashi-1, providing further evidence of a high proportion of undifferentiated and proliferative hNPC.

The hNPC also expressed CD133 mRNA, that has been attributed to *in vitro* neurosphere initiating- as well as to self-renewal capacity and was initially regarded as a "new stem cell marker" (Uchida et al., 2000; Piao et al., 2006).

It has been reported that passage number influences certain properties of *in vitro* propagated neurospheres (Svendsen et al., 1998), Piao et al. (2006). Therefore, the expression of a number of markers was investigated in young and old cell populations with low and higher passage numbers. However, in the present study the mRNA expression profiles and the immunocytochemical phenotypes of hNPC remained constant in various passages tested.

4.1.3 The hNPC Represent a Heterogeneous Cell Population

The expression of the stem/progenitor cell-related markers was observed in the majority of hNPC, despite their heterogeneous cell morphologies that developed after plating on to PLL/laminin for 24h. The range of morphological phenotypes of cells migrating out of the spheres included large flat cells, smaller bipolar and multipolar cells similar to observations of others (Piper et al., 2001; Piao et al., 2006; Weible and Chan-Ling, 2007).

Subpopulations of hNPC expressed the neuronal markers TuJ1 and MAP2ab and others expressed the glial markers GFAP, vimentin, $S100\beta$ and CD44. The expression of glial and neuronal markers has also been reported in sub-populations of isolated human foetal neural cells that were not cultured as neurospheres (Piper et al., 2000; Svendsen et al., 1997) confirming thereby that the heterogeneity of hNPC neurospheres was not caused by preparation artefacts, but rather to the heterogeneity of the source tissue (Piao et al., 2006). The expression of stem/progenitor cell-related markers and neuronal or glial markers in the present investigation indicates a mixture of stem/progenitor- as well as immature neuronal- and glial cell popula-

tions in hNPC cultures. In addition, Weible and colleagues described that contact with laminin on coverslips induced the migration of foetal spinal cord hNPC with many of them adopting a flat, polygonal, epithelial cell-like morphology, resembling type I astrocytes grown *in vitro* (Svendsen et al., 1998; Weible and Chan-Ling, 2007). In support of this, the present work demonstrated the rapid attachment of whole neurospheres to PLL/laminin coated substrate with migrating cells adopting glial cell-like morphologies (see chapter 3.1.2, Fig. 3.8).

The neuronal markers, TuJ1 and MAP2ab, also labelled some cells in the hNPC, especially those with small, intensely DAPI-stained nuchlei, which have been suggested to represent immature neuronal cells (Weible and Chan-Ling, 2007). TuJ1 and MAP2ab-positive cells were also identified in the hNPC-cryosections. MAP2ab antibody has been found to label the dendritic processes and cell bodies of more mature neurons arising from spheres (Riederer and Matus, 1985).

The annular distribution of MAP2ab+ cells was surprising (see chapter 3.1.2, Fig. 3.4C). One might speculate that the cells located at the outermost margin of the neurosphere were exposed to different environmental conditions than those in the centre, thus providing a stronger drive to differentiation into MAP2ab+ neurons. This suggestion agrees with a hypothetical model about neurosphere size and maturation level in neural progenitor/stem cells (Suslov et al., 2002). Some MAP2ab+ cells were able to grow on top of other cells (see chapter 3.1.2, Fig. 3.4D). Interestingly, the other cells were often found to be GFAP-immunoreactive. Such behaviour of MAP2ab+ cells has also been observed by others (Svendsen et al., 1998). Thus, hNPC-derived immature astrocytes seemed to provide an attractive substrate for the migrating immature neurons in this study.

The identification and quantification of the sub-population expressing glial markers was a matter of particular interest in this study. Detailed cell counting of immunoreactive cells showed that hNPC were composed of populations of cells that were vimentin+ ($96.8 \pm 1.1\%$), GFAP+ ($23.7 \pm 2.3\%$) and S100β+ ($17.6 \pm 2.1\%$). These proportions remained relatively constant at different passage numbers. In support of this, the mRNA expression profile of vimentin, GFAP and S100β remained also constant.

The distribution of GFAP+, S100β+ and vimentin+ hNPC cryosections appeared random. This is in contrast to other reports, which described a tendency for cells in the central region in sphere cryosections to express a predominantly astroglial phenotype (GFAP+, S100β+ and vimentin+) and for only few of the cells at the periphery to express these markers (Kim et al., 2006; Weible and Chan-Ling, 2007). It is possible that the source tissue (i.e human foetal brain) of the investigated hNPC caused the different marker distribution in the neurosphere to that described by

others.

The Ca^{2+} binding protein S100β modulates the assembly and disassembly of microtubules and intermediate filaments, such as GFAP and vimentin (Bianchi et al., 1993). It has been shown *in vitro* by double immunofluorescence that during cytoskeletal rearrangement, the S100β protein remains associated with the rearranged GFAP and vimentin intermediate filaments (Sorci et al., 1998). This group observed a preferential association of S100β with GFAP and vimentin near the nucleus. The immunocytochemical staining pattern in this study showed a similar distribution of S100β in hNPC with a greater intensity of signal near the nucleus, which could be clearly distinguished from the rest of the cytoplasm (see chapter 3.1.2, Fig. 3.9B). This S100β staining pattern changed following differentiation to hNP-AC (see beneath, chapter 4.1.4).

The RT-PCR demonstrated thin bands of CD44 mRNA that could be detected in hNPC extracts at different culture passages. CD44, which has been reported to identify early astrocytic differentiation (Vogel et al., 1992; Moretto et al., 1993; Liu et al., 2004) was hardly detectable with immunocytochemistry in younger passages, indicating that the proportion of this transmembrane protein, was extremely rare, but however present in the mRNA cellular level.

In this study, the potential for spontaneous differentiation could be confirmed for cells of the neuronal and astrocytic lineage, but not for oligodendroglial cells. Although, the migrating hNPC around the spheres were immunoreactive for astrocytic and neuronal markers, no immunoreactivity for the oligodendroglial markers O1, O4 and GalC could be detected. All of these antigens are found in oligodendrocytes during maturation (Sommer and Schachner, 1981; Bansal et al., 1989). The limited incidence of foetal human neural precursors spontaneously differentiating to an oligodendroglial lineage has also been reported by other authors (Svendsen et al., 1998; Carpenter et al., 1999; Quinn et al., 1999; Armstrong et al., 2000; Uchida et al., 2000; Wachs et al., 2003; Piao et al., 2006).

Several strategies have already been performed to increase oligodendroglial development in cultures of foetal human neural cells. Piao and colleagues report that the rarity of O4+ cells ($< 1\%$) could be slightly increased ($< 2\%$), when plateled-derived growth factor (PDGF) was added to the medium (Piao et al., 2006). Others reported a dose-dependent increase of O4+ cells following triiodothyronine (T3) hormone treatment (Murray and Dubois-Dalcq, 1997; Fritsche et al., 2005). An increase of oligodendroglial marker expression by neural stem/progenitor cells has also been observed after withdrawal of growth factors and in the presence of 1% FCS (Wachs et al., 2003).

There are various attempts to explain the scarcity of *in vitro* oligodendroglial differentiation including the suggestion that stem cells do not readily differentiate towards that lineage, or markers of human oligodendrocytes are inadequate both *in vivo* and *in vitro* (Uchida et al.,

2000). Another hypothesis describes that oligodendrocyte precursors may be capable of cell division for only a certain period of time and then be lost from the cultures during the extended periods of growth (Svendsen et al., 1998). All these reports are consistent with the present findings. Some oligodendrocytes (6.0 ± 4%) developed in differentiation studies of our group from young hNPC cultures after withdrawal of growth factors EGF, bFGF and replacement with PDGF-AA (20 ng/ml) and T3 hormone-containing B27 (1:50 vol:vol; Führmann et al., 2010a).

In conclusion, several possible explanations for the cellular heterogeneity of neurospheres have been described in literature. One explanation is that the cellular composition of human neurosphere cultures differs as a result of regional heterogeneity of source tissue (Piao et al., 2006). Another explanation is that different types of clone-forming stem- or progenitor cells might be present in the neurospheres with distinct developmental potential such as different response to the growth factors present in the culture medium (Suslov et al., 2002).
In aggreement with these explanations, the hNPC used in the present study contained heterogeneous cell populations, consisting of non-commited precursors as well as committed glial and neuronal cell populations at varying stages of maturation.

4.1.4 Differentiation Leads to a Highly Enriched Population of hNP-AC

The astrocytic sub-population in hNPC seemed to be an attractive surface for neurites to grow on (see chapter 3.1.2, Fig. 3.4D). Since differentiation of rat embryonic neural precursors to astrocytes prior to implantation in spinal cord microlesions has been shown to promote recovery by supporting axonal regeneration (Davies et al., 2006), we decided to epigenetically modify the hNPC with the media supplements BMP4 and LIF, according to already established protocols (Weible and Chan-Ling, 2007). It has been shown, that the combination of BMP4 and LIF reduces the proportion of oligodendroglial and neuronal cells, while increasing the proportion of GFAP immunoreactivity in human and rat neural progenitors (Bonni et al., 1997; Liu et al., 2004; Weible and Chan-Ling, 2007). The data obtained in this study are consistent with previous observations, which together attribute the astroglial lineage commitment to the synergistic effects of BMP4 and LIF.

LIF, a member of the interleukin-6 family acts through the gp130 signal transduction unit and is referred to maintain the dividing hNP-AC in a proliferative state by preventing maturation and differentiation into non astrocytic cells (Nakashima et al., 1999; Bonaguidi et al., 2005).
In the present study, progenitor cell characteristics in the hNP-AC were also maintained following exposure to BMP4 and LIF. The majority of hNP-AC, that migrated out of plated neurospheres were immunoreactive for nestin (89 ± 2.3%), SOX2 (88.0 ± 3.6%) and Musashi-1

(89.2 $\pm$ 3.8%). The RT-PCR showed no significant change of nestin- or CD133 mRNA in comparison to the non-differentiated hNPC populations. In this regard, the modification process with BMP4 and LIF did not significantly alter the hNP-AC in respect to the hNPC phenotype. However, a qualitative change in hNP-AC Musashi-1 immunoreactivity in comparison to hNPC immunoreactivity was observed. The staining pattern changed to a more patchy illumination. The relevance of this observation is not clear. Others also noticed an uneven distribution in Musashi-1 immunoreactivity in neural stem/progenitor cells, and reported that Musashi-1 is mainly localized in non-oligodendroglial progenitor cells (Kaneko et al., 2000).

BMP4, a member of the TGFβ superfamiliy, promotes differentiation in the direction of the astrocytic lineage and inhibits oligodendrocyte or neuronal lineage development (Mabie et al., 1997; Mehler et al., 1997, 2000; Zhang and Li, 2005). The present data confirm the elaboration of the astrocytic lineage with an increased detection of GFAP- (92.5 $\pm$ 3.4%) and S100β immunoreactivity (79.4 $\pm$ 1.7%). In agreement, there was a significant increase of GFAP mRNA as wells as CD44 mRNA in hNP-AC in comparison to hNPC.

Although the amount of S100β mRNA did not alter in hNP-AC (compared to hNPC), immunocytochemistry revealed a significant increase in the number of S100β-positive cells. The altered S100β staining pattern in hNP-AC contrasted to that in hNPC prior to differentiation It is likely, that S100β remained associated to the intermediate filaments GFAP and vimentin (Sorci et al., 1998), which were up-regulated due to BMP4 and LIF application. Thus, the up-regulation of S100β protein and the altered staining pattern serve as an additional indicator for the intracellular reorganisation that had occured during hNP-AC differentiation.

This study confirms, that the number of CD44 immunoreactive cells increased after application of BMP4 (Liu et al., 2004). The GFAP immunoreactive cells ($>$ 90%) all co-expressed CD44. The increase of hNP-AC CD44 immunoreactivity is in agreement with the significant increase of CD44 mRNA expression.

However, the generation of pure astrocytic aggregates, even after eight passages, was not possible in the present study. This is in contrast to reports by others, e.g. Weible and Chan-Ling (2007). A small but constant sub-population of TuJ1- and MAP2ab-immunoreactive cells could be identified in the monolayers of cells migrating from the PLL/laminin plated spheres. On the other hand, in cryosections of hNP-AC-neurospheres no cells were labeled for the neuronal markers anymore. One explanation might be that some hNP-AC showed spontaneous differentiation, when they migrated on PLL/laminin substrate.

In conclusion, the present investigation has shown that a highly enriched population of immature astrocytes can be obtained by exposure of hNPC to BMP4 and LIF. These cells could be further utilised for *in vitro* an *in vivo* studies to investigate their ability to support axon regeneration and tissue repair in experimental SCI.

4.2 Proliferation of hNPC and hNP-AC

One of the first requirements in cell implantation strategies is the generation of usable quantities of cells. Therefore, the extent to which hNPC differentiation to hNP-AC alters proliferation kinetics was assessed.

4.2.1 Optimisation of Neurosphere Culture Conditions

The hNPC and hNP-AC were kept under proliferative conditions with the media supplements B27, EGF and bFGF, which in combination have proven to optimise the proliferative activity of cultured human foetal neural progenitor/stem cells (Svendsen et al., 1998; Wachs et al., 2003; Kanemura et al., 2002; Mori et al., 2006; Weible and Chan-Ling, 2007). The amount of these supplements remained constant throughout the differentiation process to exclude possible influences on cell expansion caused by culture medium composition.
The propagation of the hNPC and hNP-AC was promoted using the neurospheres culture technique. This technique was developed by Reynolds and Weiss (1996) in rodent neural stem/ progenitor cell cultures and has been applied in many studies for human neural progenitor/stem cells. It has been suggested that the three dimensional architecture within the neurosphere creates a micro-environment that promotes proliferation of hNPC (Mori et al., 2006).
The passaging process of the neurospheres remains an important and critical parameter for cell expansion, because the selected technique has an important influence on cell survival and proliferation rates in human neural progenitor/stem cells. In the literature, a range of different dissociation methods have been described, such as classical enzymatic dissociation techniques using trypsin or the sectioning of spheres, also referred to as chopping (Svendsen et al., 1998). The chopping method maintains the cell-cell interactions but cannot be used when single cell suspensions are required. In contrast, enzymatic dissociation with trypsin generates a single cell suspension, but results in a significant loss of cells (Svendsen et al., 1998; Wachs et al., 2003). Thus, in the present study, the enzyme Accutase was used because it is regarded as a less aggressive enzymatic dissociation technique (Svendsen et al., 1998; Wachs et al., 2003) and has been proven to minimise cell loss during passaging and to achieve highest cell numbers.
Numerous studies have discussed the issue of how long human neural progenitor/stem cells can

be kept in culture conditions while maintaining their multipotency and proliferative states. In contrast to rat neurospheres, human neurospheres derived from all regions of the CNS show continual growth over the first 20 weeks of culture (Ostenfeld et al., 2002). Some groups report that neurospheres derived from human foetal tissue could be expanded in long term cultures for up to 6-8 months (Murray and Dubois-Dalcq, 1997; Kanemura et al., 2002) while others have maintained stem/progenitor cells in neurosphere-cultures up to 1 year before proliferation arrest was detected (Svendsen et al., 1999; Quinn et al., 1999). The fact that the cells underwent senescence and stopped dividing is an important characteristic, indicating that the cells had not oncogenically transformed in culture (Svendsen et al., 1999; Kanemura et al., 2002). In agreement with the findings above, hNPC and hNP-AC of the present study could be kept in a proliferative state for up to 6-8 months.

4.2.2 Methods to Assess Cell Proliferation

Traditionally, *in vitro* cell proliferation is determined directly by counting the cells. Although this method is simple and inexpensive, it is necessary to break down the neurospheres enzymatically to obtain a single cell suspension (Svendsen et al., 1997; Carpenter et al., 1999; Quinn et al., 1999; Ostenfeld et al., 2002). Furthermore, this procedure is laborious and potentially inaccurate, because of difficulties to dissociate the neurospheres into a complete single cell suspension (Kanemura et al., 2002).
Therefore, both metabolic- and morphological assays were performed for the assessment of cell numbers and proliferation of hNPC and hNP-AC.

In application of the metabolic assay with an indirect measurement of proliferative activity in hNPC and hNP-AC some technical difficulties had to be faced: the CellTiter-Blue® Reagent is designed for use as an end-point assay rather than a kinetic method of monitoring cell growth over a period of time (Promega, Technical Bulletin, 2006). Therefore, it was difficult to standardise the ideal seeding density of hNPC (or hNP-AC), for longer measuring periods ($>$6-9 days). The choice of too low cell densities slowed down the proliferation rate. In contrast, the choice of too high cell densities resulted in the eventual formation of levels of metabolised indicator dye (Resorufin) producing a too high fluorescence signal, that was out of the preliminary adjusted gain. Furthermore, it was not possible to examine intact neurospheres due to the lack of penetration of resazurin deep into the sphere-structures and the uncertainty of how easily the fluorescence product (Resofurin) can diffuse out (see chapter 2.4). Therefore hNPC and hNP-AC were examined as 2D monolayer cultures on PLL/laminin plated surface with the metabolic assay.

In contrast, the 3D morphological assay enabled assessment of proliferation in non-disrupted, complete neurospheres. Despite this favourable advantage, it has to be mentioned that there were some methodical restrictions: a problem concerning registration of diameter was the missing 3rd dimension of the neurospheres. In this study all data of diameters were based on two dimensional measurement with light microscopy.

Furthermore, there was restriction to the size of spheres that could be analysed. The morphological assay could not be properly performed in spheres with a very small ($< 50\mu$m) or a very large ($> 800\mu$m) diameter due to increasing measuring inaccuracy.

The requirement of a relatively homogenous neurosphere, composed of similar sized cells, represents a further limitation to the morphological assay (Hulspas and Quesenberry, 2000; Singec et al., 2006). Thus, the variable cellular composition of neurospheres (Svendsen et al., 1999; Bez et al., 2003) may not accurately reflect the precise proliferation activity, thereby representing an uncertainity in the sensitivity of the obtained results in the present study.

4.2.3 Proliferative Activity of hNPC and hNP-AC

The gradients of the standard curves that were generated in the metabolic assay from hNPC and hNP-AC differed, revealing the different metabolic activity of both cell types for the indicator dye, resazurin.

The sigmoid growth curve of hNPC in the metabolic assay (see chapter 3.2.1, Fig. 3.13A) showed typical proliferative activity among the different phases of cell growth (see chapter 2.4.3): the classical phases of cell growth (i.e. log-, plateau- and decline phase) were also present in hNP-AC. In the metabolic assay, logarithmic growth was only observed in the first days in hNPC- or hNP-AC-monolayer cultures, when cell density and nutrient supply offered ideal growing conditions, with a minimum DT of 1.68 days for hNPC and a minimum DT of 3.2 days for hNP-AC. When monolayer cultures reached confluency, growth became stationary and proliferation stopped. Then, the multiplication rate continuously decreased even to negative values (see chapter 3.2.1, Fig. 3.13B and chapter 3.4.1, Fig. 3.27B).

In contrast, in the morphological assay the hNPC-neurospheres and the hNP-AC-neurospheres showed constant logarithmic growth over the complete measuring period (see chapter 3.2.2, Fig. 3.14 and chapter 3.4.2, Fig. 3.28). It is likely, that the differing growth conditions in the performed assays are responsible for the contrasting growth behaviours. The propagation of cells with the neurosphere culture technique in the 3D morphological assay indicates less restrictive growth than cells grown as monolayer cultures in the 2D metabolic assay.

The arrest of proliferation in confluent monolayer cultures approximately two weeks following seeding in the metabolic assay, indicates a growth inhibition due to the cell-cell contact in hNPC as well as hNP-AC. The critical cell density, that turned the proliferating cells to the stationary phase and later to cell loss differed in between the hNPC and hNP-AC with a less high peak cell number in hNP-AC.

Furthermore, the *DT* in hNP-AC cultured as monolayers was significantly higher compared to the *DT* for hNPC in the metabolic assay. In accordance, the doubling times from the morphological assay resulting from the intact neurospheres were higher for hNP-AC as well, answering thereby the initial question, that the hNP-AC showed and altered decelerated proliferative activity after differentiation and *in vitro* propagation.

As mentioned above, the proliferative activity of non-transformed cell lines declines over time *in vitro* until eventually a finite lifespan is reached. The longer *in vitro* propagation in hNP-AC might have influenced their longer duration of *DT*.

The obtained data from the morphological assay with a *DT* of 3.46 days for hNPC- and of 5.1 days for hNP-AC-neurospheres are consistent with data from proliferation studies in intact neurospheres of other groups. Svendsen and colleagues reported about an overall growth rate of approximately 4-5 days in foetal human neural progenitor/stem cells (Svendsen et al., 1998, 1999). Kanemura and colleagues provided detailed information on growth rates in neural progenitor neurospheres derived from human foetal forebrain tissue of 7-8 gestational weeks with a *DT* of 82h (= 3.4 days) in neurospheres after 100-200 days *in vitro* and about a *DT* of 104-126h (= 4.3-5.35 days) in long term cultures, i.e. > 200 days (Kanemura et al. (2002)).

The present investigation was unable to establish a correlation between *DT*, i.e. *r*, neither in relation to the volume of spheres nor in relation to the time point investigated in the experiment. This is in contrast with Mori and colleagues, who reported a dependency of *DT* on hNPC-neurosphere volume for human foetus-derived tissue: They described an acceleration of proliferation related to diameter increases of up to 250μm, which was mainly caused by the aggregation of small neurospheres to larger ones (Mori et al., 2006). However, in the present study the parameter of self aggregation could not exert any influence on apparent proliferative activity, since spheres were cultured individually.

It has been suggested that the ability of nutrients and oxygen to diffuse to the hypoxic central regions of large neurospheres may result in slowed growth rates (Svendsen et al., 1999). However, BrdU- and Ki67-labeled cells have been found in central and peripheral regions of neurospheres (up to 350μm; Mori et al., 2005, 2006). The present study confirms the presence of proliferative, Ki67-positive, cells in the core as well as at the margin of the hNPC-and hNP-

AC neurospheres with a range of sizes (up to 500μm). Therefore the notion that the inner part of human neurospheres is unsuitable for the survival and proliferation of neural stem/progenitor cells is, according to the present data, unfounded.

4.3 Conclusions

The investigation shows that hNPC from first-trimester human foetal forebrain and the resulting differentiated hNP-AC show diversity in cellular composition and proliferation kinetics. The investigation was successful in a number of aspects:

I) The heterogeneous source of hNPC was better defined, confirming the presence of non-committed cells at varying stages of development with a spontaneous differentiation capacity to glial- and neuronal cell populations but not to an oligodendroglial cell lineage.

II) The hNPC were successfully differentiated, showing significant upregulation of astrocyte-related markers, and were thereby termed hNP-AC. They represented a highly enriched population of astrocytes, which still possessed stem/progenitor cell characteristics.

III) The proliferative activity was assessed with both a 2D metabolic and a 3D morphological assay showing a deceleration in hNP-AC compared to hNPC prior to differentiation.

Part II

Effects of Released Factors and ECM on Neurite Regeneration *in Vitro*

5 Material and Methods

To better understand the mechanisms by which hMSC and hNP-AC supported neurite regeneration in adult rat DRG neurons as in an *in vitro* model for axon regeneration (Führmann et al., 2010a,b), the possible contributions of released trophic factors (i.e. present in conditioned medium) or substrate-mediated mechanisms (via the ECM) were investigated.

5.1 Cultivation of hNP-AC and hMSC

For generation of hNP-AC derived ECM and conditioned media the hNP-AC were cultured as monolayers as described in Part A (see chapter 2.1.1). The production of the ECM substrate and the conditioned media will be described in the following (see chapter 5.2 and 5.3).
hMSC were kindly provided by K. Montzka (Clinic for Urology, University Hospital Aachen) and had been isolated from bone marrow aspirates from patients during surgery following informed consent, approved by the Ethical Committee of the University Hospital, Aachen. Characterisation of isolated hMSC was performed by K. Montzka using three criteria i) adherence to tissue culture plastic, ii) specific surface antigen expression, and iii) multipotent differentiation potential (Prockop, 1997; Dominici et al., 2006; Montzka et al., 2009). hMSC were cultured as monolayer cultures with the culture medium consisting of:

> Panserin 401 medium supplemented with 2% FCS (Biowest, Nuaille, France),
> EGF (10 ng/ml, Cell Concepts, Umkirch),
> bFGF (1 ng/ml, Cell Concepts, Umkirch),
> plateled derived growth factor BB (PDGF-BB; 1 ng/ml, Cell Concepts, Umkirch),
> and 10nM dexamethasone (10 nM, Cell Concepts, Umkirch).

Media exchange was performed every 3-4 days until cells reached confluence. For passaging, the cells were detached with trypsin/EDTA solution (Lonza, Vervieres, Belgium) and re-seeded with a density of 4000 cells/cm^2.

5.2 Conditioned Media

To study the influence of trophic factors released from hNP-AC or hMSC to promote neural outgrowth *in vitro*, DRG culture media (DRGM) was conditioned before application to DRG neurons. DRGM was conditioned for 3 days by substances released from hNP-AC monolayer cultures or from hMSC monolayer cultures. DRGM was provided to monolayers of each cell type and consisted of:

> 48ml Neurobasal-A (Invitrogen),
> 1ml B27 1x (Stock 50x; Invitrogen),
> 0.5ml Glutamax (Invitrogen),
> and 0.5ml Penicillin/Streptomycin (1:100 vol/vol, PAA).

The conditioned DRGM was termed hMSC- conditioned media (hMSC-M) or hNP-AC-conditioned media (hNP-AC-M) and stored at 4°C. The conditioned media was applied to DRG neurons within 48 hours.

5.3 ECM Substrates

ECM-coated tissue culture dishes were produced as bio-substrates from hMSC (hMSC ECM) and from hNP-AC (hNP-AC ECM) according to a published protocol (Milner and Campbell, 2002). The hNP-AC and the hMSC were plated on to PLL (0.01%) and laminin ($5\mu g$/ml) coated cell culture 12-well plates (see chapter 2.1.1). Cells were grown as monolayer cultures for a duration of 3-4 weeks and medium was changed every 3-4 days. One week after monolayer cultures reached confluency cells were lysed by exposure to sterile water for 10 minutes as described previously (Milner and Campbell, 2002). Three washing steps with sterile 0.1M PBS were performed to remove cell debris and leave only adherent ECM on the tissue culture plates. The next day, a DRG-suspension of highly enriched DRG neurons (400-500 neurons/ml) was seeded on to the tissue culture 12-well plates, either covered with hMSC ECM or with hNP-AC ECM as substrate. The PLL/laminin coating alone served as positive control substrate.

5.4 Dissection and Dissociation of Adult Rat DRG Neurons

Adult Lewis female rats served as donor experimental animals for the DRG neurons. The dissections were performed by T. Führmann (Institute of Neuropathology, University Hospital Aachen) in accordance with the local animal ethics committee.
Under terminal isoflurane (Isofluran®, Abott GmbH, Wiesbaden) anaesthesia, animals were

rapidly decapitated. To extract the vertebral column, skin as well as back muscles were removed and ribs were cut on each side. The vertebral column was cut transversely to generate 3 equal sized pieces and opened along the anterior-posterior plane, thus preventing accidental damage to the laterally positioned DRG. The opened pieces of spinal cord column and cord were placed into cold Hanks' balanced salt solution (HBSS; Invitrogen) and remnants of the spinal cord and the dura were removed under the dissecting microscope. The DRG neurons were gently removed using microsurgical tweezers and as much peripheral nerve as possible was cut away with a surgical blade (Bean, 1990; Huettner, 1990).

The freshly dissected DRG neurons in HBSS were centrifuged at 1500rpm for 2 minutes to sediment pieces. Ganglia were then incubated in collagenase buffer (100mM HEPES, 120mM NaCl, 50mM KCl, 1mM $CaCl_2$ and 5mM glucose, pH 7.4) containing 0.8% w/v collagenase (CLS I, Biochrom AG, Berlin), and 3% w/v bovine serum albumine (BSA, fraction 5, Serva, Heidelberg) for 2 hours in a shaking incubator at $37°C$. After the first enzymatic incubation, trypsin (0.5ml, 0.25%, Invitrogen) was added for a further digestion of 30 minutes. To stop the reaction, foetal calf serum (FCS, 0.5ml, PAA) was added and the mixture was centrifuged for 3 minutes at 2000rpm. The supernatant was aspirated and replaced by 1.5ml of DRGM.

The suspension was gently dissociated by trituration with a pipette 10-15 times. After 5 minutes, the supernatant was pipetted into a separate falcon tube and 1ml of fresh DRGM was added and the dissociation was repeated. A small volume (approx. 2ml) of Percoll density gradient solution (1.3ml Percoll, Amersham; 450μl 0.1M PBS; 3.2ml a.d.) was carefully added to the bottom of the DRG neuron solution and the suspension was centrifuged at 2500rpm for 10 minutes. The supernatant was removed and the residual pellet of neurons resuspended, either in DRGM or alternatively in the conditioned hMSC-M or hNP-AC-M. The DRG neurons were either applied to the cell-free ECM substrate of hNP-AC or hMSC or alternatively plated on to the positive control PLL/laminin substrate.

5.5 Experimental Test Conditions and Microscopy

For each experiment DRG neurons from at least 2 different donor animals were examined. As a positive control, dissociated DRG neurons were resuspended in non-conditioned DRGM and seeded on to PLL/laminin substrate, which is known to support neuronal adhesion and axon regrowth (Manthorpe et al., 1983; Lander et al., 1985; Lander, 1987; Tonge et al., 1997). After 24 hours DRG neurons were fixed with 4% PFA for 30 minutes. On regrowing DRG neurites and cell bodies immunocytochemistry was performed with a mixture of monoclonal anti-NF200 antibody (200kDa, NE14, Sigma) and monoclonal anti-MAP2ab antibody (Sigma) as described in Part A (see chapter 2.2). DRG neurons were visualised using an inverted Zeiss Axioplan

epifluorescence microscope coupled to an on-line digital camera (Axiovision software). Data files documenting extensive neurite outgrowth reaching over several images were merged with Adobe Photoshop Software CS2.

Figure 5.1 demonstrates the different experimental conditions, to which the regenerating DRG neurons were subjected.
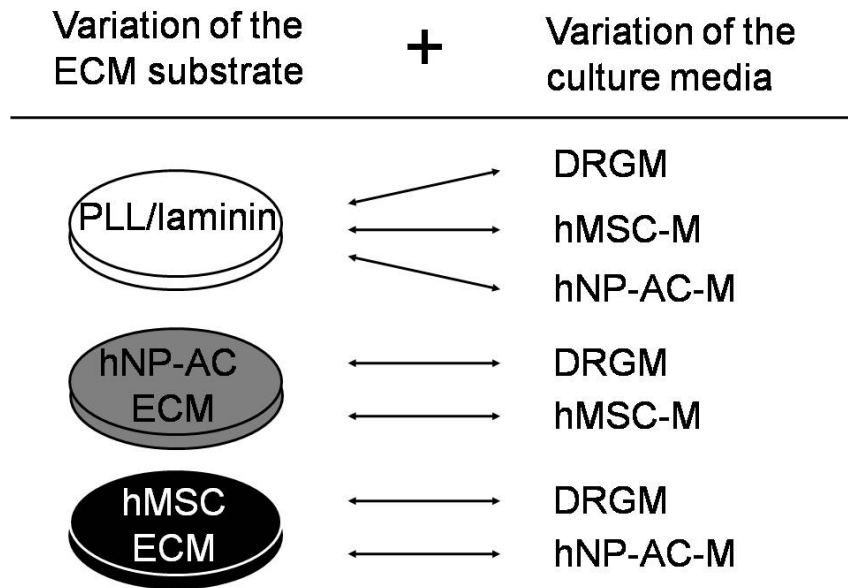
Figure 5.1: **Schematic drawing of the different experimental conditions resulting from the change of the ECM substrate and culture media for regenerating adult rat DRG.**
The DRG axon regeneration was investigated in the presence of the different ECM substrates (see left side) in combination with the applied culture media (see right side). The ECM substrate derived from hNP-AC (hNP-AC ECM, grey) and the ECM derived from hMSC (hMSC ECM, black) was studied to determine their ability to support axon regeneration by adult DRG neurons. The PLL/laminin coating (white) served as a positive control substrate. The applied culture media for the regenerating DRG neurons had been previously conditioned either by hNP-AC (hNP-AC-M) or by hMSC (hMSC-M). With this experimental approach, the effects on DRG neuron regeneration through trophic factor release and substrate-bound mechanisms were investigated. Non-conditioned DRGM served as media control.

5.6 Evaluation of Axon Regeneration by Adult Rat DRG

For each experimental condition 50 DRG neurons per donor animal were selected by the following criteria: (i) growth from solitary, well spaced out neurons, (ii) not located at the edge of a 12-well plate and (iii) clear identification of neurites belonging to one DRG soma.

Fluorescence microscopy images of neurites (e.g. Fig. 5.2A) were manually traced in Adobe Photoshop software using a graphics tablet (Intuus®, Wacom). Brush diameter was adjusted to 6 pixels. The cell soma was not traced. A threshold level value of 170 was set while con-

verting images to black and white (Fig. 5.2B). Any remaining staining artefacts were manually removed and threshold level adjusted to optimise uniformity of illumination and contrast as described previously (Pool et al., 2008).

After this manual pre-processing, images were transformed with Image J Software 1.38d. Images had to undergo a threshold level adjustment again, since 8-bit binary images were required for further processing (Fig. 5.2C). The remaining image information was processed with the "Skelettonization" function which reduced the axonal profiles to single pixel thickness (Fig. 5.2C, red box). The amount of pixels quantified reflected the total neurite outgrowth of each individual DRG neuron.

5.7 Statistical Analysis of DRG Neurite Outgrowth

In this study 800 DRG neurons were traced and analysed. Data were plotted as mean values $\pm$ SEM representing averages of experimental conditions performed in duplicate. All analysed data (i.e. total neurite outgrowth, maximal neuritic vector and number of primary neurites) was standardised in relation to the values generated on the PLL/laminin positive control substrate with DRGM as control culture medium.

Data was subjected to an analysis of variance (*ANOVA*) followed by Bonferrroni's test for multiple comparisons between pairs of means. *P* values of < 0.05 were regarded as significant (i.e. * $p < 0.05$, ** $p < 0.01$, *** $p < 0.001$). All tests were performed using the statistical software Graph Pad Prism 4.0.
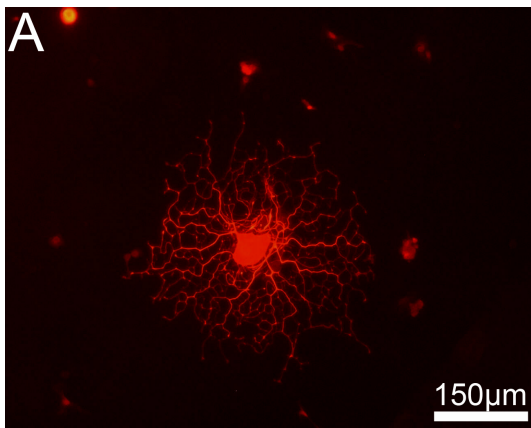
A: The image shows a sample of a rat DRG neuron on PLL/laminin control substrate and DRGM as control culture media. Regenerating neurites were stained with a combination of anti-MAP2ab antibody (red) and anti-NF200 antibody (red).
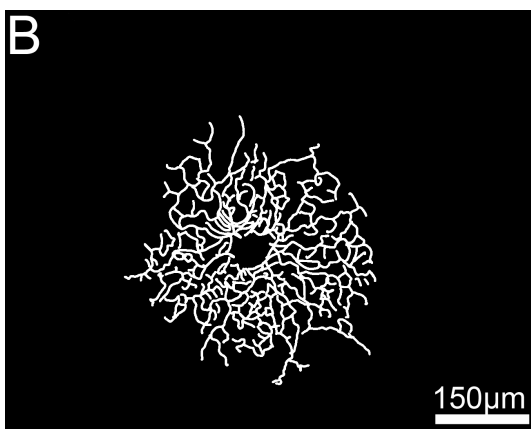
B: The neurites were traced (white) with a brush tool and the red signal was discarded.
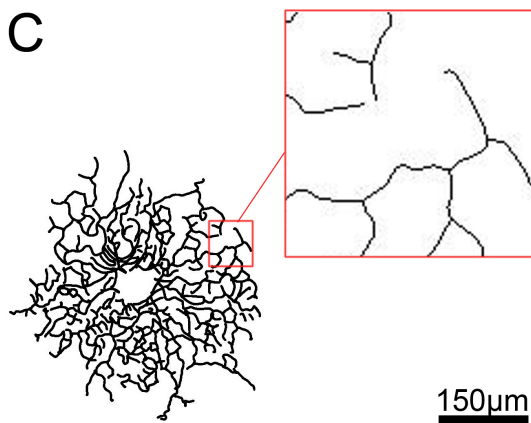
C: The thresholded images were "skeletonized" with Image J software. The amount of "skeletonized" neurites was estimated by total pixel counts. A magnification of skeletons is shown in the red box.

Figure 5.2: **Quantification of regenerating neurites by digital processing and neurite tracing.**

6 Results

In an attempt to better understand the beneficial interactions of stem/progenitor cells with regenerating neurites our group has studied the axon growth promoting effects of hMSC- and hNP-AC monolayers *in vitro* with dissociated adult rat DRG neurites as model of repair after CNS injury (Führmann et al., 2010a,b). The mechanisms by which hMSC and hNP-AC supported neurite regeneration remained unclear. Therefore, the influence of released trophic factors (i.e. conditioned media) or substrate-mediated mechanisms (i.e. the ECM) of hMSC and hNP-AC and their possible interactions to modify DRG neurite regeneration *in vitro* were investigated in the present study.

6.1 ECM Substrates derived from hNP-AC or hMSC
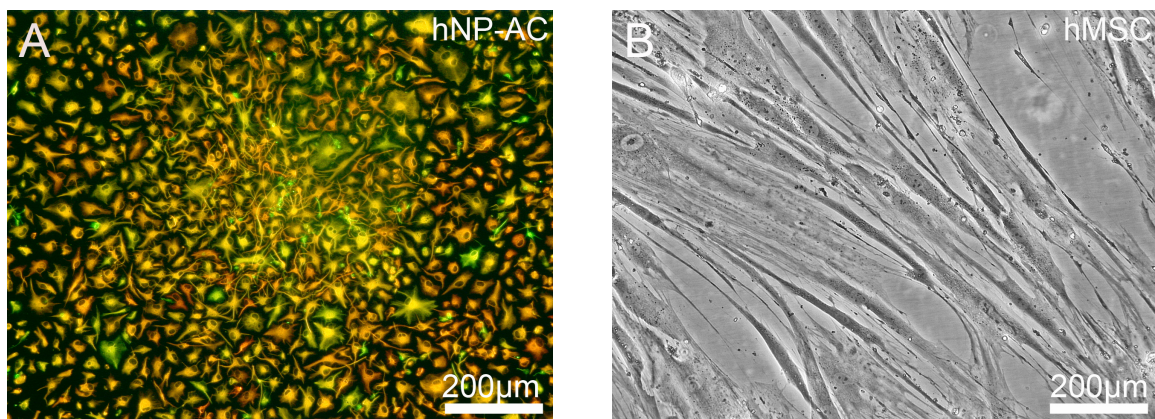
Figure 6.1: **Confluent monolayers of hNP-AC and hMSC.**
A: A confluent monolayer of hNP-AC is stained with antibodies to GFAP (green) and vimentin (red) visualising a densely packed network of cells. **B:** A phase contrast image of viable hMSC in culture demonstrates their elongated cell bodies as they approach confluence. The hMSC also show an aligned arrangement.

The ECM substrates were generated from hNP-AC (Fig. 6.1A) and hMSC (Fig. 6.1B), which had established densely packed, confluent monolayers. Several GFAP- and vimentin-positive hNP-AC showed astrocytic polymorphic or "fried egg"-shaped morphologies with diameters ranging from 30-80μm. The hMSC adhered to the tissue culture plastic and upon becoming confluent, adopted extended cell bodies which often ran in parallel with each other.

6.1.1 Quantification and Morphology of DRG Neurons
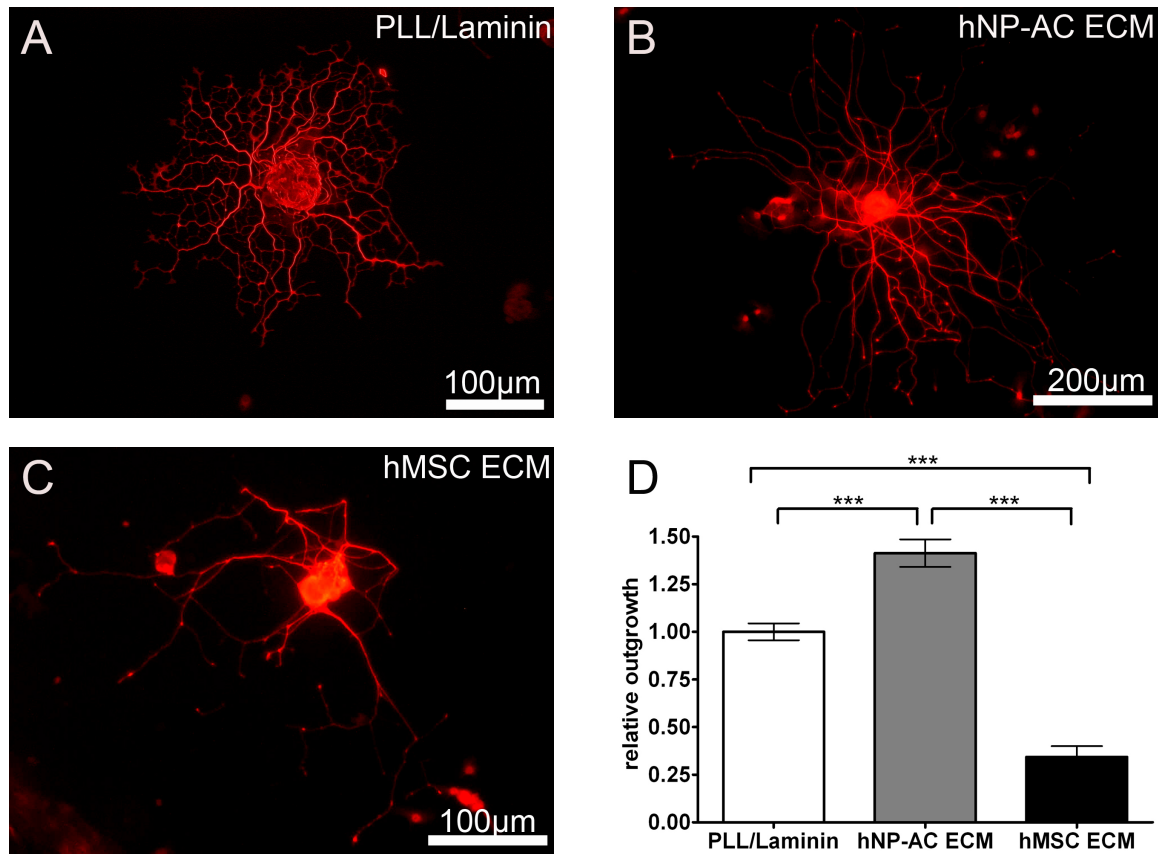
Figure 6.2: **Highest overall neurite outgrowth promoted by hNP-AC ECM.**
A-C: Examples of typical DRG neurons on the different ECM substrates. Neurons were combinatory stained for NF200 and MAP2ab (red). The DRG neurons show regeneration on all substrates: (**A**) PLL/laminin, (**B**) ECM of hNP-AC and (**C**) ECM of hMSC.
D: The histogram shows the overall neurite outgrowth on the different ECM substrates standardised to the PLL/laminin control substrate. All pairs of columns differed significantly from each other ($***$, $p < 0.001$). The overall neurite outgrowth was greatest on hNP-AC ECM substrate, and that measured on PLL/laminin was greater than on hMSC ECM substrate. Data represent means $\pm$ SEM; n = 100.

NF200/MAP2ab-positive regenerating neurites were detected on all substrates. In Figure 6.2 examples of DRG neurite regeneration over the PLL/laminin positive control (Fig. 6.2A), for hNP-AC ECM (Fig. 6.2B) and for hMSC ECM (Fig. 6.2C) are shown. To prevent a potential bias concerning the quality of the DRG dissociation on the subsequent analysis of DRG-substrate or DRG-media interactions, all data of neuritic regeneration was standardised to the PLL/laminin positive control substrate with control media (DRGM, Fig. 6.2A). Thus, data of neurite outgrowth (x) are not demonstrated as absolute values [μm], but presented as a ratio to the appropriate positive control value (i.e. ratio of x / (PLL/laminin with DRGM)). A table listing the standardised relative data used for analysis and the absolute values [µm] for all ex-

perimental conditions is attached in the appendix (see additional data, Table 9.4).

The dissociated DRG neurons rapidly attached to the test substrates and demonstrated round cell bodies (measuring $55 \pm 6\mu$m in diameter), from which multiple regenerating neuritic processes extended in all directions. The regenerating neurites often achieved substantial growth and complex aborisation patterns. Observation of growth over the PLL/laminin positive control substrate confirmed that the DRG dissociation had generated a highly enriched population of DRG neurons, with relatively little glial contamination (Delree et al., 1989; Schoenen et al., 1989).

Neurite regeneration on the PLL/laminin-coated substrate (Fig. 6.2A) appeared uniform in all directions, generating a radial growth pattern of robust primary processes, which showed multiple branching points. Regeneration of DRG neurites on hNP-AC ECM (Fig. 6.2B) showed a similar growth pattern with multiple radial sprouting processes, that seemed to be more extensive than on the control substrate. The greater overall dimension and expansion of the neuritic outgrowth on hNP-AC ECM was most striking (compare the different scale bars in Fig. 6.2A and B). Neurite regeneration over hMSC-ECM also showed a radial growth pattern, but the sprouting processes appeared to be shorter with fewer branching points (Fig. 6.2C).

6.1.2 Total and Longest Neurite Length

For quantification and comparison of the potential of the different substrates to promote neurite outgrowth, the length of all neurites was summed and represented the value of total neurite length per substrate (Fig. 6.2D). Statistical analysis showed that total neurite length on all three substrates differed significantly from each other (Fig. 6.2D, $p < 0.001$).

Whereas the overall DRG neurite outgrowth on hMSC ECM substrate was significantly ($p < 0.001$) lower than that on the PLL/laminin positive control, the neurite outgrowth measured on the hNP-AC ECM substrate was the greatest of all ($p < 0.001$).

To compare the maximal neurite outgrowth distance of DRG neurons on the different substrates, the length of the vectors between the cell soma and the tip of the longest NF200/MAP2ab-immunoreactive neurite was measured (Fig. 6.3B). Similar to the quantification for total neurite length, the values obtained were expressed as a ratio in comparison to the mean longest vector measured over the PLL/laminin control substrate. Statistical analysis showed a significant difference between the mean longest neurite length of the three experimental groups (Fig. 6.3A) with the longest neuritic vectors being recorded over the hNP-AC ECM substrate. The shortest neuritic vectors were found over the hMSC ECM substrate. The level of significance however was less strong (Fig.6.3A, $p < 0.01$) in the investigation concerning the data of the longest neurite length compared to the data of overall neurite outgrowth (Fig. 6.2D, $p < 0.001$).

The term primary neurite describes branches of neurites that sprout directly out of the DRG neuron cell soma (Fig. 6.3D). There was no apparent difference in the number of primary neurites supported by either hMSC ECM, hNP-AC ECM or the PLL/laminin control substrate (Fig. 6.3C).
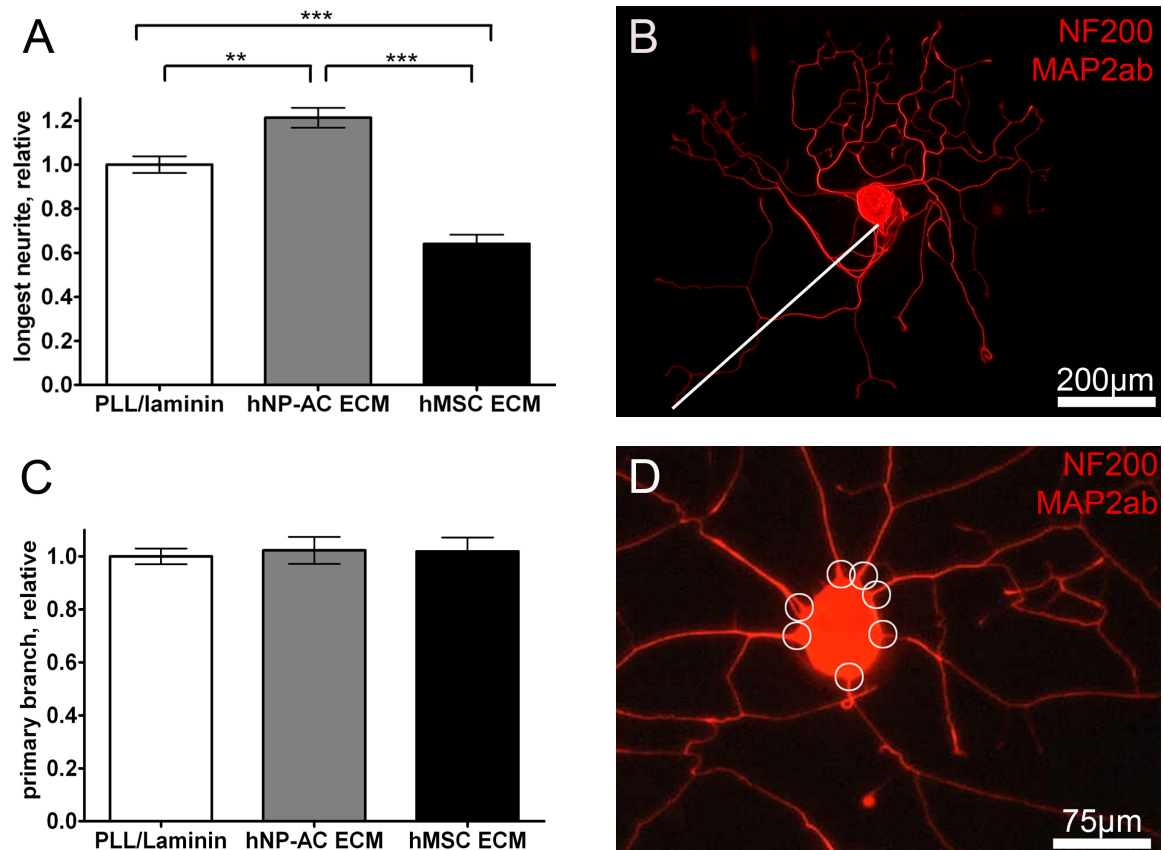
Figure 6.3: **Maximum vectors of neurite length and elaboration of primary neurites on different substrates.**
A: The graph shows a histogram summing the longest neurite length in DRG neurons for all three substrate conditions standardised to the PLL/laminin control. There is a statistically significant difference between all pairs of columns. The significantly longest neurite vectors are promoted on hNP-AC ECM substrate compared to PLL/laminin ($** p < 0.01$) and hMSC ECM substrate ($*** p < 0.001$).
B: A DRG neuron is shown on PLL/laminin substrate with DRGM combinatory stained for NF200 and MAP2ab (red). The white line demonstrates the vector of the longest neurite length of the DRG neuron.
C: There was no difference in development of primary branches in variation of the ECM substrate.
D: A representative DRG neuron is combinatory stained for NF200 and MAP2ab (red). The white circles point out the primary neurite branches sprouting out of the DRG cell soma. Data represent means $\pm$ SEM; n = 100.

6.2 Effects of Released Factors from hNP-AC or hMSC

Experimental manipulations with conditioned media of hMSC or hNP-AC resulted in regenerating DRG neurons with a complex and highly subdividing neurite architecture. Especially, the group of DRG neurons treated with hNP-AC-M (Fig. 6.5D) showed profuse and wide spread neurite expansion compared to the DRGM control group (compare the different diameters of regenerating DRG, Fig. 6.5C and D).

6.2.1 Total and Longest Neurite Length

The DRG neurons treated with conditioned media either from hMSC or hNP-AC showed significantly ($p < 0.001$) greater total neurite outgrowth than those from the control group which received unconditioned DRGM (Fig. 6.5A). There was a tendency for a lower extend of overall neurite outgrowth from neurons cultured with hMSC-M compared to those cultured in hNP-AC-M (Fig. 6.5A); however the values failed to reach the level of statistical significance.

The investigation of the vector of the longest neurite per DRG neuron (Fig. 6.5B) revealed that hNP-AC-M induced a significant increase ($p < 0.01$), when compared to DRGM or hMSC-M. Apparently, hMSC-M had no significant effect on this value.

The investigation concerning the elaboration of primary neurites in between the different media applications showed no significant differences (Fig. 6.4). There was only a slight tendency for more primary neurites to be generated by conditioned media from hMSC-M or hNP-AC-M, however the values did not reach the level of statistical significance (Fig. 6.4).
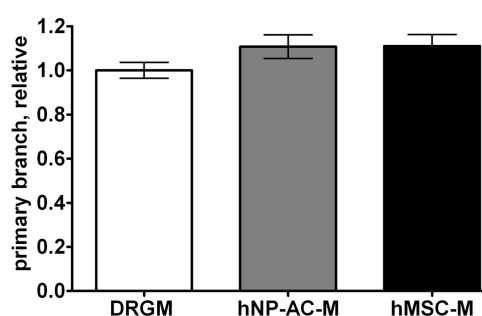
Figure 6.4: **Elaboration of primary neurites in DRG neurons, when cultured with different media.**
There was no significant difference in elaboration of primary neurites under any of the experimental conditions. Data represent means $\pm$ SEM, n = 100-200.
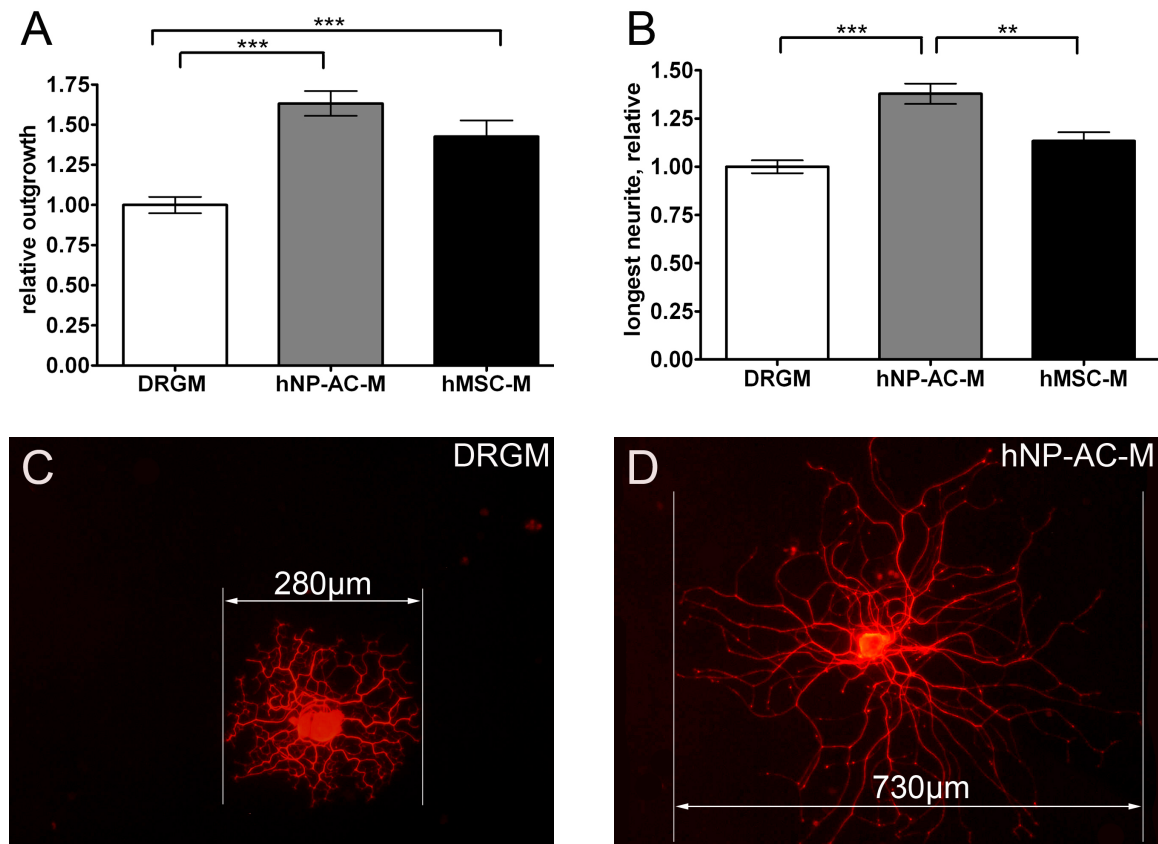
Figure 6.5: **hMSC-M and hNP-AC-M strongly support neurite outgrowth and length of longest neurite.**
A: Conditioned media of hMSC or hNP-AC promote total neurite outgrowth significantly greater than that seen with the comtrol DRGM. **B**: Analysis of the vector for longest neurite length revealed that hNP-AC-M had the greatest effect, whereas hMSC-M apparently had no significant effect on this parameter in comparison to DRGM control. Data represent means $\pm$ SEM; n = 100, *** $p < 0.001$; ** $p < 0.01$. **C-D**: Representative DRG neurons combinatory stained for NF200 and MAP2ab (red) were treated with unconditioned DRGM as control medium (**C**) or conditioned hNP-AC-M (**D**). The DRG neurons cultured with hNP-AC-M show a wide spread neurite expansion and complex growth pattern.

6.3 Interactions of Trophic Factors and ECM Substrate

The question remained, to what extent the neuronal responses to diffusible trophic factors (i.e. present in conditioned medium) could be modified by interactions with its environment (i.e. the extracellular matrix). Similarly, to what extent are the responses of the cell to its ECM environment modified by the presence of diffusible trophic factors. This issue was addressed by using combinations of cell-derived ECM substrate and conditioned media obtained from hNP-AC and hMSC. Two major experimental conditions were tested:

I) a combination of hNP-AC ECM with hMSC-M and

II) a combination of hMSC ECM with hNP-AC-M.

These combinations were compared with the effects of either the relevant ECM or conditioned medium applied individually to regenerating neurites.

There was a strong overall neurite outgrowth detectable, when the first combination (hNP-AC ECM and hMSC-M) was applied to the DRG neurons. The combination lead to a significantly ($p < 0.001$) higher promotion of neurite regeneration compared to the PLL/laminin control substrate with DRGM control media. Furthermore, the combination proved to stimulate significantly ($p < 0.05$) more overall neurite outgrowth than hNP-AC ECM individually with DRGM control or hMSC-M individually with PLL/laminin control substrate (Fig. 6.6A). Likewise, the investigation for the vector of the longest neurite length showed, that the combination of hNP-AC ECM with hMSC-M supported strong neurite regeneration. This combination supported the elaboration of significantly longer neurites compared to the control group as well as to exposure to hMSC-M alone (Fig. 6.6A). However, there was no significant difference in the value for the vector of the longest neurite length in between the combination (hNP-AC ECM and hMSC-M) compared to hNP-AC-ECM individually (Fig. 6.6B).

The elaboration of the number of primary neurites per neuronal cell body seemed not to be influenced by the combinatory approach (data not shown).

The second combination (hMSC ECM and hNP-AC-M) showed very little overall neurite outgrowth of DRG neurons (Fig. 6.6C). The neurites extended to a lesser degree than over the PLL/laminin plus DRGM control condition. The same behaviour was true when the vector for the longest neurite length was investigated (Fig. 6.6D). The total neurite outgrowth (Fig. 6.6C) as well as the length of the longest neurite (Fig. 6.6D) of the combination, containing hMSC ECM and hNP-AC-M, lay significantly ($p < 0.001$) beneath the values of the control group and the individual application of hNP-AC-M to DRG growing on the PLL/laminin control substrate. The elaboration of the number of primary neurites from the neuronal cell body seemed to be unaffected by the combinatory approach (data not shown).
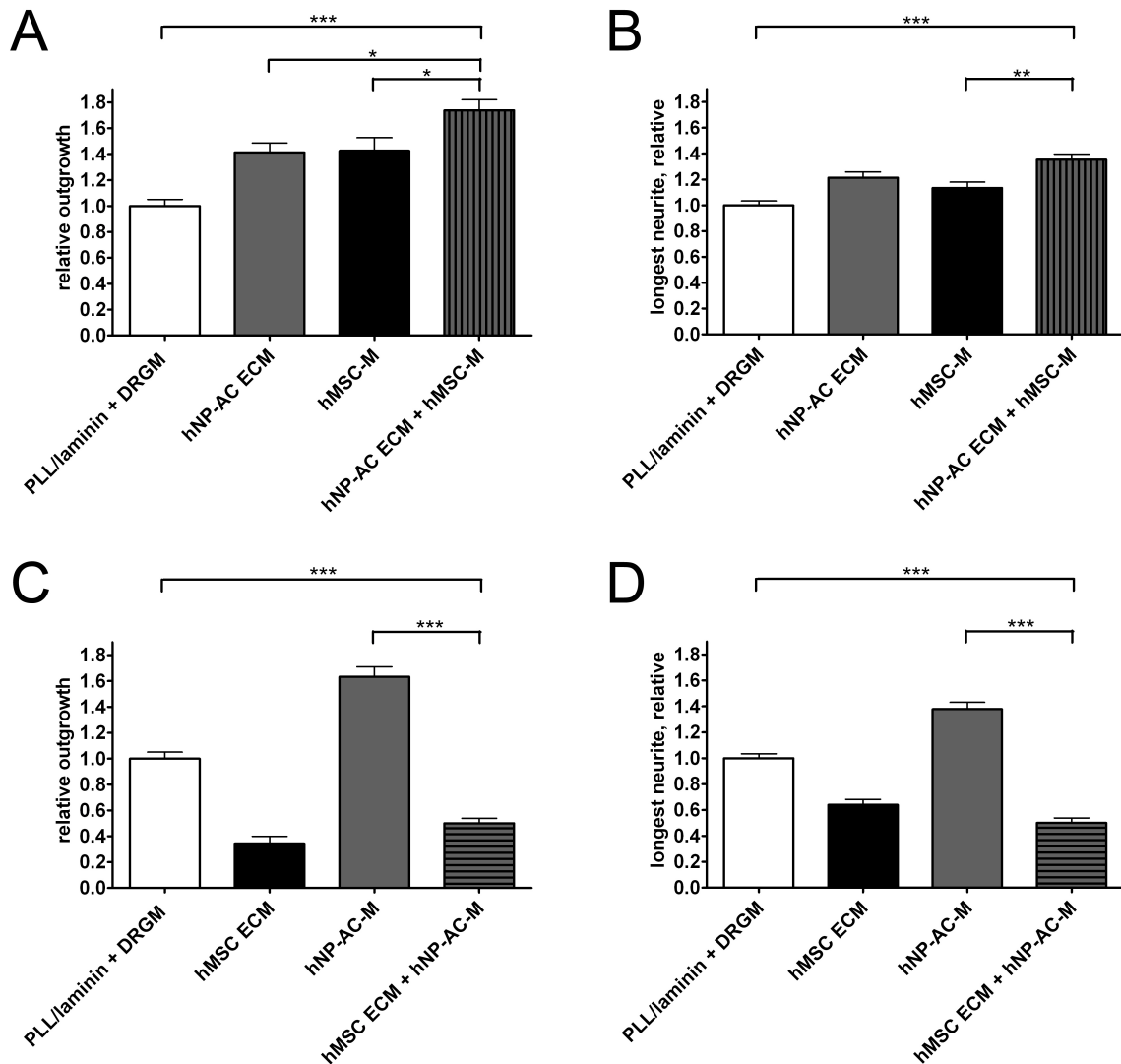
Figure 6.6: **Combinatory application of conditioned media and ECM, investigating interactions on neurite regeneration.**
A-B: A combination of hNP-AC ECM with hMSC-M (columns with vertical stripes in **A** and **B**) shows significantly greatest overall neurite outgrowth (**A**) and longest neurite length (**B**). The data of hNP-AC ECM (grey columns) and hMSC-M (black columns) have been described before in chapter 6.1 and 6.2. **C-D**: The combination of hMSC ECM with hNP-AC-M (columns with horizontal stripes in **C** and **D**) shows overall neurite outgrowth (**C**) and longest neurite length (**D**), which is significantly smaller than the PLL/laminin control and the individual application of hNP-AC-M to DRG neurons. The data of hNP-AC-M (grey columns) and hMSC ECM (black columns) have been described before in chapter 6.1 and 6.2. Data represent means $\pm$ SEM, n = 100, * $p < 0.05$, ** $p < 0.01$, *** $p < 0.001$.

6.4 Summary

In the present study, the potential of ECM and conditioned media derived from hNP-AC or hMSC to promote regeneration in adult DRG neurons was investigated. When ECM substrate was varied, DRG neuron regeneration with greatest neurite outgrowth was found on hNP-AC ECM (Fig. 6.7, 2nd column), which was significantly greater compared to the PLL/laminin control or the hMSC ECM substrate (Fig. 6.7, 3rd column). Investigations concerning the variation of media showed, that hNP-AC-M (Fig. 6.7, 5th column) as well as hMSC-M (Fig. 6.7, 6th column) promoted significantly higher neurite outgrowth than the DRGM control media. The combination of hNP-AC ECM and hMSC-M (Fig. 6.7, 8th column) to test possible interactions of trophic factors (i.e. conditioned media) and their environment (i.e ECM) provided maximum neurite outgrowth together with hNP-AC-M on PLL/laminin control substrate (Fig. 6.7, 5th column). Surprisingly, the combination of hMSC-ECM with hNP-AC-M provided relatively poor neurite outgrowth (Fig. 6.7, 9th column).
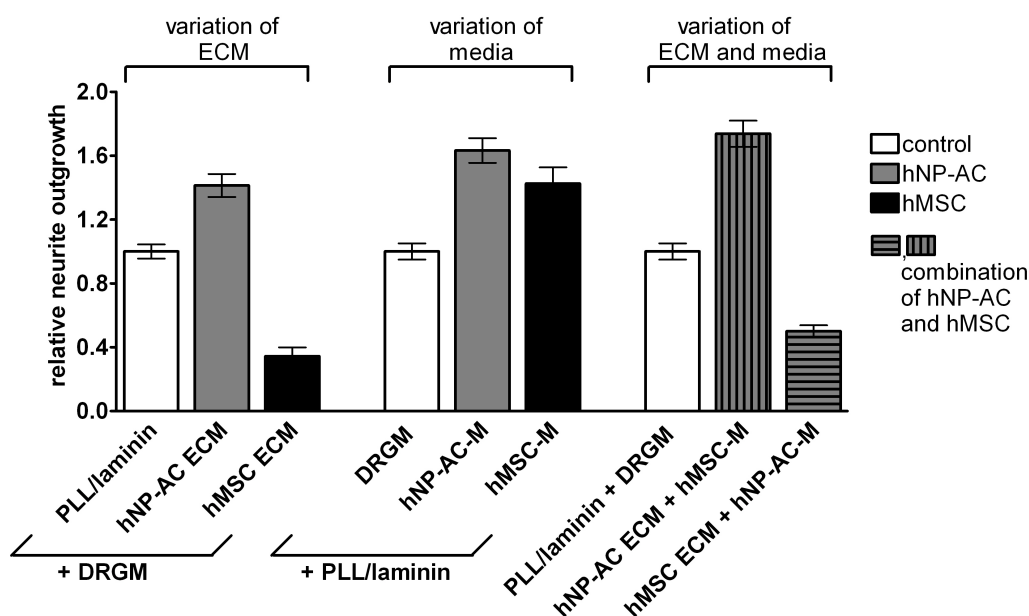
Figure 6.7: **Neurite outgrowth of DRG neurons for all experimental condtions.**
The first three columns show the overall neurite outgrowth of DRG neurons, when ECM substrate was varied. The next three columns represent the overall outgrowth, when media was varied, and the columns on the right show the overall outgrowth, when both parameters were varied.
Constant parameters were unconditioned DRGM as media in the first three columns and PLL/laminin substrate in the center columns. All data represent means ± SEM. The data of the different experimental runs can be compared, because they represent relative values, standardised to their control (PLL/laminin and DRGM with a relative value of 1.0). Absolute values [µm] for all experimental conditions are attached in the appendix (see additional data, Table 9.4).

7 Discussion

The role of cell-substrate interactions regulating neurite regeneration and outgrowth both *in vitro* and *in vivo* has been a subject of intensive study during the last decades. Recently the emphasis of cellular substrates for inducing CNS or PNS axon growth has shifted from that supported by populations of tissue cultured primary glia (Noble et al., 1984, 1985; Smith et al., 1986, 1990) to that supported by stem/progenitor cells, including embryo-derived (McDonald et al., 1999), foetal-derived or adult-derived neural stem/progenitors cells (Ogawa et al., 2002; Pfeifer et al., 2004), as well as by non-neural mesenchymal stromal cells (Chopp et al., 2000; Deng et al., 2006). In an attempt to better understand the beneficial interactions of stem/progenitor cells with regenerating neurites, our group has studied the axon growth promoting effects of hMSC and hNP-AC monolayers on neurite regeneration from dissociated adult rat DRG *in vitro* (Führmann et al., 2010a,b). Since the mechanisms by which hMSC and hNP-AC supported neurite regeneration remained poorly defined, the possible contributions of trophic factors (i.e released into conditioned medium) and substrate-mediated mechanisms (i.e. the ECM) have been investigated.

The present data supported the hypothesis that the ECM of hNP-AC is an important component for supporting strong neurite regeneration *in vitro*. Furthermore, the data indicated that diffusible trophic factors released by hNP-AC were also important for supporting strong neurite regeneration when DRG were seeded on to the control, PLL/laminin substrate (see section 7.3). In contrast and somewhat surprisingly, the major contributor to hMSC-mediated axon growth appeared to be provided by the trophic factors released from these cells, with the hMSC ECM being a relatively poor substrate for axon regeneration (see section 7.4).

Finally the question remained to what extent neuronal responses to diffusible trophic factors (i.e. present in conditioned medium) could be modified by interactions with its environment (i.e. the ECM). The combinatory application of hNP-AC ECM with hMSC-M induced the greatest degree of axonal outgrowth in the present study. However, the potent axon growth promoting effects of hNP-AC-M were found to be incapable of enhancing neurite extension over the hMSC ECM (see section 7.5).

7.1 DRG Neurons as an Experimental Model for Axon Regeneration

Adult rat DRG neurons were used as the model population for axon regeneration. They transmit a range of sensory information to the CNS including the sensory modalities of proprioception, thermoception and nociception. There are several reasons, why adult DRG neurons served as an ideal test neuron for such studies *in vitro*:

I) DRG neurons extend axonal projections into both CNS and PNS and would therefore be involved in injury to both types of nervous tissue (Golding et al., 1996, 1999),

II) DRG neurons are readily accessible, being rapidly dissected from the spinal columns of experimental animals,

III) an enrichment protocol for these neurons has already been developed (Delree et al., 1989), thereby avoiding complications of interpretation that often arise when using DRG explants (Wright et al., 2007),

IV) freshly dissected and dissociated adult DRG are able to survive and regenerate axons, in contrast to neurons from the adult CNS, that do not survive after dissociation (Björklund and Stenevi, 1984),

V) adult DRG neurons may be more appropriate than embryonic neurons for such studies because developmental changes in the sensitivity of neurons to signals from their environment have been reported (Fawcett et al., 1989),

VI) DRG neurons have already been used in numerous *in vitro* and *in vivo* axon growth and regeneration studies (Schwab and Caroni, 1988; Davies et al., 1997, 1999; Chen et al., 2000b).

The neurite lengths from these dissociated neurons were assessed by a computer assisted semi automatic manner to assure accuracy as well as simplicity of approach and because other groups had previously reported that the full automatisation of the procedure was difficult, time-consuming and not completely reliable (Pool et al., 2008).

In the present investigation, no attempt was made to separate the dissociated DRG into their well documented 3 general sub-types. These sub-types have been described as (i) large-to-medium diameter NF200-positive/neurotrophin responsive neurons, (ii) small diameter calcitonin gene related peptide (CGRP)-positive/neurotrophin responsive neurons and (iii) small diameter lectin binding immunoreactive (IB4+)/glial cell-derived neurotrophic (GDNF) factor responsive neurons (Priestley et al., 2002). It has recently been shown that adult rat DRG neuronal sub-types display different signalling requirements for axonal regeneration (Tucker et al., 2006). Fur-

thermore, the IB4-positive small diameter neurons have been reported to be unresponsive or minimally responsive to ECM signals related to PNS tissues (e.g. laminin, collagen IV and fibronectin), however, such ECM signal are required for the neurons to be able to respond to GDNF (Molliver et al., 1997; Bennett et al., 1998; Kashiba et al., 2001). The NF200-positive and the CGRP-positive neurons, on the other hand, do respond to such ECM or growth factors signals by generating axons and the combined effect of ECM (i.e. laminin) plus growth factor (i.e. NGF) stimulation supported even greater axon growth (Jones et al., 2003b; Tucker et al., 2006). It might be argued that, for some reason, the failure to demonstrate extensive neurite outgrowth over hMSC ECM in the present investigation may have been due to a technical problem of somehow only harvesting the IB4-positive sub-populations of neurons. This is, however, most improbable because the immunocytochemical detection of cell bodies and neurites included the use of NF200-staining confirming the presence of the large diameter NF-positive/neurotrophin responsive sub-type of neurons.

7.2 Neurite Outgrowth on ECM Substrates

An *in vitro* model was required to investigate the influence of hNP-AC- and hMSC-derived ECM on neurite regeneration. The ECM from confluent hNP-AC and hMSC was presented as a substrate for neuron attachment and axon extension on the floor of the tissue culture wells. The ECM from a range of cell types including skeletal muscle cell myotubes (Tomaselli et al., 1986; Bixby et al., 1987), Schwann cells (Tomaselli et al., 1986), astrocytes (Freire et al., 2004; Neugebauer et al., 1988) and olfactory ensheathing cells (Tisay and Key, 1999) has been prepared for similar cell-substrate investigations *in vitro*. The ECM produced by these cells has been shown to have a pronounced effect on neuronal morphogenesis, guidance and regeneration.

Several methods for the preparation of ECM from confluent cell monolayers have been described, such as chemical cell lysis with ethylene glycol tetraacetic acid (EGTA; Blenis and Hawkes, 1983; Leco et al., 1994), ethylendiaminetetraacetic acid (EDTA; Fairbairn et al., 1985; Wu et al., 1997), ammonium hydroxide (Niedbala et al., 1986; Rebaï et al., 2005), Triton X-100 (Carter et al., 1990) and the application of paracetic acid with freeze drying (Santucci and Barber, 2005). These rather aggressive procedures often required addition of protective components (protease inhibitors, buffer substances, dehydrating factors etc.) to keep the ECM intact (Hedman et al., 1979; Carter et al., 1990; Santucci and Barber, 2005). Alternatively, ECM has also been prepared by cell lysis provoked by incubation with sterile water for 10 minutes and ongoing washing steps in cold 0.1M PBS to remove cell debris and reduce the activity of released enzymes, thereby preventing the application of protease inhibitors. This method was

applied in the present study for several reasons:

I) it seemed to be a less aggressive approach for the preservation of the ECM framework,

II) the protocol had already been established being simple to follow (Lider et al., 1995; Doss, 1999),

III) the protocol had already been applied to astrocytic cells (Milner and Campbell, 2002).

The lysis of confluent hNP-AC and hMSC monolayers with water provided satisfactory results: after washing steps there were no large remnants of cell debris that could be detected by light microscopy, indicating the total removal of viable cells.

7.3 Support of Neurite Outgrowth by hNP-AC ECM and hNP-AC-M

The present study demonstrates that neurite outgrowth over hNP-AC ECM was significantly greater than that seen over the PLL/laminin positive control substrate ($p < 0.001$). Similarly strong neurite outgrowth was supported by viable monolayers of hNP-AC in comparison to the PLL/laminin substrate ($p < 0.001$). The greatest overall neurite outgrowth over the PLL/laminin substrate was supported by hNP-AC-M, however this effect failed to reach the level of statistical significance when compared to viable hNP-AC monolayers or hNP-AC-ECM (Fig. 7.1A, compare 2nd, 4th, 5th and 8th column; data for viable cell monolayers were kindly provided by T. Führmann and K. Montzka). This confirmed the hypothesis that both diffusible trophic factors (i.e. present in conditioned medium) and ECM-related mechanisms contributed to hNP-AC-mediated support of axon regeneration.

These findings relate to the concept that immature astrocytes play an essential role in axonal growth in the developing CNS and also in CNS regeneration via the expression of ECM molecules supportive for axon extension, and by releasing trophic factors into their environment (Noble et al., 1984; Smith et al., 1986, 1990; Silver, 1988; Davies et al., 1997; Biran et al., 2003; Tom et al., 2004; Freire et al., 2004; Chow et al., 2007). It has been reported that certain growth factors (including bFGF, EGF and TGF) as well as neurotrophins (including NGF, BDNF and NT-3) are secreted by astrocytes and play an important role in CNS development and in CNS regeneration following injury *in vitro* and *in vivo* (Giulian et al., 1993; Kane et al., 1996; Kuhn et al., 1997; White et al., 2008; Delgado-Rivera et al., 2009). The expression of the cell-adhesive ECM glycoproteins laminin (Liesi et al., 1984; Liesi and Silver, 1988) and fibronectin (Tomaselli et al., 1986; Biran et al., 2003; Tom et al., 2004) such as the ECM-related cell surface molecules N-cadherin (Neugebauer et al., 1988; Tomaselli et al., 1988) and NCAM (Neugebauer et al., 1988; Smith et al., 1990) have been suggested to play a role in

astrocyte-mediated axonal growth during development and in regeneration. Several *in vitro* studies clearly demonstrated that tissue cultured astrocytes are capable of expressing laminin matrices that support neurite regeneration (Garcia-Abreu et al., 1995; Martinez and Gomes, 2002). Since the strong influence of the ECM component laminin, on axonal growth and regeneration is well established (Manthorpe et al., 1983; Luckenbill-Edds, 1997; Freire et al., 2004), PLL/laminin substrate coating was chosen as a positive control substrate for the experiments. It has been shown in many studies that laminin as substrate is not an inert surface, but a major ECM molecule to promote strong neuronal regeneration *in vitro* (Liesi et al., 1984; Jones et al., 2003a; Tucker et al., 2005a,b). Therefore, it is very likely that the overall strong neurite outgrowth (and length of the longest neurite) observed when exposed to hNP-AC conditioned media, was influenced by the PLL/laminin substrate.

When neurite outgrowth over hNP-AC ECM was compared to our previously published data, it was surprising that the preserved ECM supported similar extent of DRG neurite regeneration as was supported by the viable cell monolayers (Fig. 7.1A, compare 2nd and 5th column; Führmann et al., 2010b). Interestingly, the length of the longest neurite sprouting away from the cell soma was significantly higher on hNP-AC ECM than on monolayers of hNP-AC (Fig. 7.1B, compare 2nd and 5th column, $p < 0.001$). This observation may be related to observations by other groups where a morphololgical heterogeneity of astrocytic monolayers has been reported: astrocytes formed either "flat" or "rocky" surface appearances, reflecting the absence or presence of bumps on the monolayer surface (Grierson et al., 1990; Meiners et al., 1995). The uneven surfaces were reported to be less permissive for neurite extension than the flat surfaces. A more recent finding confirmed this observation, where differences in the neuritogenic potential of distinct embryonic astrocyte monolayers correlated with the polygonal shaped mesh of laminin that had been secreted by the glial cells (Freire et al., 2004). It may be suggested that surface morphologies of the hNP-AC monolayers in the present investigation (see chapter 6.1, Fig. 6.1A) presented a more uneven surface than that provided by the hNP-AC ECM alone. However, this possibility remains speculative.
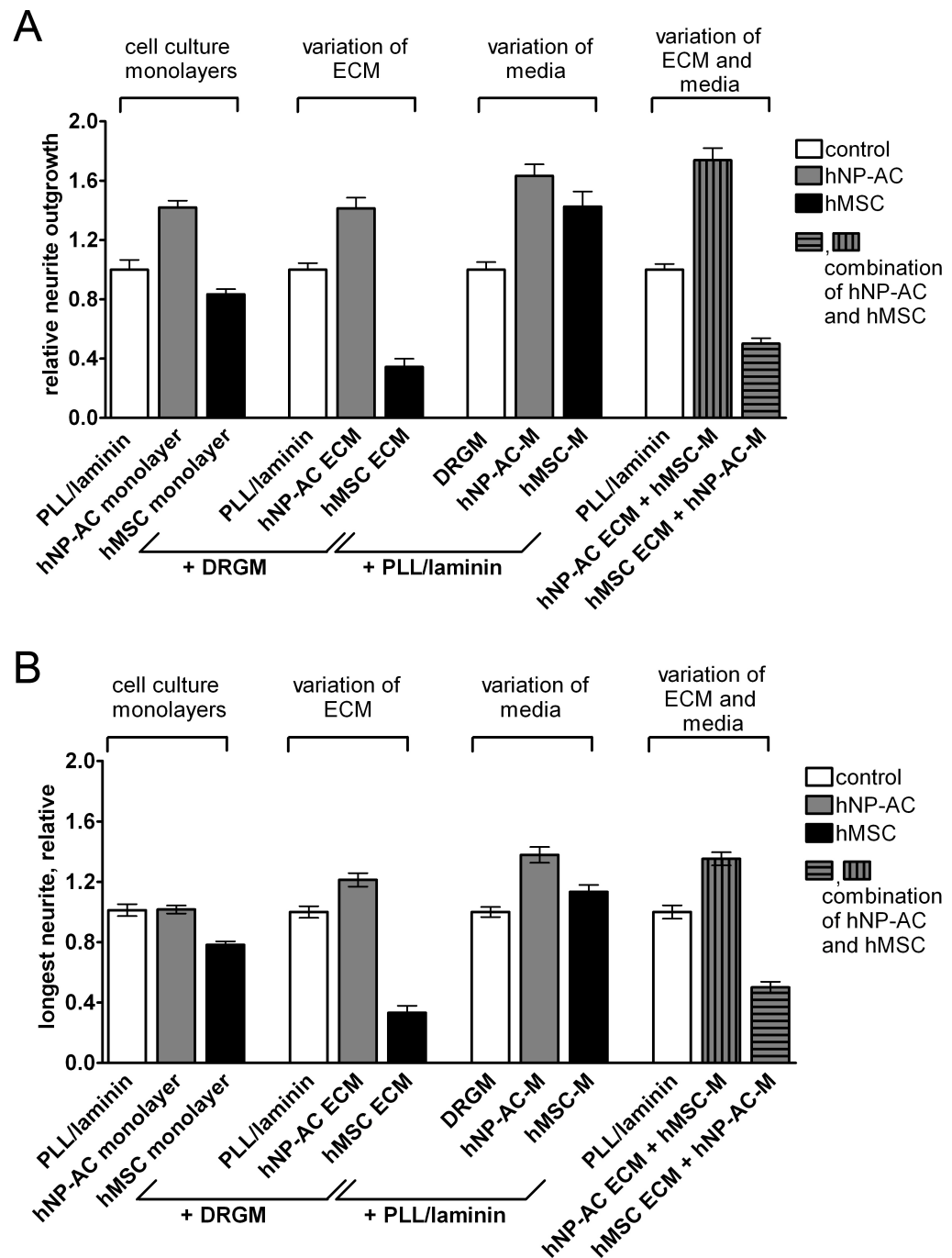
Figure 7.1: **Relative neurite outgrowth and longest neurite length for regenerating DRG neurons on cell culture monolayers compared to the experimental conditions performed in this study.**
Graph **A** is identical to Figure 6.7 in chapter 6.4 and gives an overview about relative overall neurite outgrowth, except for the first three columns: These demonstrate previous results of our group, which show neurite outgrowth on monolayer cultures of hMSC and hNP-AC. Data were kindly provided by T.Führmann and K.Montzka.
Graph **B** shows results for investigation of relative longest neurite length of DRG neurons grown on monolayers (1st to 3rd column), ECM (4th to 6th column), conditioned media (7th to 9th column) and combination of ECM with conditioned media (10th to 12th column) of hMSC and hNP-AC.

7.4 Support of Neurite Outgrowth by hMSC ECM and hMSC-M

In contrast to hNP-AC ECM, the hMSC ECM was found to be a relatively poor substrate for axon regeneration. Although hMSC-ECM and the defined DRG medium were able to support neurite outgrowth, the overall length of the regenerating neurites was significantly less extensive than that supported by the viable hMSC monolayer. This difference was even more prominent in comparison to the PLL/laminin positive control substrate (Fig. 7.1A, compare 3rd, 4th, 5th and 6th column, $p < 0.001$).

Although hMSC ECM seemed to be a relatively poor substrate for axon regeneration, a related investigation by our group revealed that its orientational cues were, to some extent, responsible for influencing the direction of neurite outgrowth. The most profound degree of neurite directionality was supported by viable hMSC and hMSC ECM (Führmann et al., 2010a). One possible explanation for the relatively poor support of neurite outgrowth over hMSC-ECM might relate to the extent of preservation of the ECM in the present study. It was assumed at the outset of the experiment that the ECM from hNP-AC and hMSC would be similarly preserved by the cell lysis protocol, however, it cannot be excluded that hMSC-ECM may have been poorly preserved. Thus, a systematic methodological error could have resulted in the observed poor neurite regeneration. Although in the present investigation there was no attempt to demonstrate the presence of the residual ECM following the water lysis protocol, this explanation remains unlikely, since the technique is already well tried and has been tested for numerous cell types (Lider et al., 1995; Doss, 1999; Milner and Campbell, 2002).

If there is no systematic error in the present experimental model, the results might imply that hMSC-ECM, alone, enables adherence of DRG neurons, but provides a relatively poor substrate for neurite extension. It has been reported, that hMSC express abundant levels of the intercellular adhesion- and ECM-related molecules such as N-cadherin, collagen I, collagen IV, fibronectin and laminin (Puch et al., 2001; Grayson et al., 2004; Schieker et al., 2007). However, it has been shown that laminin is a better neurite growth promoting ECM molecule than fibronection for a range of PNS and CNS neurons (Manthorpe et al., 1983; Luckenbill-Edds, 1997; Hynds and Snow, 2001), what might explain the significantly longer neurite outgrowth on purified laminin coating as substrate than on hMSC-ECM (Fig. 7.1A and B, compare 4th and 6th column, $p < 0.001$).

The present data clearly suggest that hMSC-derived molecules, present in conditioned medium, promote extensive neurite outgrowth. This is in contrast to Kamishina and colleagues who report the production of ECM components such as fibronectin and laminin to be the prime attributes of canine MSC's ability to promote neurite outgrowth (Kamishina et al., 2009). This would suggest the existence of species-dependent variability in the axon growth-promoting

properties of MSC.

The viable hMSC supported neurite outgrowth that was significantly greater than that observed over the hMSC-ECM (Fig. 7.1A and B, compare 3rd and 6th column, $p < 0.001$). Furthermore, the hMSC conditioned medium promoted significantly greater outgrowth over the PLL/laminin substrate than was supported by PLL/laminin and DRGM or by hMSC-ECM and DRGM (Fig. 7.1A and B, compare 6th, 7th and 9th column, $p < 0.001$). This indicates that hMSC support strong axonal growth by secreted, diffusible substances and confirms observations of others, who have suggested the beneficial effects of donor hMSC in SCI to be due to the release of growth factors and cytokines (Neuhuber et al., 2005; Himes et al., 2006). Furthermore, real-time-PCR analysis by our group demonstrated that hMSC expressed a range of important growth factors and neurotrophins, including BDNF, bFGF, EGF, NGF, NT-3, NT-4, VEGF, SDF-1 as well as cytokines IL-1, IL-6 and IL-8 (Führmann et al., 2010a). Neurotrophins are the most extensively characterised group of extracellular factors that induce axon growth (Zhou and Snider, 2006), with NGF and NT3 inducing axon growth from sympathetic ganglion cells and DRG neurons via activation of their corresponding receptors, i.e. tyrosine kinase A and C (TrkA, TrkC; Snider, 1988; Liebl et al., 1997). Furthermore, BDNF has been shown to be important for neuronal survival in adult rat DRG neurons (Acheson et al., 1995), whereas VEGF promoted regeneration through the fetal liver kinase 1 (flk-1) receptor in adult mice DRG (Sondell et al., 2000).

It has been suggested that monolayers of hMSC support the generation of a greater number of primary neurites than monolayers of hNPC, hNP-AC or PLL/laminin substrate (T. Führmann, personal communication). Therefore one may have assumed that an investigation concerning elaboration of the number of primary neurites over hMSC-ECM, hNP-AC-ECM and PLL/laminin might show similar results. This was, however, not supported by the present study. Despite the strong induction of primary neurites by viable hMSC monolayers (T. Führmann, personal communication), no such behaviour was observed over hMSC ECM substrate or control substrates that were supported by hMSC conditioned media.

7.5 Interactions of Released Factors with ECM Substrates

The question, to what extent neuronal responses to diffusible trophic factors (i.e. present in conditioned medium) could be modified by interactions with their substrate environment (i.e. the ECM) or conversely, to what extent the responses of the cell to its ECM environment were modified by the presence of diffusible trophic factors was addressed with a combinatorial experimental approach. Two major experimental settings were established, where conditioned media

and ECM substrate varied: in one experiment hNP-AC ECM was combined with hMSC-M, and in the other, hMSC-ECM was combined with hNP-AC-M (Fig. 7.1A and B, 11th and 12th column). Overall, the greatest extent of DRG neurite regeneration was supported by hNP-AC ECM combined with hMSC-M (Fig. 7.1A, 11th column). Outgrowth was significantly greater compared to outgrowth on hNP-AC ECM with DRGM (Fig. 7.1A, 5th column, $p < 0.05$), PLL/laminin substrate with hMSC-M (Fig. 7.1A, 9th column, $p < 0.05$) or the positive PLL/laminin control with DRGM (Fig 7.1A, 1st column, $p < 0.001$). Likewise there was a trend for greater neurite outgrowth, when the combination hNP-AC ECM with hMSC-M was compared to the outgrowth over viable monolayers of hNP-AC, but this failed to reach the level of statistical significance though (Fig. 7.1A, 2nd column). It seems that the interaction of hMSC-M with hNP-AC ECM, or the other way around, the interactions of hNP-AC-ECM with hMSC-M provided a favourable atmosphere for neurite regeneration and regrowth.

Interestingly, hNP-AC-M supported strong neurite regeneration when applied to PLL/laminin substrate, but not so when applied to hMSC-ECM. The combinatory application of hNP-AC-M with hMSC-ECM showed significantly less neurite outgrowth in comparison to hNP-AC-M with PLL/laminin (Fig. 7.1A, compare 10th to 12th column, $p < 0.001$). There was only a slight, statistically not significant, tendency for enhanced DRG neurite outgrowth in the combinatorial experiment compared to hMSC-ECM with DRGM (Fig. 7.1A, compare 6th to 12th column). From that it can be deduced that hNP-AC-M was apparently inable to increase DRG regeneration over the hMSC substrate.

It is well known that neurite outgrowth is influenced by a number of stimuli including diffusible nerve growth factors and ECM-mediated mechanisms (Tucker et al., 2005b; Zhou and Snider, 2006). Previous studies have demonstrated that conditioned media of hMSC contributed to the activation of intracellular signalling pathways in neurons and astrocytes: for example rat and human MSC-conditioned medium promoted the phosphorylation of mitogen-activated protein kinase (MAPK), extracellular signal-regulated protein kinase (ERK) and of total extracellular phosphoinositide 3-kinase/serine/threonine kinase (PI3K/Akt) in primary cultures of rat DRG neurons.

This suggested that MSCs trigger endogenous survival- and growth signaling pathways in neurons through their secreted soluble factors, including BDNF, VEGF, bFGF and CNTF (Gao et al., 2005b,a; Zhou and Snider, 2006; Isele et al., 2007; Gu et al., 2010). Similarly, it has been shown that hMSC conditioned media activate these two pathways in post ischemia rat astrocytes, thereby contributing to astrocytic cell survival (Gao et al., 2005b,a).

In addition to growth factors, adhesion of regenerating neurons to ECM proteins (including fibronectin and laminin) via ligation to their integrin receptors also leads to activation of the MAPK- and ERK pathway thereby stimulating cell proliferation and regrowth (Boudreau and

Jones, 1999; Danen and Yamada, 2001). It is also known that integrin-activated signalling pathways are capable of interacting with diffusible growth factor-activated pathways to promote enhanced axonal regeneration: it has been reported that growth factor-mediated signalling and integrin-mediated signalling converge in adult rat DRG neurons and even that integrin signalling may be required for certain growth factors (e.g. NGF) to promote their effect on neurite extension and branching (Tucker et al., 2005b). Similarly, cross-talk between signal transduction pathways for different growth factors (i.e. NGF and insulin like growth factor-1, IGF-1) has been reported to act synergistically in the promotion of axon growth (Jones et al., 2003b). Recent studies have suggested that both the Src tyrosine kinase and focal adhesion kinase (FAK) may act together in regulating the down-stream signalling through the activation of PI3K and Akt kinase that are required for axonal extension (Tucker and Mearow, 2008).

Other groups have reported that the axon growth inhibitory effects of chondroitin sulphate proteoglycans (CSPG), which are located in the ECM, are due to interference with integrin signalling and that certain growth factors (e.g. NGF) can induce robust axon growth, even over inhibitory CSPGs (Zhou and Snider, 2006). It may be that hMSC-M contains such factors, and that these are not present in hNP-AC-M, or that the levels of these factors are higher in hMSC-M than in hNP-AC-M. Clarification of this point would require further investigation into the molecular constituents of hMSC- and hNP-AC- conditioned media as well as the components of their respective ECM. Furthermore, the signal transduction cascades associated with the relevant growth factor and ECM molecules would also need to be investigated.

7.6 Conclusions

The investigation confirmed that both, the extracellular environment through which axons grow and the availability and action of neurotrophic factors play key roles in regulating axonal growth and regeneration. Furthermore, it was possible to extend the information about interactions between diffusible, growth factor mediated effects and those brought about by ECM-related molecules. The present study clearly indicates that:

I) hNP-AC ECM mediated mechanisms and the release of diffusible factors into the medium were both involved in the potent axon growth promoting effects of hNP-AC *in vitro*; suggesting them as a promising cell type for consideration in future tissue engineering strategies to promote functional repair in animal models of traumatic CNS and spinal cord injury.

II) There is an, as yet, undefined benefical cross-talk between hMSC-M mediated signalling and that induced by hNP-AC ECM; the result being enhanced axon-growth.

III) hMSC ECM appears to contain molecules that are detrimental to axon growth.

IV) Comparison of the extent of axon growth supported by viable hMSC (i.e. that supported by hMSC ECM and diffusible factors) with that supported by hMSC ECM only suggests that living hMSC release a factor or factors that is/are capable of over-riding the inhibitory component(s) of the hMSC ECM.

V) The factors released by hNP-AC, although capable of increasing axon growth over PLL/laminin and hNP-AC ECM substrates, are incapable of over-riding the inhibitory effects of hMSC-ECM.

Part III

Final Remarks

8 Final Remarks

The present study gives further evidence that hNP-AC and hMSC possess features that justify their consideration in future cell therapy-based strategies for repair of the injured spinal cord. In a previous study our group has described the axon growth promoting effects of hMSC-, hNPC and hNP-AC monolayers *in vitro* (Führmann et al., 2010a,b). We could show that hMSC were able to direct neurite regeneration. Furthermore, the immature hNP-AC promoted stronger neurite outgrowth than either non-differentiated hNPC or hMSC. To obtain a better understanding of the mechanisms accounting for strong neurite regeneration in hNP-AC and hMSC, further *in vitro* investigations were performed in the present study.

In Part I of this thesis, the hNPC and hNP-AC were characterised and their proliferative activity was studied in order to define the cellular changes that were induced by differentiation with the media supplements BMP4 and LIF. The investigation was successful in a number of aspects: the characterisation confirmed that the differentiated hNP-AC represented a highly enriched cell population of immature type I astrocytes, with only a few TuJ1+/MAP2ab+ neuronal cells being found. These immature hNP-AC expressed the stem/progenitor cell related markers nestin (89.2 $\pm$ 3.8%), SOX2 (88.0 $\pm$ 3.6%), musashi (91.8 $\pm$ 2.0%), CD133-and nestin mRNA in similar proportions to the hNPC, as well as elevated levels of S100β (from 17.6 $\pm$ 2.1% in hNPC to 79.4 $\pm$ 1.7% in hNP-AC), GFAP (from 23.7 $\pm$ 2.3% in hNPC to 92.5 $\pm$ 3.4% in hNP-AC) and CD44 (coexpressed in all GFAP+ hNP-AC).

The characterisation of hNPC and the differentiated hNP-AC in this study might contribute to the optimisation of protocols for the future generation of hNP-AC in regenerative medicine for CNS diseases and disorders. However, it should be considered that the establishment of exact reproducible differentiation protocols has limitations due to the heterogeneity of the source and age of the tissue used to harvest the neural stem/progenitors. Furthermore, in view of limited availability of foetal donor tissue and ethical concerns, large scale use of this source as a treatment option remains challenging. On the other hand, recent progress in the research of neural stem/progenitor cell biology has made it possible to routinely expand neural stem cells obtained from a small amount of foetal CNS tissue *in vitro* (Svendsen et al., 1999; Wachs et al., 2003). To realise preliminary clinical studies in patients in the future, high amounts of cellular material will be essential. Thus, the proliferative activity of the cells remains an important characteristic

to be observed. In awareness of the limitations, that are present in an *in vitro* investigation, the proliferation experiments of this study revealed that the differentiated hNP-AC showed decelerated proliferation kinetics with a *DT* of 5.1 days (in the morphological assay), i.e. 3.2 days (in the metabolic assay) in comparison to non-differentiated hNPC with a *DT* of 3.5 days (in the morphological assay), i.e. 1.7 days (in the metabolic assay). However, it should be considered that the investigations concerning proliferation kinetics cannot reveal exact and generally valid data. In registration of the varying obtained values in dependency of the performed assays, the determined doubling times represent approximated values.

In part II of this thesis, the axon growth promoting effects of ECM and conditioned media derived from hNP-AC and hMSC were investigated *in vitro*. The conditioned media of both cell types promoted strong neurite regeneration, indicating the release of axon growth promoting substances into the culture media. The ECM derived from hNP-AC supported strong neurite regeneration whereas that derived from hMSC only promoted poor regeneration.
A better understanding of the molecular mechanisms involved in such behaviour will require the identification of which ECM- and diffusible components are produced by both cell types and which signal transduction cascades they are capable of activating. This information will be important for understanding the beneficial mechanisms of action of donor cells as well as influencing the final choice of cell type to be used in future regenerative medicine strategies.

Part IV

Appendix

9 Additional Data

9.1 Formula to Calculate *DT* in the Morphological Assay

$$DT = \frac{ln2}{\alpha} \tag{9.1}$$

to calculate the Doubling Time (DT) from all neurosphere in the morphological assay has been derived from the following differential equation:

$$\frac{\partial V}{\partial t} = \alpha V \tag{9.2}$$

That means proliferation ($\partial V / \partial t$) is propotional to the actual Volume (V), i.e. cell number. Transformation and integration resulted in

$$\frac{1}{V}\partial V = \alpha \partial t \stackrel{Integration}{\longrightarrow} \int_{V_{t=0}}^{V_t} \frac{1}{V}\partial V = \int_{t=0}^{t} \alpha \partial t. \tag{9.3}$$

The integration leads to

$$ln\, V_t - ln\, V_{t=0} = ln\, \frac{V_t}{V_{t=0}} = \alpha(t - 0) \tag{9.4}$$

Using common logarithms this equation leads to the exponential function:

$$V_t = V_{t=0} e^{\alpha t} \tag{9.5}$$

Inserting DT the ratio between the volume V_{DT} and the volume $V_{t=0}$ becomes two.

$$V_{DT} = V_{t=0}\, e^{\alpha DT} \Rightarrow \frac{V_{DT}}{V_{t=0}} = 2 = e^{\alpha DT} \tag{9.6}$$

Using logarithms the equation for the Doubling time becomes

$$ln2 = \alpha DT \Rightarrow DT = \frac{ln2}{\alpha}. \tag{9.7}$$

This formula enabled a calculation of mean DT including all neurospheres from the morphological assay.

9.2 Quantification of hNPC and hNP-AC

Table 9.1: **Overview of quantified immunocytochemical phenotypes in hNPC and hNP-AC**

Markers	hNPC [%]	hNP-AC [%]
Stem/ Progenitor Cell Markers		
Nestin	91.0 ± 3.4	89.2 ± 3.8
SOX2	89.2 ± 2.7	88.0 ± 3.6
Musashi	91.8 ± 2.0	89.2 ± 3.8
Astroglial Markers		
Vimentin	96.8 ± 1.1	92.9 ± 3.8
GFAP	23.7 ± 2.3	92.5 ± 3.4
S100β	17.6 ± 2.1	79.4 ± 1.7
CD44	-	coexpression in all GFAP+ hNP-AC

The table summarises the immunocytochemical phenotypes, that were counted in hNPC and differentiated hNP-AC for stem/ progenitor cell- and astroglial markers. The proportion of cells labeled for immunocytochemical markers was analysed in cell monolayers, that hat emerged around PLL/laminin plated neurospheres after 24 hours.

9.3 Overview of RT-PCR
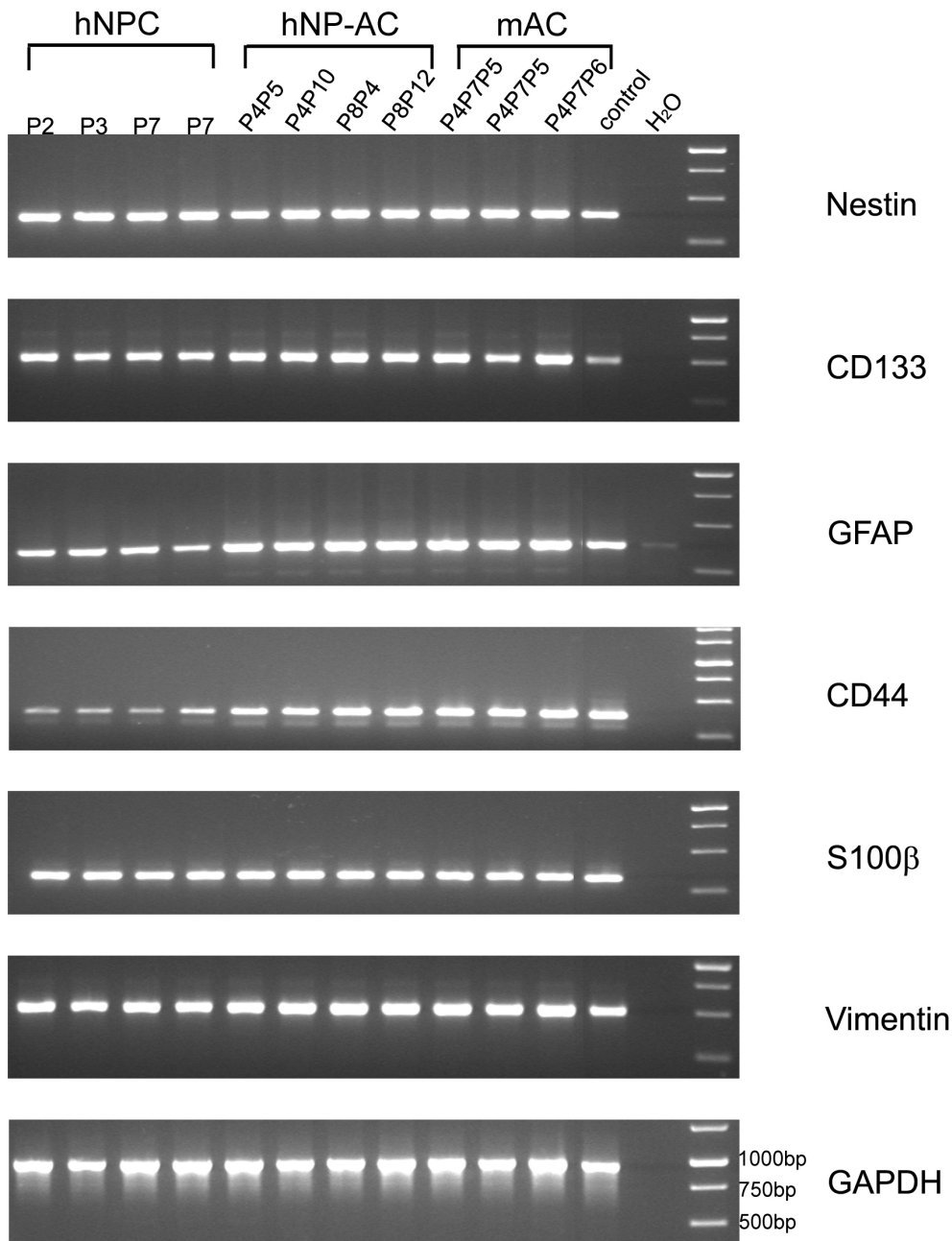
Figure 9.1: **Overview of RT-PCR performed in this study.**
RT-PCR was performed for hNPC, hNP-AC (and mature astrocytes, mAC) with the stem/progenitor cell markers nestin and CD133 such as the glial markers GFAP, CD44, S100β and vimentin. The first four bands show samples of different hNPC culture passages and the next four bands show samples of different hNP-AC culture passages. The four bands of mature astrocytes (mAC) are not relevant for this study, but were processed in the same experimental runs as hNPC and hNP-AC. As positive control the cell lines U373, THP-1 and MCF-7 were used. H_2O was used as negative control. On the left of each row the the number of bp is marked by the Gene-Ruler^{TM} 1kb-ladder. The bottom row of DNA bands shows the internal control with the house keeping gene GAPDH for each sample.

9.4 Effect of Trophic Factors and ECM on DRG Neurite Regeneration *in Vitro*

Table 9.2: **Relative and Absolute Values for All Experimental Conditions**

experimental condition	overall neurite outgrowth	longest neurite length	primary branches	outgrowth per branch
	[μm]/[-]*	[μm]/[-]*	[-]/[-]	[μm]/[-]*
PLL/laminin +DRGM	3516 ±223 **1.0**	237 ±7.5 **1.0**	4.9 ±0.15 **1.0**	935.8 ±57 **1.0**
hNP-AC ECM +DRGM	6137 ±314 **1.41 ±0.07**	296 ±11 **1.21 ±0.05**	5.8 ±0.3 **1.02 ±0.05**	1421 ±121 **1.54 ±0.13**
hMSC ECM +DRGM	1226 ±199 **0.34 ±0.06**	160 ±10 **0.64 ±0.04**	3.7 ±0.2 **1.02 ±0.05**	441 ±90 **0.40 ±0.08**
PLL/laminin +hNP-AC-M	7089 ±335 **1.63 ±0.08**	337 ±13 **1.38 ±0.05**	6.3 ±0.3 **1.11 ±0.05**	1557 ±155 **1.69 ±0.17**
PLL/laminin +hMSC-M	3765 ±267 **1.43 ±0.1**	248 ±10 **1.13 ±0.05**	5.0 ±0.2 **1.11 ±0.05**	990 ±114 **1.28 ±0.15**
hNP-AC ECM +hMSC-M	7545 ±256 **1.74 ±0.08**	330 ±11 **1.35 ±0.04**	7.0 ±0.4 **1.24 ±0.07**	1468 ±155 **1.60 ±0.17**
hMSC ECM +hNP-AC-M	2175 ±161 **0.5 ±0.04**	122 ±9 **0.56 ±0.01**	4.8 ±0.3 **1.06 ±0.06**	453 ±64 **0.78 ±0.8**

The data represent means ± SEM of 100 analysed DRG neurons per experimental condition, except for the experimental positive control (PLL/laminin + DRGM) which includes means ± SEM of 300 DRG neurons. For statistical anaylsis relative values were used.

* The **bold** numbers represent the relative values set in ratio to the positive control (PLL/laminin + DRGM).

10 Bibliography

Acheson A., Conover J.C., Fandl J.P., DeChiara T.M., Russell M., Thadani A., Squinto S.P., Yancopoulos G.D., Lindsay R.M., 1995: A BDNF autocrine loop in adult sensory neurons prevents cell death., *Nature* **374**(6521) 450–453.

Anderberg L., Aldskogius H., Holtz A., 2007: Spinal cord injury–scientific challenges for the unknown future., *Ups J Med Sci* **112**(3) 259–288.

Armstrong R.J., Watts C., Svendsen C.N., Dunnett S.B., Rosser A.E., 2000: Survival, neuronal differentiation, and fiber outgrowth of propagated human neural precursor grafts in an animal model of Huntington's disease., *Cell Transplant* **9**(1) 55–64.

Asher R.A., Morgenstern D.A., Fidler P.S., Adcock K.H., Oohira A., Braistead J.E., Levine J.M., Margolis R.U., Rogers J.H., Fawcett J.W., 2000: Neurocan is upregulated in injured brain and in cytokine-treated astrocytes., *J Neurosci* **20**(7) 2427–2438.

Azizi S.A., Stokes D., Augelli B.J., DiGirolamo C., Prockop D.J., 1998: Engraftment and migration of human bone marrow stromal cells implanted in the brains of albino rats–similarities to astrocyte grafts., *Proc Natl Acad Sci U S A* **95**(7) 3908–3913.

Bandtlow C.E., Löschinger J., 1997: Developmental changes in neuronal responsiveness to the CNS myelin-associated neurite growth inhibitor NI-35/250., *Eur J Neurosci* **9**(12) 2743–2752.

Bansal R., Warrington A.E., Gard A.L., Ranscht B., Pfeiffer S.E., 1989: Multiple and novel specificities of mon-oclonal antibodies O1, O4, and R-mAb used in the analysis of oligodendrocyte development., *J Neurosci Res* **24**(4) 548–557.

Bareyre F.M., 2008: Neuronal repair and replacement in spinal cord injury., *J Neurol Sci* **265**(1-2) 63–72.

Barkho B.Z., Song H., Aimone J.B., Smrt R.D., Kuwabara T., Nakashima K., Gage F.H., Zhao X., 2006: Identification of astrocyte-expressed factors that modulate neural stem/progenitor cell differentiation., *Stem Cells Dev* **15**(3) 407–421.

Barrett C.P., Donati E.J., Guth L., 1984: Differences between adult and neonatal rats in their astroglial response to spinal injury., *Exp Neurol* **84**(2) 374–385.

Barrett C.P., Guth L., Donati E.J., Krikorian J.G., 1981: Astroglial reaction in the gray matter lumbar segments after midthoracic transection of the adult rat spinal cord., *Exp Neurol* **73**(2) 365–377.

Bartsch U., Bandtlow C.E., Schnell L., Bartsch S., Spillmann A.A., Rubin B.P., Hillenbrand R., Montag D., Schwab M.E., Schachner M., 1995: Lack of evidence that myelin-associated glycoprotein is a major inhibitor of axonal regeneration in the CNS., *Neuron* **15**(6) 1375–1381.

Bean B.P., 1990: ATP-activated channels in rat and bullfrog sensory neurons: concentration dependence and kinetics., *J Neurosci* **10**(1) 1–10.

Beattie M.S., Farooqui A.A., Bresnahan J.C., 2000: Review of current evidence for apoptosis after spinal cord injury., *J Neurotrauma* **17**(10) 915–925.

Bennett D.L., Michael G.J., Ramachandran N., Munson J.B., Averill S., Yan Q., McMahon S.B., Priestley J.V., 1998: A distinct subgroup of small DRG cells express GDNF receptor components and GDNF is protective for these neurons after nerve injury., *J Neurosci* **18**(8) 3059–3072.

Bez A., Corsini E., Curti D., Biggiogera M., Colombo A., Nicosia R.F., Pagano S.F., Parati E.A., 2003: Neurosphere and neurosphere-forming cells: morphological and ultrastructural characterization., *Brain Res* **993**(1-2) 18–29.

Bianchi R., Giambanco I., Donato R., 1993: S-100 protein, but not calmodulin, binds to the glial fibrillary acidic protein and inhibits its polymerization in a Ca(2+)-dependent manner., *J Biol Chem* **268**(17) 12669–12674.

Biran R., Noble M.D., Tresco P.A., 2003: Directed nerve outgrowth is enhanced by engineered glial substrates., *Exp Neurol* **184**(1) 141–152.

Bixby J.L., Pratt R.S., Lilien J., Reichardt L.F., 1987: Neurite outgrowth on muscle cell surfaces involves extracellular matrix receptors as well as Ca2+-dependent and -independent cell adhesion molecules., *Proc Natl Acad Sci U S A* **84**(8) 2555–2559.

Björklund A., 1993: Neurobiology. Better cells for brain repair., *Nature* **362**(6419) 414–415.

Björklund A., Stenevi U., 1984: Intracerebral neural implants: neuronal replacement and reconstruction of damaged circuitries., *Annu Rev Neurosci* **7** 279–308.

Blenis J., Hawkes S.P., 1983: Transformation-sensitive protein associated with the cell substratum of chicken embryo fibroblasts., *Proc Natl Acad Sci U S A* **80**(3) 770–774.

Bonaguidi M.A., McGuire T., Hu M., Kan L., Samanta J., Kessler J.A., 2005: LIF and BMP signaling generate separate and discrete types of GFAP-expressing cells., *Development* **132**(24) 5503–5514.

Bonni A., Sun Y., Nadal-Vicens M., Bhatt A., Frank D.A., Rozovsky I., Stahl N., Yancopoulos G.D., Greenberg M.E., 1997: Regulation of gliogenesis in the central nervous system by the JAK-STAT signaling pathway., *Science* **278**(5337) 477–483.

Boudreau N.J., Jones P.L., 1999: Extracellular matrix and integrin signalling: the shape of things to come., *Biochem J* **339 (Pt 3)** 481–488.

Breasted J., 1930: Edwin Smith Surgical Papyrus in Facsimile and Hieroglyphic Transliteration With Translation and Commentary., *Chicago, IL: University of Chicago Oriental Institute Publications* **2 Vols**.

Bregman B.S., Coumans J.V., Dai H.N., Kuhn P.L., Lynskey J., McAtee M., Sandhu F., 2002: Transplants and neurotrophic factors increase regeneration and recovery of function after spinal cord injury, *Prog Brain Res* **137** 257–273.

Brook G.A., Houweling D.A., Gieling R.G., Hermanns T., Joosten E.A., Bär D.P., Gispen W.H., Schmitt A.B., Leprince P., Noth J., Nacimiento W., 2000: Attempted endogenous tissue repair following experimental spinal cord injury in the rat: involvement of cell adhesion molecules L1 and NCAM?, *Eur J Neurosci* **12**(9) 3224–3238.

Brook G.A., Pérez-Bouza A., Noth J., Nacimiento W., 1999: Astrocytes re-express nestin in deafferented target territories of the adult rat hippocampus., *Neuroreport* **10**(5) 1007–1011.

Bunge M.B., 2008: Novel combination strategies to repair the injured mammalian spinal cord., *J Spinal Cord Med* **31**(3) 262–269.

Buss A., Pech K., Kakulas B.A., Martin D., Schoenen J., Noth J., Brook G.A., 2008: TGF-beta1 and TGF-beta2 expression after traumatic human spinal cord injury., *Spinal Cord* **46**(5) 364–371.

Buss A., Schwab M.E., 2003: Sequential loss of myelin proteins during Wallerian degeneration in the rat spinal cord., *Glia* **42**(4) 424–432.

Cajal S., 1928: Degeneration and Regeneration of the Nervous System, *Oxford, UK: Oxford University Press [transl. R. M. May]* .

do Carmo Cunha J., de Freitas Azevedo Levy B., de Luca B.A., de Andrade M.S.R., Gomide V.C., Chadi G., 2007: Responses of reactive astrocytes containing S100beta protein and fibroblast growth factor-2 in the border and in the adjacent preserved tissue after a contusion injury of the spinal cord in rats: implications for wound repair and neuroregeneration., *Wound Repair Regen* **15**(1) 134–146.

Caroni P., Savio T., Schwab M.E., 1988: Central nervous system regeneration: oligodendrocytes and myelin as non-permissive substrates for neurite growth., *Prog Brain Res* **78** 363–370.

Caroni P., Schwab M.E., 1988: Antibody against myelin-associated inhibitor of neurite growth neutralizes nonpermissive substrate properties of CNS white matter., *Neuron* **1**(1) 85–96.

Carpenter M.K., Cui X., Hu Z.Y., Jackson J., Sherman S., Seiger A., Wahlberg L.U., 1999: In vitro expansion of a multipotent population of human neural progenitor cells., *Exp Neurol* **158**(2) 265–278.

Carter W.G., Kaur P., Gil S.G., Gahr P.J., Wayner E.A., 1990: Distinct functions for integrins alpha 3 beta 1 in focal adhesions and alpha 6 beta 4/bullous pemphigoid antigen in a new stable anchoring contact (SAC) of keratinocytes: relation to hemidesmosomes., *J Cell Biol* **111**(6 Pt 2) 3141–3154.

Chen J., Li Y., Chopp M., 2000a: Intracerebral transplantation of bone marrow with BDNF after MCAo in rat., *Neuropharmacology* **39**(5) 711–716.

Chen M.S., Huber A.B., van der Haar M.E., Frank M., Schnell L., Spillmann A.A., Christ F., Schwab M.E., 2000b: Nogo-A is a myelin-associated neurite outgrowth inhibitor and an antigen for monoclonal antibody IN-1., *Nature* **403**(6768) 434–439.

Cheng L., Hammond H., Ye Z., Zhan X., Dravid G., 2003: Human adult marrow cells support prolonged expansion of human embryonic stem cells in culture., *Stem Cells* **21**(2) 131–142.

Chopp M., Zhang X.H., Li Y., Wang L., Chen J., Lu D., Lu M., Rosenblum M., 2000: Spinal cord injury in rat: treatment with bone marrow stromal cell transplantation., *Neuroreport* **11**(13) 3001–3005.

Chow W.N., Simpson D.G., Bigbee J.W., Colello R.J., 2007: Evaluating neuronal and glial growth on electrospun polarized matrices: bridging the gap in percussive spinal cord injuries., *Neuron Glia Biol* **3**(2) 119–126.

Chu Y., Hughes S., Chan-Ling T., 2001: Differentiation and migration of astrocyte precursor cells and astrocytes in human fetal retina: relevance to optic nerve coloboma., *FASEB J* **15**(11) 2013–2015.

Clarke S.R., Shetty A.K., Bradley J.L., Turner D.A., 1994: Reactive astrocytes express the embryonic intermediate neurofilament nestin., *Neuroreport* **5**(15) 1885–1888.

Clemente C.D., 1964: REGENERATION IN THE VERTEBRATE CENTRAL NERVOUS SYSTEM., *Int Rev Neurobiol* **6** 257–301.

Cummings B.J., Uchida N., Tamaki S.J., Salazar D.L., Hooshmand M., Summers R., Gage F.H., Anderson A.J., 2005: Human neural stem cells differentiate and promote locomotor recovery in spinal cord-injured mice., *Proc Natl Acad Sci U S A* **102**(39) 14069–14074.

Dahl D., Bignami A., Weber K., Osborn M., 1981a: Filament proteins in rat optic nerves undergoing Wallerian degeneration: localization of vimentin, the fibroblastic 100-A filament protein, in normal and reactive astrocytes., *Exp Neurol* **73**(2) 496–506.

Dahl D., Rueger D.C., Bignami A., Weber K., Osborn M., 1981b: Vimentin, the 57 000 molecular weight protein of fibroblast filaments, is the major cytoskeletal component in immature glia., *Eur J Cell Biol* **24**(2) 191–196.

Danen E.H., Yamada K.M., 2001: Fibronectin, integrins, and growth control., *J Cell Physiol* **189**(1) 1–13.

Davies J., Pröschel C., Zhang N., Noble M., Mayer-Pröschel M., Davies S., 2008: Transplanted astrocytes derived from BMP- or CNTF-treated glial-restricted precursors have opposite effects on recovery and allodynia after spinal cord injury., *J Biol* **7**(7) 24.

Davies J.E., Huang C., Proschel C., Noble M., Mayer-Proschel M., Davies S.J.A., 2006: Astrocytes derived from glial-restricted precursors promote spinal cord repair., *J Biol* **5**(3) 7.

Davies S.J., Fitch M.T., Memberg S.P., Hall A.K., Raisman G., Silver J., 1997: Regeneration of adult axons in white matter tracts of the central nervous system., *Nature* **390**(6661) 680–683.

Davies S.J., Goucher D.R., Doller C., Silver J., 1999: Robust regeneration of adult sensory axons in degenerating white matter of the adult rat spinal cord., *J Neurosci* **19**(14) 5810–5822.

Deans R.J., Moseley A.B., 2000: Mesenchymal stem cells: biology and potential clinical uses., *Exp Hematol* **28**(8) 875–884.

Dehmelt L., Halpain S., 2005: The MAP2/Tau family of microtubule-associated proteins., *Genome Biol* **6**(1) 204.

Delgado-Rivera R., Harris S.L., Ahmed I., Babu A.N., Patel R.P., Ayres V., Flowers D., Meiners S., 2009: Increased FGF-2 secretion and ability to support neurite outgrowth by astrocytes cultured on polyamide nanofibrillar matrices., *Matrix Biol* .

Delree P., Leprince P., Schoenen J., Moonen G., 1989: Purification and culture of adult rat dorsal root ganglia neurons., *J Neurosci Res* **23**(2) 198–206.

Deng Y.B., Liu X.G., Liu Z.G., Liu X.L., Liu Y., Zhou G.Q., 2006: Implantation of BM mesenchymal stem cells into injured spinal cord elicits de novo neurogenesis and functional recovery: evidence from a study in rhesus monkeys., *Cytotherapy* **8**(3) 210–214.

Dominici M., Blanc K.L., Mueller I., Slaper-Cortenbach I., Marini F., Krause D., Deans R., Keating A., Prockop D., Horwitz E., 2006: Minimal criteria for defining multipotent mesenchymal stromal cells. The International Society for Cellular Therapy position statement., *Cytotherapy* **8**(4) 315–317.

Donovan W.H., 2007: Donald Munro Lecture. Spinal cord injury–past, present, and future., *J Spinal Cord Med* **30**(2) 85–100.

Doss R.P., 1999: Composition and enzymatic activity of the extracellular matrix secreted by germlings of botrytis cinerea., *Appl Environ Microbiol* **65**(2) 404–408.

Dou C.L., Levine J.M., 1995: Differential effects of glycosaminoglycans on neurite growth on laminin and L1 substrates., *J Neurosci* **15**(12) 8053–8066.

Dumont A.S., Dumont R.J., Oskouian R.J., 2002: Will improved understanding of the pathophysiological mechanisms involved in acute spinal cord injury improve the potential for therapeutic intervention?, *Curr Opin Neurol* **15**(6) 713–720.

Eftekharpour E., Karimi-Abdolrezaee S., Fehlings M.G., 2008: Current status of experimental cell replacement approaches to spinal cord injury., *Neurosurg Focus* **24**(3-4) E19.

Ellis P., Fagan B.M., Magness S.T., Hutton S., Taranova O., Hayashi S., McMahon A., Rao M., Pevny L., 2004: SOX2, a persistent marker for multipotential neural stem cells derived from embryonic stem cells, the embryo or the adult., *Dev Neurosci* **26**(2-4) 148–165.

Eng L.F., 1985: Glial fibrillary acidic protein (GFAP): the major protein of glial intermediate filaments in differentiated astrocytes., *J Neuroimmunol* **8**(4-6) 203–214.

Eng L.F., Reier P.J., Houle J.D., 1987: Astrocyte activation and fibrous gliosis: glial fibrillary acidic protein immunostaining of astrocytes following intraspinal cord grafting of fetal CNS tissue., *Prog Brain Res* **71** 439–455.

Enzmann G.U., Benton R.L., Woock J.P., Howard R.M., Tsoulfas P., Whittemore S.R., 2005: Consequences of noggin expression by neural stem, glial, and neuronal precursor cells engrafted into the injured spinal cord., *Exp Neurol* **195**(2) 293–304.

Fairbairn S., Gilbert R., Ojakian G., Schwimmer R., Quigley J.P., 1985: The extracellular matrix of normal chick embryo fibroblasts: its effect on transformed chick fibroblasts and its proteolytic degradation by the transformants., *J Cell Biol* **101**(5 Pt 1) 1790–1798.

Fallon J.R., 1985a: Neurite guidance by non-neuronal cells in culture: preferential outgrowth of peripheral neurites on glial as compared to nonglial cell surfaces., *J Neurosci* **5**(12) 3169–3177.

Fallon J.R., 1985b: Preferential outgrowth of central nervous system neurites on astrocytes and Schwann cells as compared with nonglial cells in vitro., *J Cell Biol* **100**(1) 198–207.

Faulkner J., Keirstead H.S., 2005: Human embryonic stem cell-derived oligodendrocyte progenitors for the treatment of spinal cord injury., *Transpl Immunol* **15**(2) 131–142.

Fawcett J.W., Fersht N., Housden L., Schachner M., Pesheva P., 1992: Axonal growth on astrocytes is not inhibited by oligodendrocytes., *J Cell Sci* **103 (Pt 2)** 571–579.

Fawcett J.W., Housden E., Smith-Thomas L., Meyer R.L., 1989: The growth of axons in three-dimensional astrocyte cultures., *Dev Biol* **135**(2) 449–458.

Führmann T., Hillen L.M., Montzka K., Wöltje M., Brook G.A., 2010a: Cell-cell interactions of human neural progenitor-derived astrocytes within a microstructured 3D-scaffold., *Biomaterials* **31**(30) 7705–7715.

Führmann T., Montzka K., Hillen L.M., Hodde D., Dreier A., Bozkurt A., Wöltje M., Brook G.A., 2010b: Axon growth-promoting properties of human bone marrow mesenchymal stromal cells., *Neurosci Lett* **474**(1) 37–41.

Fong H., Hohenstein K.A., Donovan P.J., 2008: Regulation of self-renewal and pluripotency by Sox2 in human embryonic stem cells., *Stem Cells* **26**(8) 1931–1938.

Franklin R.J., Blakemore W.F., 1990: The peripheral nervous system–central nervous system regeneration dichotomy: a role for glial cell transplantation., *J Cell Sci* **95 (Pt 2)** 185–190.

Freire E., Gomes F.C.A., Jotha-Mattos T., Neto V.M., Filho F.C.S., Coelho-Sampaio T., 2004: Sialic acid residues on astrocytes regulate neuritogenesis by controlling the assembly of laminin matrices., *J Cell Sci* **117**(Pt 18) 4067–4076.

Frisén J., Johansson C.B., Török C., Risling M., Lendahl U., 1995: Rapid, widespread, and longlasting induction of nestin contributes to the generation of glial scar tissue after CNS injury., *J Cell Biol* **131**(2) 453–464.

Fritsche E., Cline J.E., Nguyen N.H., Scanlan T.S., Abel J., 2005: Polychlorinated biphenyls disturb differentiation of normal human neural progenitor cells: clue for involvement of thyroid hormone receptors., *Environ Health Perspect* **113**(7) 871–876.

Gage F.H., 2000: Mammalian neural stem cells., *Science* **287**(5457) 1433–1438.

Gao Q., Katakowski M., Chen X., Li Y., Chopp M., 2005a: Human marrow stromal cells enhance connexin43 gap junction intercellular communication in cultured astrocytes., *Cell Transplant* **14**(2-3) 109–117.

Gao Q., Li Y., Chopp M., 2005b: Bone marrow stromal cells increase astrocyte survival via upregulation of phosphoinositide 3-kinase/threonine protein kinase and mitogen-activated protein kinase kinase/extracellular signal-regulated kinase pathways and stimulate astrocyte trophic factor gene expression after anaerobic insult., *Neuroscience* **136**(1) 123–134.

Garbuzova-Davis S., Willing A.E., Saporta S., Bickford P.C., Gemma C., Chen N., Sanberg C.D., Klasko S.K., Borlongan C.V., Sanberg P.R., 2006: Novel cell therapy approaches for brain repair., *Prog Brain Res* **157** 207–222.

Garcia-Abreu J., Neto V.M., Carvalho S.L., Cavalcante L.A., 1995: Regionally specific properties of midbrain glia: I. Interactions with midbrain neurons., *J Neurosci Res* **40**(4) 471–477.

Giulian D., Vaca K., Corpuz M., 1993: Brain glia release factors with opposing actions upon neuronal survival., *J Neurosci* **13**(1) 29–37.

Golding J.P., Bird C., McMahon S., Cohen J., 1999: Behaviour of DRG sensory neurites at the intact and injured adult rat dorsal root entry zone: postnatal neurites become paralysed, whilst injury improves the growth of embryonic neurites., *Glia* **26**(4) 309–323.

Golding J.P., Shewan D., Berry M., Cohen J., 1996: An in vitro model of the rat dorsal root entry zone reveals developmental changes in the extent of sensory axon growth into the spinal cord., *Mol Cell Neurosci* **7**(3) 191–203.

Goldman S., 2005: Stem and progenitor cell-based therapy of the human central nervous system., *Nat Biotechnol* **23**(7) 862–871.

Good P., Yoda A., Sakakibara S., Yamamoto A., Imai T., Sawa H., Ikeuchi T., Tsuji S., Satoh H., Okano H., 1998: The human Musashi homolog 1 (MSI1) gene encoding the homologue of Musashi/Nrp-1, a neural RNA-binding protein putatively expressed in CNS stem cells and neural progenitor cells., *Genomics* **52**(3) 382–384.

GrandPré T., Nakamura F., Vartanian T., Strittmatter S.M., 2000: Identification of the Nogo inhibitor of axon regeneration as a Reticulon protein., *Nature* **403**(6768) 439–444.

Grayson W.L., Ma T., Bunnell B., 2004: Human mesenchymal stem cells tissue development in 3D PET matrices., *Biotechnol Prog* **20**(3) 905–912.

Grierson J.P., Petroski R.E., Ling D.S., Geller H.M., 1990: Astrocyte topography and tenascin cytotactin expression: correlation with the ability to support neuritic outgrowth., *Brain Res Dev Brain Res* **55**(1) 11–19.

Grimpe B., Silver J., 2002: The extracellular matrix in axon regeneration., *Prog Brain Res* **137** 333–349.

Gris P., Tighe A., Levin D., Sharma R., Brown A., 2007: Transcriptional regulation of scar gene expression in primary astrocytes., *Glia* **55**(11) 1145–1155.

Gross R.E., Mehler M.F., Mabie P.C., Zang Z., Santschi L., Kessler J.A., 1996: Bone morphogenetic proteins promote astroglial lineage commitment by mammalian subventricular zone progenitor cells., *Neuron* **17**(4) 595–606.

Gu Y., Wang J., Ding F., Hu N., Wang Y., Gu X., 2010: Neurotrophic actions of bone marrow stromal cells on primary culture of dorsal root ganglion tissues and neurons., *J Mol Neurosci* **40**(3) 332–341.

Guth L., 1956: Regeneration in the mammalian peripheral nervous system., *Physiol Rev* **36**(4) 441–478.

Hall S.M., 1989: Regeneration in the peripheral nervous system., *Neuropathol Appl Neurobiol* **15**(6) 513–529.

Hatten M.E., Liem R.K., Shelanski M.L., Mason C.A., 1991: Astroglia in CNS injury., *Glia* **4**(2) 233–243.

Hedman K., Kurkinen M., Alitalo K., Vaheri A., Johansson S., Höök M., 1979: Isolation of the pericellular matrix of human fibroblast cultures., *J Cell Biol* **81**(1) 83–91.

Herszfeld D., Wolvetang E., Langton-Bunker E., Chung T.L., Filipczyk A.A., Houssami S., Jamshidi P., Koh K., Laslett A.L., Michalska A., Nguyen L., Reubinoff B.E., Tellis I., Auerbach J.M., Ording C.J., Looijenga L.H.J., Pera M.F., 2006: CD30 is a survival factor and a biomarker for transformed human pluripotent stem cells., *Nat Biotechnol* **24**(3) 351–357.

Himes B.T., Neuhuber B., Coleman C., Kushner R., Swanger S.A., Kopen G.C., Wagner J., Shumsky J.S., Fischer I., 2006: Recovery of function following grafting of human bone marrow-derived stromal cells into the injured spinal cord., *Neurorehabil Neural Repair* **20**(2) 278–296.

Hofstetter C.P., Holmström N.A.V., Lilja J.A., Schweinhardt P., Hao J., Spenger C., Wiesenfeld-Hallin Z., Kurpad S.N., Frisén J., Olson L., 2005: Allodynia limits the usefulness of intraspinal neural stem cell grafts; directed differentiation improves outcome., *Nat Neurosci* **8**(3) 346–353.

Hofstetter C.P., Schwarz E.J., Hess D., Widenfalk J., Manira A.E., Prockop D.J., Olson L., 2002: Marrow stromal cells form guiding strands in the injured spinal cord and promote recovery., *Proc Natl Acad Sci U S A* **99**(4) 2199–2204.

Huettner J.E., 1990: Glutamate receptor channels in rat DRG neurons: activation by kainate and quisqualate and blockade of desensitization by Con A., *Neuron* **5**(3) 255–266.

Hughes J.T., 1988: The Edwin Smith Surgical Papyrus: an analysis of the first case reports of spinal cord injuries., *Paraplegia* **26**(2) 71–82.

Hulspas R., Quesenberry P.J., 2000: Characterization of neurosphere cell phenotypes by flow cytometry., *Cytometry* **40**(3) 245–250.

Hynds D.L., Snow D.M., 2001: Fibronectin and laminin elicit differential behaviors from SH-SY5Y growth cones contacting inhibitory chondroitin sulfate proteoglycans., *J Neurosci Res* **66**(4) 630–642.

Ignatova T.N., Kukekov V.G., Laywell E.D., Suslov O.N., Vrionis F.D., Steindler D.A., 2002: Human cortical glial tumors contain neural stem-like cells expressing astroglial and neuronal markers in vitro., *Glia* **39**(3) 193–206.

Ikeda O., Murakami M., Ino H., Yamazaki M., Nemoto T., Koda M., Nakayama C., Moriya H., 2001: Acute up-regulation of brain-derived neurotrophic factor expression resulting from experimentally induced injury in the rat spinal cord., *Acta Neuropathol* **102**(3) 239–245.

Isele N.B., Lee H.S., Landshamer S., Straube A., Padovan C.S., Plesnila N., Culmsee C., 2007: Bone marrow stromal cells mediate protection through stimulation of PI3-K/Akt and MAPK signaling in neurons., *Neurochem Int* **50**(1) 243–250.

Iwanami A., Kaneko S., Nakamura M., Kanemura Y., Mori H., Kobayashi S., Yamasaki M., Momoshima S., Ishii H., Ando K., Tanioka Y., Tamaoki N., Nomura T., Toyama Y., Okano H., 2005: Transplantation of human neural stem cells for spinal cord injury in primates., *J Neurosci Res* **80**(2) 182–190.

Jones L.L., Margolis R.U., Tuszynski M.H., 2003a: The chondroitin sulfate proteoglycans neurocan, brevican, phosphacan, and versican are differentially regulated following spinal cord injury., *Exp Neurol* **182**(2) 399–411.

Jones L.L., Oudega M., Bunge M.B., Tuszynski M.H., 2001: Neurotrophic factors, cellular bridges and gene therapy for spinal cord injury., *J Physiol* **533**(Pt 1) 83–89.

Jones L.L., Sajed D., Tuszynski M.H., 2003b: Axonal regeneration through regions of chondroitin sulfate proteoglycan deposition after spinal cord injury: a balance of permissiveness and inhibition., *J Neurosci* **23**(28) 9276–9288.

Kalia M., 2008: Brain development: anatomy, connectivity, adaptive plasticity, and toxicity., *Metabolism* **57 Suppl 2** S2–S5.

Kamishina H., Cheeseman J.A., Clemmons R.M., 2009: The effects of canine bone marrow stromal cells on neuritogenesis from dorsal root ganglion neurons in vitro., *Vet Res Commun* **33**(7) 645–657.

Kane C.J., Brown G.J., Phelan K.D., 1996: Transforming growth factor-beta 2 both stimulates and inhibits neurogenesis of rat cerebellar granule cells in culture., *Brain Res Dev Brain Res* **96**(1-2) 46–51.

Kaneko Y., Sakakibara S., Imai T., Suzuki A., Nakamura Y., Sawamoto K., Ogawa Y., Toyama Y., Miyata T., Okano H., 2000: Musashi1: an evolutionally conserved marker for CNS progenitor cells including neural stem cells., *Dev Neurosci* **22**(1-2) 139–153.

Kanemura Y., Mori H., Kobayashi S., Islam O., Kodama E., Yamamoto A., Nakanishi Y., Arita N., Yamasaki M., Okano H., Hara M., Miyake J., 2002: Evaluation of in vitro proliferative activity of human fetal neural stem/progenitor cells using indirect measurements of viable cells based on cellular metabolic activity., *J Neurosci Res* **69**(6) 869–879.

Kashiba H., Uchida Y., Senba E., 2001: Difference in binding by isolectin B4 to trkA and c-ret mRNA-expressing neurons in rat sensory ganglia., *Brain Res Mol Brain Res* **95**(1-2) 18–26.

Katoh-Semba R., Matsuda M., Kato K., Oohira A., 1995: Chondroitin sulphate proteoglycans in the rat brain: candidates for axon barriers of sensory neurons and the possible modification by laminin of their actions., *Eur J Neurosci* **7**(4) 613–621.

Keirstead H.S., Nistor G., Bernal G., Totoiu M., Cloutier F., Sharp K., Steward O., 2005: Human embryonic stem cell-derived oligodendrocyte progenitor cell transplants remyelinate and restore locomotion after spinal cord injury., *J Neurosci* **25**(19) 4694–4705.

Kim H.T., Kim I.S., Lee I.S., Lee J.P., Snyder E.Y., Park K.I., 2006: Human neurospheres derived from the fetal central nervous system are regionally and temporally specified but are not committed., *Exp Neurol* **199**(1) 222–235.

Kiryushko D., Berezin V., Bock E., 2004: Regulators of neurite outgrowth: role of cell adhesion molecules., *Ann N Y Acad Sci* **1014** 140–154.

Kitada M., Dezawa M., 2008: [Neural repair], *Nippon Rinsho* **66**(5) 921–925.

Klimanskaya I., Chung Y., Becker S., Lu S.J., Lanza R., 2006: Human embryonic stem cell lines derived from single blastomeres., *Nature* **444**(7118) 481–485.

Krenz N.R., Weaver L.C., 2000: Nerve growth factor in glia and inflammatory cells of the injured rat spinal cord., *J Neurochem* **74**(2) 730–739.

Kuhn H.G., Winkler J., Kempermann G., Thal L.J., Gage F.H., 1997: Epidermal growth factor and fibroblast growth factor-2 have different effects on neural progenitors in the adult rat brain., *J Neurosci* **17**(15) 5820–5829.

Lagord C., Berry M., Logan A., 2002: Expression of TGFbeta2 but not TGFbeta1 correlates with the deposition of scar tissue in the lesioned spinal cord., *Mol Cell Neurosci* **20**(1) 69–92.

Lander A.D., 1987: Molecules that make axons grow., *Mol Neurobiol* **1**(3) 213–245.

Lander A.D., Fujii D.K., Reichardt L.F., 1985: Laminin is associated with the "neurite outgrowth-promoting factors" found in conditioned media., *Proc Natl Acad Sci U S A* **82**(7) 2183–2187.

Leco K.J., Khokha R., Pavloff N., Hawkes S.P., Edwards D.R., 1994: Tissue inhibitor of metalloproteinases-3 (TIMP-3) is an extracellular matrix-associated protein with a distinctive pattern of expression in mouse cells and tissues., *J Biol Chem* **269**(12) 9352–9360.

Lee M.Y., Kim C.J., Shin S.L., Moon S.H., Chun M.H., 1998: Increased ciliary neurotrophic factor expression in reactive astrocytes following spinal cord injury in the rat., *Neurosci Lett* **255**(2) 79–82.

Li M., Shibata A., Li C., Braun P.E., McKerracher L., Roder J., Kater S.B., David S., 1996: Myelin-associated glycoprotein inhibits neurite/axon growth and causes growth cone collapse., *J Neurosci Res* **46**(4) 404–414.

Li Y., Chen J., Zhang C.L., Wang L., Lu D., Katakowski M., Gao Q., Shen L.H., Zhang J., Lu M., Chopp M., 2005: Gliosis and brain remodeling after treatment of stroke in rats with marrow stromal cells., *Glia* **49**(3) 407–417.

Liang P., hong Jin L., Liang T., zhong Liu E., guang Zhao S., 2006: Human neural stem cells promote corticospinal axons regeneration and synapse reformation in injured spinal cord of rats., *Chin Med J (Engl)* **119**(16) 1331–1338.

Liberto C.M., Albrecht P.J., Herx L.M., Yong V.W., Levison S.W., 2004: Pro-regenerative properties of cytokine-activated astrocytes., *J Neurochem* **89**(5) 1092–1100.

Lider O., Cahalon L., Gilat D., Hershkoviz R., Siegel D., Margalit R., Shoseyov O., Cohen I.R., 1995: A disaccharide that inhibits tumor necrosis factor alpha is formed from the extracellular matrix by the enzyme heparanase., *Proc Natl Acad Sci U S A* **92**(11) 5037–5041.

Liebl D.J., Tessarollo L., Palko M.E., Parada L.F., 1997: Absence of sensory neurons before target innervation in brain-derived neurotrophic factor-, neurotrophin 3-, and TrkC-deficient embryonic mice., *J Neurosci* **17**(23) 9113–9121.

Liesi P., Dahl D., Vaheri A., 1984: Neurons cultured from developing rat brain attach and spread preferentially to laminin., *J Neurosci Res* **11**(3) 241–251.

Liesi P., Silver J., 1988: Is astrocyte laminin involved in axon guidance in the mammalian CNS?, *Dev Biol* **130**(2) 774–785.

Lin J., Cai W., 2004: Effect of vimentin on reactive gliosis: in vitro and in vivo analysis., *J Neurotrauma* **21**(11) 1671–1682.

Liu B.P., Cafferty W.B.J., Budel S.O., Strittmatter S.M., 2006: Extracellular regulators of axonal growth in the adult central nervous system., *Philos Trans R Soc Lond B Biol Sci* **361**(1473) 1593–1610.

Liu Y., Han S.S.W., Wu Y., Tuohy T.M.F., Xue H., Cai J., Back S.A., Sherman L.S., Fischer I., Rao M.S., 2004: CD44 expression identifies astrocyte-restricted precursor cells., *Dev Biol* **276**(1) 31–46.

Luckenbill-Edds L., 1997: Laminin and the mechanism of neuronal outgrowth., *Brain Res Brain Res Rev* **23**(1-2) 1–27.

Mabie P.C., Mehler M.F., Marmur R., Papavasiliou A., Song Q., Kessler J.A., 1997: Bone morphogenetic proteins induce astroglial differentiation of oligodendroglial-astroglial progenitor cells., *J Neurosci* **17**(11) 4112–4120.

Manthorpe M., Engvall E., Ruoslahti E., Longo F.M., Davis G.E., Varon S., 1983: Laminin promotes neuritic regeneration from cultured peripheral and central neurons., *J Cell Biol* **97**(6) 1882–1890.

Maric D., Barker J.L., 2004: Neural stem cells redefined: a FACS perspective., *Mol Neurobiol* **30**(1) 49–76.

Martin G.F., Terman J.R., Wang X.M., 2000: Regeneration of descending spinal axons after transection of the thoracic spinal cord during early development in the North American opossum, Didelphis virginiana., *Brain Res Bull* **53**(5) 677–687.

Martinez R., Gomes F.C.A., 2002: Neuritogenesis induced by thyroid hormone-treated astrocytes is mediated by epidermal growth factor/mitogen-activated protein kinase-phosphatidylinositol 3-kinase pathways and involves modulation of extracellular matrix proteins., *J Biol Chem* **277**(51) 49311–49318.

McAteer J.A D.J., 2001: *Basic Cell Culture, Second Edition, Practical Approach*, IRL Press, Oxford.

McDonald J.W., Liu X.Z., Qu Y., Liu S., Mickey S.K., Turetsky D., Gottlieb D.I., Choi D.W., 1999: Transplanted embryonic stem cells survive, differentiate and promote recovery in injured rat spinal cord., *Nat Med* **5**(12) 1410–1412.

McGee A.W., Strittmatter S.M., 2003: The Nogo-66 receptor: focusing myelin inhibition of axon regeneration., *Trends Neurosci* **26**(4) 193–198.

McKay R., 1997: Stem cells in the central nervous system., *Science* **276**(5309) 66–71.

McKeon R.J., Jurynec M.J., Buck C.R., 1999: The chondroitin sulfate proteoglycans neurocan and phosphacan are expressed by reactive astrocytes in the chronic CNS glial scar., *J Neurosci* **19**(24) 10778–10788.

McKerracher L., David S., Jackson D.L., Kottis V., Dunn R.J., Braun P.E., 1994: Identification of myelin-associated glycoprotein as a major myelin-derived inhibitor of neurite growth., *Neuron* **13**(4) 805–811.

Mehler M.F., Mabie P.C., Zhang D., Kessler J.A., 1997: Bone morphogenetic proteins in the nervous system., *Trends Neurosci* **20**(7) 309–317.

Mehler M.F., Mabie P.C., Zhu G., Gokhan S., Kessler J.A., 2000: Developmental changes in progenitor cell responsiveness to bone morphogenetic proteins differentially modulate progressive CNS lineage fate., *Dev Neurosci* **22**(1-2) 74–85.

Meiners S., Powell E.M., Geller H.M., 1995: A distinct subset of tenascin/CS-6-PG-rich astrocytes restricts neuronal growth in vitro., *J Neurosci* **15**(12) 8096–8108.

Menet V., Ribotta M.G.Y., Sandillon F., Privat A., 2000: GFAP null astrocytes are a favorable substrate for neuronal survival and neurite growth., *Glia* **31**(3) 267–272.

Milner R., Campbell I.L., 2002: Cytokines regulate microglial adhesion to laminin and astrocyte extracellular matrix via protein kinase C-dependent activation of the alpha6beta1 integrin., *J Neurosci* **22**(5) 1562–1572.

Mocchetti I., Rabin S.J., Colangelo A.M., Whittemore S.R., Wrathall J.R., 1996: Increased basic fibroblast growth factor expression following contusive spinal cord injury., *Exp Neurol* **141**(1) 154–164.

Molliver D.C., Wright D.E., Leitner M.L., Parsadanian A.S., Doster K., Wen D., Yan Q., Snider W.D., 1997: IB4-binding DRG neurons switch from NGF to GDNF dependence in early postnatal life., *Neuron* **19**(4) 849–861.

Montzka K., Lassonczyk N., Tschöke B., Neuss S., Führmann T., Franzen R., Smeets R., Brook G.A., Wöltje M., 2009: Neural differentiation potential of human bone marrow-derived mesenchymal stromal cells: misleading marker gene expression., *BMC Neurosci* **10** 16.

Moon L.D., Fawcett J.W., 2001: Reduction in CNS scar formation without concomitant increase in axon regeneration following treatment of adult rat brain with a combination of antibodies to TGFbeta1 and beta2., *Eur J Neurosci* **14**(10) 1667–1677.

Moretto G., Xu R.Y., Kim S.U., 1993: CD44 expression in human astrocytes and oligodendrocytes in culture., *J Neuropathol Exp Neurol* **52**(4) 419–423.

Morgenstern D.A., Asher R.A., Fawcett J.W., 2002: Chondroitin sulphate proteoglycans in the CNS injury response., *Prog Brain Res* **137** 313–332.

Mori H., Kanemura Y., Onaya J., Hara M., Miyake J., Yamasaki M., Kariya Y., 2005: Effects of heparin and its 6-O- and 2-O-desulfated derivatives with low anticoagulant activity on proliferation of human neural stem/progenitor cells., *J Biosci Bioeng* **100**(1) 54–61.

Mori H., Ninomiya K., Kino-oka M., Shofuda T., Islam M.O., Yamasaki M., Okano H., Taya M., Kanemura Y., 2006: Effect of neurosphere size on the growth rate of human neural stem/progenitor cells., *J Neurosci Res* **84**(8) 1682–1691.

Mukhopadhyay G., Doherty P., Walsh F.S., Crocker P.R., Filbin M.T., 1994: A novel role for myelin-associated glycoprotein as an inhibitor of axonal regeneration., *Neuron* **13**(3) 757–767.

Murray K., Dubois-Dalcq M., 1997: Emergence of oligodendrocytes from human neural spheres., *J Neurosci Res* **50**(2) 146–156.

Nakashima K., Yanagisawa M., Arakawa H., Kimura N., Hisatsune T., Kawabata M., Miyazono K., Taga T., 1999: Synergistic signaling in fetal brain by STAT3-Smad1 complex bridged by p300., *Science* **284**(5413) 479–482.

Naor D., Sionov R.V., Ish-Shalom D., 1997: CD44: structure, function, and association with the malignant process., *Adv Cancer Res* **71** 241–319.

Neugebauer K.M., Tomaselli K.J., Lilien J., Reichardt L.F., 1988: N-cadherin, NCAM, and integrins promote retinal neurite outgrowth on astrocytes in vitro., *J Cell Biol* **107**(3) 1177–1187.

Neuhuber B., Himes B.T., Shumsky J.S., Gallo G., Fischer I., 2005: Axon growth and recovery of function supported by human bone marrow stromal cells in the injured spinal cord exhibit donor variations., *Brain Res* **1035**(1) 73–85.

Nicholls J., Saunders N., 1996: Regeneration of immature mammalian spinal cord after injury., *Trends Neurosci* **19**(6) 229–234.

Niedbala M.J., Crickard K., Bernacki R.J., 1986: Adhesion, growth and morphology of human mesothelial cells on extracellular matrix., *J Cell Sci* **85** 133–147.

Nistor G.I., Totoiu M.O., Haque N., Carpenter M.K., Keirstead H.S., 2005: Human embryonic stem cells differentiate into oligodendrocytes in high purity and myelinate after spinal cord transplantation., *Glia* **49**(3) 385–396.

Noble M., Albrechtsen M., Møller C., Lyles J., Bock E., Goridis C., Watanabe M., Rutishauser U., 1985: Glial cells express N-CAM/D2-CAM-like polypeptides in vitro., *Nature* **316**(6030) 725–728.

Noble M., Fok-Seang J., Cohen J., 1984: Glia are a unique substrate for the in vitro growth of central nervous system neurons., *J Neurosci* **4**(7) 1892–1903.

Ogawa D., Okada Y., Nakamura M., Kanemura Y., Okano H.J., Matsuzaki Y., Shimazaki T., Ito M., Ikeda E., Tamiya T., Nagao S., Okano H., 2009: Evaluation of human fetal neural stem/progenitor cells as a source for cell replacement therapy for neurological disorders: properties and tumorigenicity after long-term in vitro maintenance., *J Neurosci Res* **87**(2) 307–317.

Ogawa Y., Sawamoto K., Miyata T., Miyao S., Watanabe M., Nakamura M., Bregman B.S., Koike M., Uchiyama Y., Toyama Y., Okano H., 2002: Transplantation of in vitro-expanded fetal neural progenitor cells results in neurogenesis and functional recovery after spinal cord contusion injury in adult rats., *J Neurosci Res* **69**(6) 925–933.

Ohta M., Suzuki Y., Noda T., Ejiri Y., Dezawa M., Kataoka K., Chou H., Ishikawa N., Matsumoto N., Iwashita Y., Mizuta E., Kuno S., Ide C., 2004: Bone marrow stromal cells infused into the cerebrospinal fluid promote functional recovery of the injured rat spinal cord with reduced cavity formation., *Exp Neurol* **187**(2) 266–278.

Okano H., Imai T., Okabe M., 2002: Musashi: a translational regulator of cell fate., *J Cell Sci* **115**(Pt 7) 1355–1359.

Okano H., Ogawa Y., Nakamura M., Kaneko S., Iwanami A., Toyama Y., 2003: Transplantation of neural stem cells into the spinal cord after injury., *Semin Cell Dev Biol* **14**(3) 191–198.

Ostenfeld T., Joly E., Tai Y.T., Peters A., Caldwell M., Jauniaux E., Svendsen C.N., 2002: Regional specification of rodent and human neurospheres., *Brain Res Dev Brain Res* **134**(1-2) 43–55.

Ostenfeld T., Svendsen C.N., 2004: Requirement for neurogenesis to proceed through the division of neuronal pro-
genitors following differentiation of epidermal growth factor and fibroblast growth factor-2-responsive human
neural stem cells., *Stem Cells* **22**(5) 798–811.

Oudega M., 2007: Schwann cell and olfactory ensheathing cell implantation for repair of the contused spinal cord.,
Acta Physiol (Oxf) **189**(2) 181–189.

Parr A.M., Tator C.H., Keating A., 2007: Bone marrow-derived mesenchymal stromal cells for the repair of central
nervous system injury., *Bone Marrow Transplant* **40**(7) 609–619.

Pfeifer K., Vroemen M., Blesch A., Weidner N., 2004: Adult neural progenitor cells provide a permissive guiding
substrate for corticospinal axon growth following spinal cord injury., *Eur J Neurosci* **20**(7) 1695–1704.

Piao J.H., Odeberg J., Samuelsson E.B., Kjaeldgaard A., Falci S., Seiger A., Sundström E., Akesson E., 2006:
Cellular composition of long-term human spinal cord- and forebrain-derived neurosphere cultures., *J Neurosci
Res* **84**(3) 471–482.

Pindzola R.R., Doller C., Silver J., 1993: Putative inhibitory extracellular matrix molecules at the dorsal root entry
zone of the spinal cord during development and after root and sciatic nerve lesions., *Dev Biol* **156**(1) 34–48.

Piper D.R., Mujtaba T., Keyoung H., Roy N.S., Goldman S.A., Rao M.S., Lucero M.T., 2001: Identification
and characterization of neuronal precursors and their progeny from human fetal tissue., *J Neurosci Res* **66**(3)
356–368.

Piper D.R., Mujtaba T., Rao M.S., Lucero M.T., 2000: Immunocytochemical and physiological characterization of
a population of cultured human neural precursors., *J Neurophysiol* **84**(1) 534–548.

Pool M., Thiemann J., Bar-Or A., Fournier A.E., 2008: NeuriteTracer: a novel ImageJ plugin for automated
quantification of neurite outgrowth., *J Neurosci Methods* **168**(1) 134–139.

Pot C., Simonen M., Weinmann O., Schnell L., Christ F., Stoeckle S., Berger P., Rülicke T., Suter U., Schwab
M.E., 2002: Nogo-A expressed in Schwann cells impairs axonal regeneration after peripheral nerve injury., *J
Cell Biol* **159**(1) 29–35.

Powell E.M., Meiners S., DiProspero N.A., Geller H.M., 1997: Mechanisms of astrocyte-directed neurite guid-
ance., *Cell Tissue Res* **290**(2) 385–393.

Pérez-Bouza A., Wigley C.B., Nacimiento W., Noth J., Brook G.A., 1998: Spontaneous orientation of transplanted
olfactory glia influences axonal regeneration., *Neuroreport* **9**(13) 2971–2975.

Priestley J.V., Michael G.J., Averill S., Liu M., Willmott N., 2002: Regulation of nociceptive neurons by nerve
growth factor and glial cell line derived neurotrophic factor., *Can J Physiol Pharmacol* **80**(5) 495–505.

Prinjha R., Moore S.E., Vinson M., Blake S., Morrow R., Christie G., Michalovich D., Simmons D.L., Walsh F.S.,
2000: Inhibitor of neurite outgrowth in humans., *Nature* **403**(6768) 383–384.

Prockop D.J., 1997: Marrow stromal cells as stem cells for nonhematopoietic tissues., *Science* **276**(5309) 71–74.

Puch S., Armeanu S., Kibler C., Johnson K.R., Müller C.A., Wheelock M.J., Klein G., 2001: N-cadherin is developmentally regulated and functionally involved in early hematopoietic cell differentiation., *J Cell Sci* **114**(Pt 8) 1567–1577.

Quinn S.M., Walters W.M., Vescovi A.L., Whittemore S.R., 1999: Lineage restriction of neuroepithelial precursor cells from fetal human spinal cord., *J Neurosci Res* **57**(5) 590–602.

Ramón-Cueto A., Cordero M.I., Santos-Benito F.F., Avila J., 2000: Functional recovery of paraplegic rats and motor axon regeneration in their spinal cords by olfactory ensheathing glia., *Neuron* **25**(2) 425–435.

Ramón-Cueto A., Nieto-Sampedro M., 1994: Regeneration into the spinal cord of transected dorsal root axons is promoted by ensheathing glia transplants., *Exp Neurol* **127**(2) 232–244.

Ramón-Cueto A., Plant G.W., Avila J., Bunge M.B., 1998: Long-distance axonal regeneration in the transected adult rat spinal cord is promoted by olfactory ensheathing glia transplants., *J Neurosci* **18**(10) 3803–3815.

Rebaï O., Petit-Thevenin J.L., Bruneau N., Lombardo D., Vérine A., 2005: In vitro angiogenic effects of pancreatic bile salt-dependent lipase., *Arterioscler Thromb Vasc Biol* **25**(2) 359–364.

Reynolds B.A., Weiss S., 1992: Generation of neurons and astrocytes from isolated cells of the adult mammalian central nervous system., *Science* **255**(5052) 1707–1710.

Reynolds B.A., Weiss S., 1996: Clonal and population analyses demonstrate that an EGF-responsive mammalian embryonic CNS precursor is a stem cell., *Dev Biol* **175**(1) 1–13.

Ridet J.L., Malhotra S.K., Privat A., Gage F.H., 1997: Reactive astrocytes: cellular and molecular cues to biological function., *Trends Neurosci* **20**(12) 570–577.

Riederer B., Matus A., 1985: Differential expression of distinct microtubule-associated proteins during brain development., *Proc Natl Acad Sci U S A* **82**(17) 6006–6009.

Santucci R.A., Barber T.D., 2005: Resorbable extracellular matrix grafts in urologic reconstruction., *Int Braz J Urol* **31**(3) 192–203.

Sasaki M., Li B., Lankford K.L., Radtke C., Kocsis J.D., 2007: Remyelination of the injured spinal cord., *Prog Brain Res* **161** 419–433.

Savio T., Schwab M.E., 1990: Lesioned corticospinal tract axons regenerate in myelin-free rat spinal cord., *Proc Natl Acad Sci U S A* **87**(11) 4130–4133.

Schieker M., Pautke C., Haasters F., Schieker J., Docheva D., Böcker W., Guelkan H., Neth P., Jochum M., Mutschler W., 2007: Human mesenchymal stem cells at the single-cell level: simultaneous seven-colour immunofluorescence., *J Anat* **210**(5) 592–599.

Schlüter C., Duchrow M., Wohlenberg C., Becker M.H., Key G., Flad H.D., Gerdes J., 1993: The cell proliferation-associated antigen of antibody Ki-67: a very large, ubiquitous nuclear protein with numerous repeated elements, representing a new kind of cell cycle-maintaining proteins., *J Cell Biol* **123**(3) 513–522.

Schnell L., Schwab M.E., 1990: Axonal regeneration in the rat spinal cord produced by an antibody against myelin-associated neurite growth inhibitors., *Nature* **343**(6255) 269–272.

Schoenen J., Delree P., Leprince P., Moonen G., 1989: Neurotransmitter phenotype plasticity in cultured dissociated adult rat dorsal root ganglia: an immunocytochemical study., *J Neurosci Res* **22**(4) 473–487.

Schultz S.S., 2005: Adult stem cell application in spinal cord injury., *Curr Drug Targets* **6**(1) 63–73.

Schwab M.E., 2002: Increasing plasticity and functional recovery of the lesioned spinal cord., *Prog Brain Res* **137** 351–359.

Schwab M.E., Bartholdi D., 1996: Degeneration and regeneration of axons in the lesioned spinal cord., *Physiol Rev* **76**(2) 319–370.

Schwab M.E., Caroni P., 1988: Oligodendrocytes and CNS myelin are nonpermissive substrates for neurite growth and fibroblast spreading in vitro., *J Neurosci* **8**(7) 2381–2393.

Schwab M.E., Thoenen H., 1985: Dissociated neurons regenerate into sciatic but not optic nerve explants in culture irrespective of neurotrophic factors., *J Neurosci* **5**(9) 2415–2423.

Schwartz P.H., Bryant P.J., Fuja T.J., Su H., O'Dowd D.K., Klassen H., 2003: Isolation and characterization of neural progenitor cells from post-mortem human cortex., *J Neurosci Res* **74**(6) 838–851.

Seaberg R.M., van der Kooy D., 2003: Stem and progenitor cells: the premature desertion of rigorous definitions., *Trends Neurosci* **26**(3) 125–131.

Shewan D., Berry M., Cohen J., 1995: Extensive regeneration in vitro by early embryonic neurons on immature and adult CNS tissue., *J Neurosci* **15**(3 Pt 1) 2057–2062.

Shimode K., Iwasaki N., Majima T., Funakoshi T., Sawaguchi N., Onodera T., Minami A., 2007: Bone marrow stromal cells act as feeder cells for tendon fibroblasts through soluble factors., *Tissue Eng* **13**(2) 333–341.

Shuman S.L., Bresnahan J.C., Beattie M.S., 1997: Apoptosis of microglia and oligodendrocytes after spinal cord contusion in rats., *J Neurosci Res* **50**(5) 798–808.

Silver J., 1988: Transplantation strategies using embryonic astroglial cells to promote CNS axon regeneration in neonatal and adult mammals., *Clin Res* **36**(3) 196–199.

Silver J., Miller J.H., 2004: Regeneration beyond the glial scar., *Nat Rev Neurosci* **5**(2) 146–156.

Silver J., Ogawa M.Y., 1983: Postnatally induced formation of the corpus callosum in acallosal mice on glia-coated cellulose bridges., *Science* **220**(4601) 1067–1069.

Singec I., Knoth R., Meyer R.P., Maciaczyk J., Volk B., Nikkhah G., Frotscher M., Snyder E.Y., 2006: Defining the actual sensitivity and specificity of the neurosphere assay in stem cell biology., *Nat Methods* **3**(10) 801–806.

Singer M., Nordlander R.H., Egar M., 1979: Axonal guidance during embryogenesis and regeneration in the spinal cord of the newt: the blueprint hypothesis of neuronal pathway patterning., *J Comp Neurol* **185**(1) 1–21.

Smith G.M., Jacobberger J.W., Miller R.H., 1993: Modulation of adhesion molecule expression on rat cortical astrocytes during maturation., *J Neurochem* **60**(4) 1453–1466.

Smith G.M., Miller R.H., Silver J., 1986: Changing role of forebrain astrocytes during development, regenerative failure, and induced regeneration upon transplantation., *J Comp Neurol* **251**(1) 23–43.

Smith G.M., Rutishauser U., Silver J., Miller R.H., 1990: Maturation of astrocytes in vitro alters the extent and molecular basis of neurite outgrowth., *Dev Biol* **138**(2) 377–390.

Snider W.D., 1988: Nerve growth factor enhances dendritic arborization of sympathetic ganglion cells in developing mammals., *J Neurosci* **8**(7) 2628–2634.

Snow D.M., Brown E.M., Letourneau P.C., 1996: Growth cone behavior in the presence of soluble chondroitin sulfate proteoglycan (CSPG), compared to behavior on CSPG bound to laminin or fibronectin., *Int J Dev Neurosci* **14**(3) 331–349.

Snow D.M., Lemmon V., Carrino D.A., Caplan A.I., Silver J., 1990: Sulfated proteoglycans in astroglial barriers inhibit neurite outgrowth in vitro., *Exp Neurol* **109**(1) 111–130.

Snyder E.Y., Yoon C., Flax J.D., Macklis J.D., 1997: Multipotent neural precursors can differentiate toward replacement of neurons undergoing targeted apoptotic degeneration in adult mouse neocortex., *Proc Natl Acad Sci U S A* **94**(21) 11663–11668.

Sohur U.S., Emsley J.G., Mitchell B.D., Macklis J.D., 2006: Adult neurogenesis and cellular brain repair with neural progenitors, precursors and stem cells., *Philos Trans R Soc Lond B Biol Sci* **361**(1473) 1477–1497.

Someya Y., Koda M., Dezawa M., Kadota T., Hashimoto M., Kamada T., Nishio Y., Kadota R., Mannoji C., Miyashita T., Okawa A., Yoshinaga K., Yamazaki M., 2008: Reduction of cystic cavity, promotion of axonal regeneration and sparing, and functional recovery with transplanted bone marrow stromal cell-derived Schwann cells after contusion injury to the adult rat spinal cord., *J Neurosurg Spine* **9**(6) 600–610.

Sommer I., Schachner M., 1981: Monoclonal antibodies (O1 to O4) to oligodendrocyte cell surfaces: an immunocytological study in the central nervous system., *Dev Biol* **83**(2) 311–327.

Sondell M., Sundler F., Kanje M., 2000: Vascular endothelial growth factor is a neurotrophic factor which stimulates axonal outgrowth through the flk-1 receptor., *Eur J Neurosci* **12**(12) 4243–4254.

Sorci G., Agneletti A.L., Bianchi R., Donato R., 1998: Association of S100B with intermediate filaments and microtubules in glial cells., *Biochim Biophys Acta* **1448**(2) 277–289.

Steindler D.A., Laywell E.D., 2003: Astrocytes as stem cells: nomenclature, phenotype, and translation., *Glia* **43**(1) 62–69.

Stoll G., Jander S., Myers R.R., 2002: Degeneration and regeneration of the peripheral nervous system: from Augustus Waller's observations to neuroinflammation., *J Peripher Nerv Syst* **7**(1) 13–27.

Suslov O.N., Kukekov V.G., Ignatova T.N., Steindler D.A., 2002: Neural stem cell heterogeneity demonstrated by molecular phenotyping of clonal neurospheres., *Proc Natl Acad Sci U S A* **99**(22) 14506–14511.

Svendsen C.N., ter Borg M.G., Armstrong R.J., Rosser A.E., Chandran S., Ostenfeld T., Caldwell M.A., 1998: A new method for the rapid and long term growth of human neural precursor cells., *J Neurosci Methods* **85**(2) 141–152.

Svendsen C.N., Caldwell M.A., Ostenfeld T., 1999: Human neural stem cells: isolation, expansion and transplantation., *Brain Pathol* **9**(3) 499–513.

Svendsen C.N., Caldwell M.A., Shen J., ter Borg M.G., Rosser A.E., Tyers P., Karmiol S., Dunnett S.B., 1997: Long-term survival of human central nervous system progenitor cells transplanted into a rat model of Parkinson's disease., *Exp Neurol* **148**(1) 135–146.

Tang X., Davies J.E., Davies S.J.A., 2003: Changes in distribution, cell associations, and protein expression levels of NG2, neurocan, phosphacan, brevican, versican V2, and tenascin-C during acute to chronic maturation of spinal cord scar tissue., *J Neurosci Res* **71**(3) 427–444.

Tarasenko Y.I., Gao J., Nie L., Johnson K.M., Grady J.J., Hulsebosch C.E., McAdoo D.J., Wu P., 2007: Human fetal neural stem cells grafted into contusion-injured rat spinal cords improve behavior., *J Neurosci Res* **85**(1) 47–57.

Tate C.C., Tate M.C., LaPlaca M.C., 2007: Fibronectin and laminin increase in the mouse brain after controlled cortical impact injury., *J Neurotrauma* **24**(1) 226–230.

Thomson J.A., Itskovitz-Eldor J., Shapiro S.S., Waknitz M.A., Swiergiel J.J., Marshall V.S., Jones J.M., 1998: Embryonic stem cell lines derived from human blastocysts., *Science* **282**(5391) 1145–1147.

Tisay K.T., Key B., 1999: The extracellular matrix modulates olfactory neurite outgrowth on ensheathing cells., *J Neurosci* **19**(22) 9890–9899.

Tom V.J., Doller C.M., Malouf A.T., Silver J., 2004: Astrocyte-associated fibronectin is critical for axonal regeneration in adult white matter., *J Neurosci* **24**(42) 9282–9290.

Tomaselli K.J., Neugebauer K.M., Bixby J.L., Lilien J., Reichardt L.F., 1988: N-cadherin and integrins: two receptor systems that mediate neuronal process outgrowth on astrocyte surfaces., *Neuron* **1**(1) 33–43.

Tomaselli K.J., Reichardt L.F., Bixby J.L., 1986: Distinct molecular interactions mediate neuronal process outgrowth on non-neuronal cell surfaces and extracellular matrices., *J Cell Biol* **103**(6 Pt 2) 2659–2672.

Tonge D.A., Golding J.P., Edbladh M., Kroon M., Ekström P.E., Edström A., 1997: Effects of extracellular matrix components on axonal outgrowth from peripheral nerves of adult animals in vitro.Tonge1997, *Exp Neurol* **146**(1) 81–90.

Tsai R.Y.L., McKay R.D.G., 2002: A nucleolar mechanism controlling cell proliferation in stem cells and cancer cells., *Genes Dev* **16**(23) 2991–3003.

Tucker B.A., Mearow K.M., 2008: Peripheral sensory axon growth: from receptor binding to cellular signaling., *Can J Neurol Sci* **35**(5) 551–566.

Tucker B.A., Rahimtula M., Mearow K.M., 2005a: Integrin activation and neurotrophin signaling cooperate to enhance neurite outgrowth in sensory neurons., *J Comp Neurol* **486**(3) 267–280.

Tucker B.A., Rahimtula M., Mearow K.M., 2005b: A procedure for selecting and culturing subpopulations of neurons from rat dorsal root ganglia using magnetic beads., *Brain Res Brain Res Protoc* **16**(1-3) 50–57.

Tucker B.A., Rahimtula M., Mearow K.M., 2006: Laminin and growth factor receptor activation stimulates differential growth responses in subpopulations of adult DRG neurons., *Eur J Neurosci* **24**(3) 676–690.

Uchida N., Buck D.W., He D., Reitsma M.J., Masek M., Phan T.V., Tsukamoto A.S., Gage F.H., Weissman I.L., 2000: Direct isolation of human central nervous system stem cells., *Proc Natl Acad Sci U S A* **97**(26) 14720–14725.

Ueki T., Tanaka M., Yamashita K., Mikawa S., Qiu Z., Maragakis N.J., Hevner R.F., Miura N., Sugimura H., Sato K., 2003: A novel secretory factor, Neurogenesin-1, provides neurogenic environmental cues for neural stem cells in the adult hippocampus., *J Neurosci* **23**(37) 11732–11740.

Vaquero J., Zurita M., 2009: Bone marrow stromal cells for spinal cord repair: a challenge for contemporary neurobiology., *Histol Histopathol* **24**(1) 107–116.

Verheijen R., Kuijpers H.J., Schlingemann R.O., Boehmer A.L., van Driel R., Brakenhoff G.J., Ramaekers F.C., 1989: Ki-67 detects a nuclear matrix-associated proliferation-related antigen. I. Intracellular localization during interphase., *J Cell Sci* **92 (Pt 1)** 123–130.

Vogel H., Butcher E.C., Picker L.J., 1992: H-CAM expression in the human nervous system: evidence for a role in diverse glial interactions., *J Neurocytol* **21**(5) 363–373.

Wachs F.P., Couillard-Despres S., Engelhardt M., Wilhelm D., Ploetz S., Vroemen M., Kaesbauer J., Uyanik G., Klucken J., Karl C., Tebbing J., Svendsen C., Weidner N., Kuhn H.G., Winkler J., Aigner L., 2003: High efficacy of clonal growth and expansion of adult neural stem cells., *Lab Invest* **83**(7) 949–962.

Wagner W., Wein F., Roderburg C., Saffrich R., Diehlmann A., Eckstein V., Ho A.D., 2008: Adhesion of human hematopoietic progenitor cells to mesenchymal stromal cells involves CD44., *Cells Tissues Organs* **188**(1-2) 160–169.

Wang L., Li Y., Chen X., Chen J., Gautam S.C., Xu Y., Chopp M., 2002: MCP-1, MIP-1, IL-8 and ischemic cerebral tissue enhance human bone marrow stromal cell migration in interface culture., *Hematology* **7**(2) 113–117.

Watanabe K., Nakamura M., Iwanami A., Fujita Y., Kanemura Y., Toyama Y., Okano H., 2004: Comparison between fetal spinal-cord- and forebrain-derived neural stem/progenitor cells as a source of transplantation for spinal cord injury., *Dev Neurosci* **26**(2-4) 275–287.

Weible M.W., Chan-Ling T., 2007: Phenotypic characterization of neural stem cells from human fetal spinal cord: synergistic effect of LIF and BMP4 to generate astrocytes., *Glia* **55**(11) 1156–1168.

White R.E., Yin F.Q., Jakeman L.B., 2008: TGF-alpha increases astrocyte invasion and promotes axonal growth into the lesion following spinal cord injury in mice., *Exp Neurol* .

Wictorin K., Björklund A., 1992: Axon outgrowth from grafts of human embryonic spinal cord in the lesioned adult rat spinal cord., *Neuroreport* **3**(12) 1045–1048.

Wilhelmsson U., Li L., Pekna M., Berthold C.H., Blom S., Eliasson C., Renner O., Bushong E., Ellisman M., Morgan T.E., Pekny M., 2004: Absence of glial fibrillary acidic protein and vimentin prevents hypertrophy of astrocytic processes and improves post-traumatic regeneration., *J Neurosci* **24**(21) 5016–5021.

Willerth S.M., Sakiyama-Elbert S.E., 2007: Approaches to neural tissue engineering using scaffolds for drug delivery., *Adv Drug Deliv Rev* **59**(4-5) 325–338.

Willerth S.M., Sakiyama-Elbert S.E., 2008: Cell therapy for spinal cord regeneration., *Adv Drug Deliv Rev* **60**(2) 263–276.

Wright K.T., Masri W.E., Osman A., Roberts S., Chamberlain G., Ashton B.A., Johnson W.E.B., 2007: Bone marrow stromal cells stimulate neurite outgrowth over neural proteoglycans (CSPG), myelin associated glyco-protein and Nogo-A., *Biochem Biophys Res Commun* **354**(2) 559–566.

Wright L.S., Li J., Caldwell M.A., Wallace K., Johnson J.A., Svendsen C.N., 2003: Gene expression in human neural stem cells: effects of leukemia inhibitory factor., *J Neurochem* **86**(1) 179–195.

Wu A., Pangalos M.N., Efthimiopoulos S., Shioi J., Robakis N.K., 1997: Appican expression induces morpholog-ical changes in C6 glioma cells and promotes adhesion of neural cells to the extracellular matrix., *J Neurosci* **17**(13) 4987–4993.

Wu P., Tarasenko Y.I., Gu Y., Huang L.Y.M., Coggeshall R.E., Yu Y., 2002: Region-specific generation of cholin-ergic neurons from fetal human neural stem cells grafted in adult rat., *Nat Neurosci* **5**(12) 1271–1278.

Wu S., Suzuki Y., Ejiri Y., Noda T., Bai H., Kitada M., Kataoka K., Ohta M., Chou H., Ide C., 2003: Bone marrow stromal cells enhance differentiation of cocultured neurosphere cells and promote regeneration of injured spinal cord., *J Neurosci Res* **72**(3) 343–351.

Xie F., Zheng B., 2008: White matter inhibitors in CNS axon regeneration failure., *Exp Neurol* **209**(2) 302–312.

Yiu G., He Z., 2006: Glial inhibition of CNS axon regeneration., *Nat Rev Neurosci* **7**(8) 617–627.

Yong V.W., Moumdjian R., Yong F.P., Ruijs T.C., Freedman M.S., Cashman N., Antel J.P., 1991: Gamma-interferon promotes proliferation of adult human astrocytes in vitro and reactive gliosis in the adult mouse brain in vivo., *Proc Natl Acad Sci U S A* **88**(16) 7016–7020.

Zeng X., 2007: Human embryonic stem cells: mechanisms to escape replicative senescence?, *Stem Cell Rev* **3**(4) 270–279.

Zhang J., Li L., 2005: BMP signaling and stem cell regulation., *Dev Biol* **284**(1) 1–11.

Zheng T., Steindler D.A., Laywell E.D., 2002: Transplantation of an indigenous neural stem cell population leading to hyperplasia and atypical integration., *Cloning Stem Cells* **4**(1) 3–8.

Zhou F.Q., Snider W.D., 2006: Intracellular control of developmental and regenerative axon growth., *Philos Trans R Soc Lond B Biol Sci* **361**(1473) 1575–1592.

11 Acknowledgements

12 Data Handling

Erklärung § 5 Abs. 1 zur Datenaufbewahrung

Hiermit erkläre ich, Lisa Maria Hillen, dass die dieser Dissertation zu Grunde liegenden Originaldaten bei meinem Betreuer, Herrn Privatdozent Ph.D.B.Sc. Gary Brook, Institut für Neuropathologie, des Universitätsklinikums Aachen, hinterlegt sind.

13 Curriculum Vitae

Lisa Maria Hillen

Date/Place of Birth	14. December 1984 in Aachen
Nationality	German

University Education

08/2004 - 10/2010	Medical student at the RWTH-Aachen University Medical School
10/2007	First State Examination (Ärztliche Basisprüfung)
10/2010	Second State Examination (Ärztliche Prüfung)

Education

08/1991 - 06/1995	Grundschule Walheim, Aachen
08/1995 - 06/2004	Inda Gymnasium Kornelimünster, Aachen
06/2001 - 12/2001	Pine Ridge Secondary School, Toronto
06/2004	German university-entrance diploma (Abitur)

Doctoral Thesis

10/2007-12/2010	Title of Thesis: "*In vitro* Characterisation of Foetal Human Neural Progenitors, their Astroglial Derivates, and Effects of Released Factors and Extracellular Matrix on Axon Regeneration"

Supervisor: Ph.D.B.Sc. Gary Brook

Department of Neuropathology, Aachen University Medical School

EC FP6 project RESCUE (LSHB-CT-2005-518233)

Publications

T. Führmann, K. Montzka, **L. M. Hillen**, D. Hodde, A. Dreier, A. Bozkurt, M. Wöltje, G.A. Brook. Axon growth-promoting properties of human bone marrow mesenchymal stromal cells. *Neuroscience Letters 2010,* ***474****:37-41*

T. Führmann, **L. M. Hillen**, K. Montzka, M. Wöltje, G. A. Brook. Novel Cell-Cell Interactions of Human Neural Progenitor-Derived Astrocytes within a Microstructured 3D-Scaffold. *Biomaterials 2010,* ***31****:7705-7715*

Abstracts and Posters

T. Führmann, **L. M. Hillen**, K. Montzka, Dr. M. Wöltje, I. Heschel and Dr. G. Brook. 2010. Cell-Cell interactions within an orientated type-I collagen scaffold. *Abstract and poster presentation*, Biomedica Summit, Aachen, Germany.

T. Führmann, **L. M. Hillen**, K. Montzka, Dr. M. Wöltje and PD Dr. G. A. Brook. 2009. An In vitro study of the Effect of Human Foetal Neural Progenitor-derived Astrocytes on Axon Regeneration in 2D and 3D Culture Systems. *Abstract and poster presentation*, 7th International Stem Cell School in Regenerative Medicine, Prague, Czech Republic.

T. Führmann, K. Montzka, **L. M. Hillen**, G. A. Brook. 2009. An in vitro investigation of the effects of multipotent human progenitors and their astroglial derivates on DRG axonal growth. *Abstract and poster presentation*, 5th International Meeting of the Stem Cell Network NRW, Aachen, Germany.

T. Führmann, K. Montzka, **L. M. Hillen** and G.A. Brook. 2008. Multipotent stem/progenitor cells and their derivatives promote adult rat DRG neurite outgrowth. *Abstract and poster presentation*, BioStar, the 3rd International Congress on Regenerative Biology and Medicine and the 3rd Congress of the German Society for Stem Cell Research, Stuttgart, Germany.

T. Führmann, K. Montzka, **L. M. Hillen** and G.A. Brook. 2008. Investigation of adult rat DRG neurite outgrowth on multipotent stem/progenitor cells and their derivatives. *Abstract and poster presentation*, 25th International Summer School of Brain Research, Amsterdam, Netherlands.